



HAL
open science

Bounding global aerosol radiative forcing of climate change

N. Bellouin, J. Quaas, E Gryspeerdt, S. Kinne, P. Stier, D Watson-Parris, O. Boucher, K. Carslaw, M Christensen, A.-L Daniau, et al.

► **To cite this version:**

N. Bellouin, J. Quaas, E Gryspeerdt, S. Kinne, P. Stier, et al.. Bounding global aerosol radiative forcing of climate change. *Reviews of Geophysics*, 2020, 10.1029/2019RG000660 . hal-02322106

HAL Id: hal-02322106

<https://hal.science/hal-02322106>

Submitted on 21 Oct 2019

HAL is a multi-disciplinary open access archive for the deposit and dissemination of scientific research documents, whether they are published or not. The documents may come from teaching and research institutions in France or abroad, or from public or private research centers.

L'archive ouverte pluridisciplinaire **HAL**, est destinée au dépôt et à la diffusion de documents scientifiques de niveau recherche, publiés ou non, émanant des établissements d'enseignement et de recherche français ou étrangers, des laboratoires publics ou privés.

Bounding global aerosol radiative forcing of climate change

N. Bellouin¹, J. Quaas², E. Gryspeerdt³, S. Kinne⁴, P. Stier⁵,
 D. Watson-Parris⁵, O. Boucher⁶, K.S. Carslaw⁷, M. Christensen⁵,
 A.-L. Daniaou⁸, J.-L. Dufresne⁹, G. Feingold¹⁰, S. Fiedler⁴, P. Forster¹¹,
 A. Gettelman¹², J. M. Haywood^{13,14}, U. Lohmann¹⁵, F. Malavelle¹³,
 T. Mauritsen¹⁶, D.T. McCoy⁷, G. Myhre¹⁷, J. Mülmenstädt², D. Neubauer¹⁵,
 A. Possner^{18,25}, M. Rugenstein⁴, Y. Sato^{19,26}, M. Schulz²⁰, S. E. Schwartz²¹,
 O. Sourdeval^{2,22}, T. Storelvmo²³, V. Toll^{1,27}, D. Winker²⁴, and B. Stevens⁴

¹Department of Meteorology, University of Reading, Reading RG6 6BB, UK

²Institute for Meteorology, Universität Leipzig, D-04103 Leipzig, Germany

³Space and Atmospheric Physics Group, Imperial College London, London SW7 2AZ, UK

⁴Max Planck Institute for Meteorology, D-20146 Hamburg, Germany

⁵Atmospheric, Oceanic and Planetary Physics, Department of Physics, University of Oxford, Oxford OX1 3PU, UK

⁶Institut Pierre-Simon Laplace, Sorbonne Université / CNRS, Paris F-75252, France

⁷School of Earth and Environment, University of Leeds, Leeds LS2 9JT, UK.

⁸EPOC, UMR 5805, CNRS - Université de Bordeaux, 33615 Pessac Cedex, France

⁹Laboratoire de Météorologie Dynamique/IPSL, CNRS, Sorbonne Université, Ecole Normale Supérieure,

PSL Research University, Ecole Polytechnique, 75252, Paris, France

¹⁰NOAA ESRL Chemical Sciences Division, Boulder, CO, 80305, USA

¹¹Priestley International Centre for Climate, University of Leeds, Leeds LS2 9JT, UK

¹²National Center for Atmospheric Research, Boulder, CO, 80301, USA

¹³CEMPS, University of Exeter, Exeter, EX4 4QE, UK

¹⁴UK Met Office Hadley Centre, Exeter, EX1 3PB, UK

¹⁵Institute for Atmospheric and Climate Science, ETH Zürich, 8092 Zurich, Switzerland

¹⁶Department of Meteorology, Stockholm University, SE-106 91 Stockholm, Sweden

¹⁷Center for International Climate and Environmental Research–Oslo (CICERO), N-0318 Oslo, Norway

¹⁸Department of Global Ecology, Carnegie Institution for Science, Stanford, CA, 94305, USA

¹⁹Department of Applied Energy, Graduate School of Engineering, Nagoya University, Nagoya, 464-8603,

Japan

²⁰Climate Modelling and Air Pollution Section, Research and Development Department, Norwegian Meteorological Institute, 0313 Oslo, Norway

²¹Brookhaven National Laboratory Environmental & Climate Sciences Department, Upton, NY

11973-5000, USA

²²Laboratoire d'Optique Atmosphérique, Université de Lille, 59655 Villeneuve d'Ascq Cedex, France

²³Department of Geosciences, University of Oslo, Norway

²⁴NASA Langley Research Center, Hampton, VA 23681, United States

²⁵now at Institute for Atmospheric and Environmental Sciences, Goethe University, 60438

Frankfurt/Main, Germany

²⁶now at Faculty of Science, Department of Earth and Planetary Sciences, Hokkaido University, Sapporo,

060-0810, Japan

²⁷now at Institute of Physics, University of Tartu, 50411 Tartu, Estonia

Key Points:

- An assessment of multiple lines of evidence supported by a conceptual model provides ranges for aerosol radiative forcing of climate change;
- Aerosol effective radiative forcing is assessed to be between -1.60 and -0.65 W m^{-2} at the 16-84% confidence level;
- Although key uncertainties remain, new ways of using observations provide stronger constraints for models.

Corresponding author: Nicolas Bellouin, n.bellouin@reading.ac.uk

Abstract

Aerosols interact with radiation and clouds. Substantial progress made over the past 40 years in observing, understanding, and modeling these processes helped quantify the imbalance in the Earth’s radiation budget caused by anthropogenic aerosols, called aerosol radiative forcing, but uncertainties remain large. This review provides a new range of aerosol radiative forcing over the industrial era based on multiple, traceable and arguable lines of evidence, including modelling approaches, theoretical considerations, and observations. Improved understanding of aerosol absorption and the causes of trends in surface radiative fluxes constrain the forcing from aerosol-radiation interactions. A robust theoretical foundation and convincing evidence constrain the forcing caused by aerosol-driven increases in liquid cloud droplet number concentration. However, the influence of anthropogenic aerosols on cloud liquid water content and cloud fraction is less clear, and the influence on mixed-phase and ice clouds remains poorly constrained. Observed changes in surface temperature and radiative fluxes provide additional constraints. These multiple lines of evidence lead to a 68% confidence interval for the total aerosol effective radiative forcing of -1.60 to -0.65 W m^{-2} , or -2.0 to -0.4 W m^{-2} with a 90% likelihood. Those intervals are of similar width to the last Intergovernmental Panel on Climate Change assessment but shifted towards more negative values. The uncertainty will narrow in the future by continuing to critically combine multiple lines of evidence, especially those addressing industrial-era changes in aerosol sources and aerosol effects on liquid cloud amount and on ice clouds.

1 Introduction

At steady state and averaged over a suitably long period, the heat content in the Earth system, defined here as the ocean, the atmosphere, the land surface and the cryosphere, remains constant because incoming radiative fluxes balance their outgoing counterparts. Perturbations to the radiative balance force the state of the system to change. Those perturbations can be natural, for example due to variations in the astronomical parameters of the Earth, a change in solar radiative output or injections of gases and aerosol particles by volcanic eruptions. Perturbations can also be due to human activities, which change the composition of the atmosphere.

A key objective of Earth system sciences is to understand historical changes in the energy budget of the Earth over the industrial period (Myhre et al., 2017) and how they translate into changes in the state variables of the atmosphere, land and ocean; to attribute observed temperature change since preindustrial times to specific perturbations (Jones et al., 2016); and to predict the impact of projected emission changes on the climate system. From that understanding climate scientists can derive estimates of the amount of committed warming that can be expected from past emissions (Pincus & Mauritsen, 2017; Schwartz, 2018), estimates of net carbon dioxide emissions that would be consistent with maintaining the increase in global mean surface temperature below agreed targets (Allen et al., 2018), or the efficacy of climate engineering to possibly mitigate against climate changes in the future (Kravitz et al., 2015).

A sustained radiative perturbation imposed on the climate system initially exerts a transient imbalance in the energy budget, which is called a radiative forcing (RF; denoted as \mathcal{F} ; Figure 1a). The system then responds by eventually reaching a new steady state whereby its heat content once again remains fairly constant. The equilibrium change in global mean surface temperature ΔT_s , in K, is given by

$$\Delta T_s = \lambda \mathcal{F} \quad (1)$$

where \mathcal{F} is the global mean radiative forcing, in W m^{-2} , and λ is the climate sensitivity parameter that quantifies the combined effect of feedbacks, in $\text{K (W m}^{-2})^{-1}$ (Ramanathan, 1975). For multiple reasons, including lack of knowledge of λ and the long response time

101 of T_s to RF (Schwartz, 2012; Forster, 2016; Knutti et al., 2017), it has become custom-
 102 ary to compare the strengths of different perturbations by their RFs rather than by the
 103 changes in T_s that ultimately ensue.

104 Temperatures in the stratosphere, a region of the atmosphere which is largely un-
 105 coupled from the troposphere-land-ocean system below, respond on a timescale of months,
 106 adjusting the magnitude and in the case of ozone perturbations even the sign of the initial
 107 radiative forcing (Figure 1b) (J. Hansen et al., 1997). This adjusted RF is defined
 108 by the 5th Assessment Report (AR5) of the Intergovernmental Panel on Climate Change
 109 (IPCC) (Myhre, Shindell, et al., 2013) as the change in net downward radiative flux at
 110 the tropopause, holding tropospheric state variables fixed at their unperturbed state but
 111 allowing for stratospheric temperatures to adjust to radiative equilibrium. This defini-
 112 tion is adopted by this review.

113 In addition to exerting a radiative forcing, changes in atmospheric composition af-
 114 fect other global mean quantities, such as temperature, moisture, surface radiative and
 115 heat fluxes, and wind fields, as well as their spatio-temporal patterns. Some of these re-
 116 sponses occur on timescales much faster than the adjustment timescales of ocean sur-
 117 face temperatures. These responses are called rapid adjustments and occur independently
 118 of surface temperature change (Shine et al., 2003; J. Hansen et al., 2005). Rapid adjust-
 119 ment mechanisms can augment or offset the initial radiative forcing by a sizable frac-
 120 tion, because they involve changes to the radiative properties of the atmosphere, includ-
 121 ing clouds, and/or the surface, which all contribute substantially to the Earth’s energy
 122 budget. Consequently, effective radiative forcing (ERF; denoted \mathcal{E} ; Figure 1c), which is
 123 the sum of radiative forcing and the associated rapid adjustments, is a better predictor
 124 of ΔT_s than RF (Figure 1d). Sherwood et al. (2015) make a pedagogical presentation
 125 of the concept of rapid adjustments that was used in IPCC AR5 (Boucher et al., 2013;
 126 Myhre, Shindell, et al., 2013). This review also adopts the definition of ERF introduced
 127 in the IPCC AR5 (Boucher et al., 2013; Myhre, Shindell, et al., 2013), which is the change
 128 in net top-of-atmosphere downward radiative flux that includes adjustments of temper-
 129 atures, water vapor and clouds throughout the atmosphere, including the stratosphere,
 130 but with sea surface temperature maintained fixed. In addition to its influence on global
 131 temperature change, ERF is also an efficient predictor of changes in globally-averaged
 132 precipitation rate (T. Andrews et al., 2010). Those changes arise from a balance between
 133 radiative changes within the atmosphere and changes in the latent and sensible heat fluxes
 134 at the surface (Richardson et al., 2016). Accounting for rapid adjustments when quan-
 135 tifying radiative changes is essential to obtain the full response of precipitation.

136 [INSERT FIGURE 1 HERE]

137 RF can be induced in multiple ways: changes in atmospheric composition, both in
 138 the gaseous and particulate phases, induced by volcanic or anthropogenic emissions; changes
 139 in surface albedo; and variations in solar irradiance. An estimated full range of anthro-
 140 pogenic aerosol RF based on an elicitation of 24 experts of -0.3 W m^{-2} to -2.1 W m^{-2}
 141 at the 90% confidence level was presented by Morgan et al. (2006). Individual experts,
 142 however, allowed for the possibility of much more negative, but also the possibility even
 143 of net positive, RF. A similar degree of uncertainty has been reflected in an evolving series
 144 of IPCC assessment reports (Table 1), where best estimates and uncertainty ranges
 145 of aerosol RF are also based at least partly on expert judgment. Since radiative forcings
 146 are additive within the forcing-response paradigm, the uncertainty attached to the aerosol
 147 ERF translates to the entire anthropogenic ERF (Schwartz & Andreae, 1996). Recog-
 148 nition of this fact has motivated a tremendous effort, now lasting several decades, to bet-
 149 ter understand how aerosols influence radiation, clouds, and ultimately the large-scale
 150 trajectory of the climate system, involving field measurements, laboratory studies, and
 151 modeling from microphysical to global scales (e.g. S. J. Ghan & Schwartz, 2007; Kul-
 152 mala et al., 2011; Seinfeld et al., 2016).

153 [INSERT TABLE 1 HERE]

154 In spring 2018, under the auspices of the World Climate Research Programme’s Grand
 155 Science Challenge on Clouds, Circulation and Climate Sensitivity, thirty-six experts gath-
 156 ered at Schloss Ringberg, in the mountains of Southern Germany, to take a fresh and
 157 comprehensive look at the present state of understanding of aerosol ERF, and identify
 158 prospects for progress on some of the most pressing open questions, thereby drawing the
 159 outlines for this review. The participants at that workshop expressed a wide range of
 160 views regarding the mechanisms and magnitudes of aerosol influences on the Earth’s en-
 161 ergy budget. This review represents a synthesis of these views and the underlying ev-
 162 idence.

163 This review is structured as follows. Section 2 reviews the physical mechanisms by
 164 which anthropogenic aerosols exert an RF of climate, and sets the scope of this review.
 165 Section 3 presents a conceptual model of globally-averaged aerosol ERF and the differ-
 166 ent lines of evidence used to quantify the uncertainty bounds in the terms of that con-
 167 ceptual model. Section 4 quantifies changes in aerosol amounts between preindustrial
 168 and present-day conditions. Sections 5 and 6 review current knowledge of aerosol inter-
 169 actions with radiation and clouds, respectively, to propose bounds for their RF, while
 170 sections 7 and 8, respectively, do the same for their rapid adjustments. Section 9 reviews
 171 the knowledge, and gaps thereof, in aerosol-cloud interactions in ice clouds. Section 10
 172 reviews estimates of aerosol ERF based on the response of the climate system over the
 173 last century. Finally, section 11 brings all lines of evidence together to bound total global
 174 aerosol ERF, and outlines open questions and research directions that could further con-
 175 tribute to narrow uncertainty or reduce the likelihood of surprises.

176 **2 Mechanisms, scope and terminology**

177 **2.1 Aerosol radiative forcing mechanisms**

178 The term “atmospheric aerosol” denotes a suspension of microscopic and submi-
 179 croscopic particles in air. These particles may be primary, meaning emitted directly in
 180 the liquid or solid phase, or secondary, meaning that they are produced in the atmosphere
 181 from gaseous precursors. In both cases, sources may be natural, for example sand storms,
 182 sea spray, volcanoes, natural wildfires, and biogenic emissions, or result from human ac-
 183 tivities, like construction and cement production, agriculture, and combustion of biomass
 184 and fossil fuels (Hoesly et al., 2018). Once in the atmosphere, aerosols undergo micro-
 185 physical (e.g. coagulation, condensation) and chemical (e.g. oxidation) transformation
 186 and are transported with the atmospheric flow. Tropospheric aerosols, the aerosols of
 187 main concern here, remain in the atmosphere for days to weeks (e.g. Kristiansen et al.,
 188 2012). Those relatively short residence times, compared to greenhouse gases, are caused
 189 by efficient removal processes, either by direct deposition to the surface by sedimenta-
 190 tion, diffusion or turbulence, or by scavenging by and into cloud droplets and ice crys-
 191 tals, and subsequent precipitation. As a consequence of these relatively rapid removal
 192 processes together with spatially heterogeneous distribution of sources, tropospheric aerosols
 193 are highly non-uniform spatially and temporally: a mean residence time of approximately
 194 5 days results in typical transport distances of about 2000 km. In consequence, aerosols
 195 are concentrated in and downwind of source regions such as cities and industrialized re-
 196 gions. In contrast, aerosols introduced into the stratosphere, for example by explosive
 197 volcanic eruptions, may have residence times of several months to a few years because
 198 of slow particle sedimentation velocities and secondary aerosol production.

199 Aerosols modify the Earth’s radiative budget directly through scattering and ab-
 200 sorption of radiation, denoted here aerosol radiative interaction, *ari*, and indirectly by
 201 modifying the microphysical properties of clouds, affecting their reflectivity and persis-
 202 tence, denoted here aerosol cloud interactions, *aci* (Figure 2). Aerosols may also affect

203 the reflectivity of the surface, as absorbing aerosol deposited on snow-covered surfaces
 204 may decrease their reflectivity. As a result of these processes, anthropogenic emissions
 205 of aerosols and their gaseous precursors have over the Anthropocene exerted an ERF,
 206 which is thought to have been strengthening over time for much of the industrial period,
 207 but is locally and instantaneously highly variable. All of this heterogeneity combines to
 208 make the aerosol ERF challenging to quantify, not just locally, but also in the global and
 209 annual mean.

210 [INSERT FIGURE 2 HERE]

211 Aerosol-radiation interactions are readily discerned by human observers as smoke,
 212 haze, and dust (See Box). As early as the 15th century, Leonardo da Vinci in instruc-
 213 tions on how to paint a battle scene, noted that the distribution of light in a mineral dust
 214 and biomass-burning plume was such that “*from the side whence the light comes this mix-*
 215 *ture of air and smoke and dust will seem far brighter than on the opposite side*” (Paris
 216 Manuscript A, circa 1492), a manifestation of the angular distribution of light scatter-
 217 ing that must be accurately represented in calculation of the RF. Volcanic aerosols and
 218 their impact on sunsets have also influenced a wide range of artists as shown by Zerefos
 219 et al. (2014). In this context the possibility that anthropogenic and volcanic aerosols de-
 220 crease atmospheric transmittance of solar radiation globally was therefore considered rel-
 221 atively early in climate change studies (e.g., McCormick & Ludwig, 1967; J. M. J. Mitchell,
 222 1971).

223 Improvements in the physical understanding of atmospheric scattering and absorp-
 224 tion, combined with a good constraint on ocean surface reflectance, allowed J. M. Hay-
 225 wood et al. (1999) to show that ari was needed to explain satellite-retrieved top-of-atmosphere
 226 shortwave radiative fluxes under cloud-free conditions. Aerosol contributions to outgo-
 227 ing shortwave radiative fluxes can exceed 100 W m^{-2} in some cases, as estimated for ex-
 228 ample by J. Haywood et al. (2003) from aircraft measurements of a mineral dust plume
 229 over the ocean. In addition to these direct effects of scattering and absorption, rapid ad-
 230 justments to ari, originally called semi-direct effects, were postulated by Grassl (1975),
 231 then again more recently from global modelling (J. Hansen et al., 1997), and observa-
 232 tions made during the Indian Ocean Experiment (INDOEX) field campaign (A. Ack-
 233 erman et al., 2000). Those adjustments stem from changes in the distribution of atmospheric
 234 radiative fluxes and heating rates induced by the aerosols, especially light-absorbing aerosols,
 235 which then modify surface radiative and heat fluxes, temperature and water vapor pro-
 236 files, atmospheric stability, and the conditions for cloud formation (Stjern et al., 2017).
 237 Correlations between satellite retrievals of aerosol, clouds, and planetary albedo consis-
 238 tent with the expected signature of semi-direct effects have been reported, e.g., over the
 239 subtropical South Atlantic Ocean (Wilcox, 2012) and North Atlantic marine stratocu-
 240 mulus decks (Amiri-Farahani et al., 2017).

241 [INSERT FOLLOWING AS A BOX TITLED “Impact of absorption on aerosol-radiation
 242 interactions”]

243 Aerosol particles scatter and absorb solar (also called shortwave) and terrestrial
 244 (or longwave) radiation, hereafter denoted aerosol-radiation interaction (ari). The effi-
 245 ciency at which they do so depends on the wavelength of the radiation, the distribution
 246 of particle sizes, their shapes, and on their refractive index, which is determined by their
 247 chemical composition and mixing state (J. E. Hansen & Travis, 1974). For each parti-
 248 cle, both scattering and absorption contribute to the extinction of radiation, and the single-
 249 scattering albedo (SSA), denoted ϖ_0 , quantifies the contribution of scattering to total
 250 extinction:

$$251 \quad \varpi_0 = \frac{\sigma_{\text{sca}}}{\sigma_{\text{sca}} + \sigma_{\text{abs}}} \quad (2)$$

252 where σ_{sca} and σ_{abs} are the scattering and absorption cross sections, respectively, in units
 253 of area. This key quantity can be likewise defined for a population of aerosol particles.

254 Locally and seen from the top of the atmosphere, aerosol particles can both increase
 255 or decrease the amount of radiation reflected to space, depending on the contrast between
 256 the brightness of the aerosols and that of the underlying surface. Bright (scattering) aerosols
 257 increase the local albedo when over dark surfaces but have less of an impact when over
 258 brighter surfaces. Conversely, dark (absorbing) aerosols decrease the albedo over bright
 259 surfaces but have less of an impact over darker surfaces. This effect is clearly demon-
 260 strated by the satellite image shown in Figure 3 showing biomass burning aerosol over
 261 the Iberian Peninsula. The absorbing smoke plume brightens the image when located
 262 over dark land and ocean surfaces, but darkens it when overlying the bright cloud to the
 263 northwest.

264 [INSERT FIGURE 3 HERE]

265 Mathematically, that change in sign of the aerosol-radiation interactions means that
 266 there exists a SSA, named critical SSA (Chýlek & Coakley, 1974) and denoted ϖ_0^{crit} , where
 267 aerosols have the same brightness as the underlying surface, thus exert no radiative per-
 268 turbation in spite of interacting with radiation. J. M. Haywood and Shine (1995) have
 269 expressed ϖ_0^{crit} as a function of the surface albedo, α_s , and the mean fraction of radi-
 270 ation up-scattered to space by the aerosols, β , as:

$$271 \quad \varpi_0^{\text{crit}} = \frac{2 \alpha_s}{\beta(1 - \alpha_s)^2 + 2 \alpha_s} \quad (3)$$

272 Quantities in this equation are integrated and weighted over the solar spectrum. (Stephens
 273 et al., 2015) In practice, the critical single-scattering albedo ranges from 0.7 and 0.8 over
 274 land surfaces (e.g., Gonzi et al., 2007) and is up to 0.9 over clouds (Costantino, 2012).
 275 Most aerosols from natural and human sources have a SSA larger than 0.9 and there-
 276 fore typically increase reflection of radiation to space, but aerosols from agricultural and
 277 forest fires are often more strongly absorbing, and decrease reflection of radiation when
 278 located above clouds (e.g. Leahy et al., 2007; Zuidema et al., 2016). The point where
 279 the radiative effect of aerosol-radiation interactions switches sign from negative to posi-
 280 tive has alternatively been characterised as a critical surface albedo (King et al., 1999)
 281 or a critical cloud fraction (Chand et al., 2009).

282 [END OF BOX]

283 Clouds affect aerosol populations. They act as a source of aerosol mass, because
 284 heterogeneous chemistry converts precursor gases into low- or non-volatile chemical com-
 285 ponents of aerosol, and as a sink of aerosols because precipitation is the main pathway
 286 for removing aerosols from the atmosphere. But aerosols also affect clouds.

287 Aerosol-cloud interactions are based, for liquid clouds, on the role aerosol particles
 288 play as cloud condensation nuclei (CCN), first identified by Aitken (1880) and then de-
 289 scribed thermodynamically by Köhler (1936). An anthropogenically driven increase in
 290 CCN concentrations therefore leads to more cloud droplets. Conover (1966), Hobbs et
 291 al. (1970) and Twomey (1974) presented observational evidence for increases in CCN re-
 292 sulting in increases in droplet number. More numerous droplets present an increased scat-
 293 tering cross-section leading to an increase of the albedo of the cloud when LWP is held
 294 constant. In radiative transfer the particle size is often measured by a droplet effective
 295 radius, r_e , rather than the droplet number concentration, N_d , so it is often stated that
 296 an increase in N_d , for a given cloud liquid water content, implies a decrease in r_e . This
 297 was the original formulation by Twomey (1977). Ship tracks, the quasi-linear features
 298 of enhanced cloud albedo along the track of ships (Conover, 1966), are commonly cited
 299 as evidence for that cloud brightening.

300 Ice clouds also contribute to aci. This is the case when ice crystals form via homo-
 301 geneous freezing of water droplets or aqueous aerosol particles, and because some aerosols
 302 serve as ice nucleating particles (INPs) (DeMott et al., 1997). Changes to liquid droplets
 303 may also have later implications for the ice phase in mixed-phase clouds (Norgren et al.,

2018; Coopman et al., 2018). Observations of higher concentrations of smaller ice crystals in cirrus clouds polluted by aircraft exhaust were first made by Ström and Ohlsson (1998) and Zhao et al. (2018) found similar correlations in satellite retrievals, although seasonal variations in water vapor overwhelm the aerosol signature. Vergara-Temprado, Miltenberger, et al. (2018) have shown by comparing a global model to satellite retrievals of radiative fluxes that INP concentrations can strongly alter the reflectivity of shallow mixed-phase clouds. However, evidence for a Twomey effect acting on ice clouds is far from being as strong as for liquid clouds.

The list of rapid adjustments associated with aci is long. Because of different processes, adjustments in liquid clouds, in mixed-phase and ice clouds are usually considered separately. But even among clouds of the same phase, differences in cloud dynamics or environmental conditions may influence the sign of the adjustment. Adjustments in liquid clouds have been hypothesized through aerosol increases driving delays in precipitation rates (Albrecht, 1989) and increases in cloud thickness (Pincus & Baker, 1994) that would manifest themselves as increases in cloud liquid water path (LWP) or changes in cloud fraction (CF). Altered droplet size distributions also affect entrainment-mixing of clouds with environmental air, possibly reducing LWP (A. S. Ackerman et al., 2004; Small et al., 2009). The latter adjustments might reduce the increase in cloud albedo (Stevens & Feingold, 2009). Adjustments in mixed-phase and ice clouds stem from different mechanisms. Responses of these clouds to aerosols include more frequent glaciation of supercooled water because of preferential freezing onto increased INP (Lohmann, 2002), de-activation of INP because of changes in aerosol mixing state (Girard et al., 2004; Hoose et al., 2008; Storelvmo et al., 2008), changes in precipitation and consequently cloud water path and cloud reflectivity (Vergara-Temprado, Miltenberger, et al., 2018), invigoration of convection from suppression of precipitation and latent heat release (Khain et al., 2001; Koren et al., 2005), and increase in lightning occurrence in deep convective clouds (Thornton et al., 2017).

Aerosols may also exert an RF after their removal from the atmosphere. Aerosol-surface interactions refer to changes in albedo from the deposition of absorbing aerosols on to bright – e.g., snow- and ice-covered – surfaces. Initially hypothesized by Bloch (1965) to explain past changes in sea level, the impact of aerosols on snow albedo was quantified by Warren and Wiscombe (1980), who showed that including in-snow aerosol absorption in a radiative transfer model better fits albedo measurements made in the Arctic and Antarctica. Rapid adjustments to aerosol-surface interactions involve changes in snow grain size and the timing of melting of the snow pack (Flanner et al., 2007). Since such effects are relevant only in confined regions, they are not assessed in detail in this review.

Compared to greenhouse gases, aerosols exhibit much more variable chemical compositions and much shorter atmospheric residence times, but much greater forcing per unit mass from interaction with radiation. For ari, aerosol scattering and absorption cross sections depend on the wavelength of the radiation and the physical and chemical properties of the aerosol (see Box). The sign and strength of the RF due to ari, RF_{ari}, is modulated further by environmental factors, including incident radiation, relative humidity, and the albedo of the underlying ocean, land surface or cloud (See Figure 3). For aci, the ability of aerosol particles to serve as CCN or INPs depends on the number concentration, size distribution, solubility, shape and surface chemical properties of the particles. In addition, cloud type or cloud regime, i.e. discrimination between cumuliform and stratiform clouds, as well as clouds in different altitudes (WMO, 2017) is a strong determinant of the complex responses of cloud processes to an aerosol-driven increase in drop number, and those cloud processes may be more important and uncertain for aci than aerosol processes (Gettelman, 2015). Even if all of these issues could be addressed accurately, uncertainty would remain due to uncertainty in the reference state (Carslaw et al., 2013), increasingly so the further back in time one adopts a baseline.

357

2.2 Scope and definitions

358

359

360

361

362

363

364

365

366

367

368

The scope of this review is globally-averaged aerosol ERF because the concept of ERF is mostly relevant to the understanding of climate change in a global sense. Consequently, ERF from aerosol-surface interactions due to deposition of absorbing aerosols onto snow and ice is not considered here because it comes primarily from local areas within high latitude regions or high mountain ranges and does not contribute much to the globally-averaged ERF (Jiao et al., 2014). The strong regional variations in aerosol distributions and ERF may matter for determining impacts of aerosol ERF on several aspects of the Earth system (e.g. Bollasina et al., 2011; Chung & Soden, 2017; Kasoar et al., 2018), but those considerations are also not addressed in this review. Both RF and ERF are measured in W m^{-2} and cover both the solar (shortwave, SW) and terrestrial (longwave, LW) parts of the electromagnetic spectrum.

369

370

371

372

373

374

375

376

377

378

379

380

381

382

383

384

385

386

387

388

389

Although this review adopts the IPCC definitions of RF and ERF (Myhre, Shindell, et al., 2013), it differs from previous IPCC practices in two ways. First, the reference year is chosen to be 1850 instead of 1750. Although 1750 represents a preindustrial state when fossil-fuel combustion emissions were negligible, there is no evidence for 1750 being special from an aerosol point of view, as agricultural fires occurred well before that. In addition, 1850 matches the start of most surface temperature records and also the start of the historical climate simulations of the Coupled Model Intercomparison Project (CMIP; Eyring et al., 2016). This match is important because having coincidence in the starting year is beneficial to comparing the change in forcing with the change in temperature. The difference in RF between the two reference years is smaller than 0.1 W m^{-2} (Myhre, Shindell, et al., 2013; Carslaw et al., 2017) because industrialization was still in its early stages in 1850. For present-day, Myhre, Shindell, et al. (2013) used 2011 but this review is slightly more generic so present-day refers here to average aerosol concentrations over the period 2005-2015. Second, this review will not attempt to bound aerosol RF mechanisms for which lines of evidence remain fragile, which increases the possibility that the bounds derived here are too conservative. Consequently, uncertainty ranges are given in this review as 16-84% confidence intervals (68% likelihood of being in the ranges given, equivalent to $\pm 1\text{-}\sigma$ for a normal distribution) instead of the 5-95% confidence interval (90% likelihood of being in the range) generally considered in IPCC Assessment Reports. The main uncertainty ranges are however translated to 5-95% confidence intervals in Section 11 and Table 5 to make comparison easier.

390

391

392

393

394

395

396

To quantify the confidence intervals for RF and ERF, this review will need to combine the 16-84% confidence intervals obtained for different quantities. To do so, each 16-84% confidence interval is first expanded to a full interval (0-100% confidence) by assuming that probabilities are uniformly distributed within the interval, i.e. by extending the range by a factor 100/68. Full intervals are then sampled randomly 10 million times in a Monte-Carlo framework similar to that of Boucher and Haywood (2001). Finally, the resulting intervals are reported with 16-84% confidence.

397

3 Conceptual model and lines and evidence

398

3.1 Conceptual model

399

400

401

402

403

404

405

406

The net radiative flux, R , at the top of the atmosphere is the difference between the globally and annually averaged absorbed insolation (SW), $R_{\text{SW}}^{\downarrow} (1 - \alpha)$, and outgoing terrestrial (LW) irradiance, R_{LW}^{\uparrow} :

$$R = R_{\text{SW}}^{\downarrow} (1 - \alpha) - R_{\text{LW}}^{\uparrow} \approx 0 \quad (4)$$

where the near equality of the two denotes a state of stationarity. The albedo, α , the fraction of the insolation that is scattered back to space, depends on the properties of the atmosphere, the surface, and the angle of illumination. Aerosol perturbations primarily affect α , in which context their effect stems from changes in the column-integrated

407 extinction coefficient of the aerosol, called aerosol optical depth and denoted τ_a , and in
 408 cloud droplet number concentrations, N_d . τ_a is usually dominated by scattering, but some
 409 sub-components of the aerosol are also absorbing in the SW or LW parts of the electro-
 410 magnetic spectrum and contribute to the net irradiance absorbed by the atmosphere,
 411 R_{atm} . Similarly to extinction, aerosol absorption is usually quantified by the aerosol ab-
 412 sorption optical depth, τ_{abs} . N_d depends on another sub-component of the aerosol, namely
 413 the number of hygroscopic aerosol particles that serve as CCN. Anthropogenic aerosol,
 414 through its forcing and consequent rapid adjustments of clouds, as well as through its
 415 direct interaction with terrestrial radiation, may also contribute to changes in R_{LW}^\uparrow . Aerosol-
 416 induced changes in ice clouds may also influence R . Changes in surface properties are
 417 assumed small relative to the magnitude of the other components in the global annual
 418 mean.

419 Adopting this description leads to the expectation that a change in the amount or
 420 properties of aerosol influences the net irradiance, and thus exerts an RF, \mathcal{F} , as follows

$$421 \quad \mathcal{F} = \Delta R = \Delta\tau_a \frac{\partial R}{\partial \tau_a} + \Delta \ln N_d \left. \frac{\partial R}{\partial \ln N_d} \right|_{\mathcal{L}, \mathcal{C}} \quad (5)$$

422 where $\Delta\tau_a$ and $\Delta \ln N_d$ denote the perturbation in global aerosol optical depth and re-
 423 lative perturbation in cloud droplet number concentration, respectively, taken here as the
 424 difference between 1850 and an average year between 2005 and 2015, hereafter called for
 425 convenience “preindustrial” and “present-day”, respectively. \mathcal{L} denotes the cloud liquid
 426 water path and \mathcal{C} the cloud fraction, and the second partial derivative therefore excludes
 427 changes in those quantities, following Twomey (1974). Eq. 5 is valid for a given point in
 428 space and time. Perturbations in τ_a and N_d are not independent, but the two terms in
 429 Eq. 5 assume a decoupling between radiative changes originating in the clear part of the
 430 atmosphere from those originating in the cloudy part of the atmosphere. However it should
 431 be noted that this assumption is not equivalent to decoupling changes in clear-sky and
 432 cloudy-sky radiative fluxes.

433 Rapid adjustments are added to \mathcal{F} to obtain the ERF, \mathcal{E} . For ari, this consists of
 434 a term describing changes to R_{atm} driven by changes in τ_a . Changes in R_{atm} then im-
 435 pact R , including R_{LW}^\uparrow , and cloud amount. For aci, this modifies the sensitivity of R to
 436 changes in N_d to allow for changes in \mathcal{L} and \mathcal{C} , in cloud-top temperature and hence R_{LW}^\uparrow ,
 437 and in ice clouds. The inclusion of rapid adjustments is represented mathematically by
 438 moving from partial to total derivatives:

$$439 \quad \mathcal{E} = \Delta\tau_a \frac{\partial R}{\partial \tau_a} + \Delta\tau_a \frac{dR}{dR_{\text{atm}}} \frac{dR_{\text{atm}}}{d\tau_a} + \Delta \ln N_d \frac{dR}{d \ln N_d}. \quad (6)$$

440 The literature does not decompose rapid adjustments of τ_a or τ_{abs} on cloud prop-
 441 erties into adjustments of \mathcal{C} and \mathcal{L} separately (Koch & Del Genio, 2010; Bond et al., 2013),
 442 so these rapid adjustments are included in the overall sensitivity of R_{atm} to τ_a through
 443 the second term on the right-hand side of Eq. 6. In contrast, such decomposition is com-
 444 monly performed for aci (Sekiguchi et al., 2003; Quaas et al., 2008; Chen et al., 2014;
 445 Gryspeerdt, Goren, et al., 2019; Mülmenstädt et al., 2019). For a given point in space
 446 and time, the sensitivity of R to changes in N_d , $\frac{dR}{d \ln N_d}$, neglecting the changes in ice clouds
 447 and in cloud-top temperature, consists of the change in response solely due to changes
 448 in N_d with everything else constant – relevant for the radiative forcing due to aci, RFaci
 449 (Eq. 5) – and the radiative impact of the adjustments. The sensitivity is best expressed
 450 as logarithmic in N_d , because most cloud processes are sensitive to a relative, rather than
 451 absolute, change in N_d (Carslaw et al., 2013, see also Eq. 17). This approach is also sup-
 452 ported by satellite data analyses (e.g. Nakajima et al., 2001; Sekiguchi et al., 2003; Kauf-
 453 man & Koren, 2006). The total response of R to relative perturbations in N_d can there-
 454 fore be expanded as

$$455 \quad \frac{dR}{d \ln N_d} \approx \left. \frac{\partial R}{\partial \ln N_d} \right|_{\mathcal{L}, \mathcal{C}} + \frac{\partial R}{\partial \mathcal{C}} \frac{d\mathcal{C}}{d \ln N_d} + \frac{\partial R}{\partial \mathcal{L}} \frac{d\mathcal{L}}{d \ln N_d} = S_N + S_{\mathcal{C}, N} + S_{\mathcal{L}, N}. \quad (7)$$

456 The first and third terms are restricted to cloudy regions. The last step defines the de-
 457 notation of the three terms as radiative sensitivities, S_N , $S_{C,N}$, and $S_{\mathcal{L},N}$.

458 In some cases, usually under idealized conditions, the sensitivities expressed by the
 459 partial derivatives in Eq. (6) and (7) can be calculated theoretically, or inferred obser-
 460 vationally. For instance, under clear skies $\partial R/\partial\tau_a$ can be calculated locally and averaged
 461 over different scenes to get a global sensitivity of top-of-atmosphere net radiation to changes
 462 in τ_a . To relate this global sensitivity to the global, all-sky response requires also account-
 463 ing for situations where there is little sensitivity. For instance, over a sufficiently bright
 464 background, like a snow-covered surface or a cloud, increasing the clear-sky scattering
 465 will have no appreciable effect on α , irrespective of the magnitude of the aerosol pertur-
 466 bation. Likewise, over a dark surface increasing aerosol absorption has little effect on α
 467 (see Box).

468 This assessment targets the global, annual mean aerosol ERF so there is a need to
 469 integrate Eqs. 6 and 7, which are valid at a given location in space and time, globally and
 470 over periods of time long enough to eliminate variability from changes in the weather.
 471 In particular, the aci sensitivities defined in Eq. 7 require averaging globally over the dif-
 472 ferent cloud regimes that experience changes in N_d . Weighting factors are introduced
 473 to account for those spatial and temporal dependencies, following (Stevens, 2015). Al-
 474 though these weighting factors are related to cloud amount, clouds span a distribution
 475 of optical depths and their optical depth differently mediates the extent to which they
 476 mask ari or express aci. So the weighting factors are effective cloud fractions, denoted
 477 c , and the effective clear-sky fraction need not be the complement of the effective cloudy-
 478 sky fraction. The introduction of the weighting factors allows for an attractive frame-
 479 work to quantify the aerosol RFs and their uncertainties, at the expense of having to quan-
 480 tify the uncertainties of the weighting factors themselves. These uncertainties may be
 481 larger than the uncertainty on CF but arguments can be made to estimate them.

482 Effective cloud fractions c_τ , c_N , c_C , and $c_{\mathcal{L}}$ are therefore introduced for each term
 483 in Eq. 8. They are formally defined, and quantified from the literature, in sections
 484 5, 6, and 8, respectively. Consequently, the individual terms in Eqs. 6 and 7 are param-
 485 eterized as a product of the change in the global aerosol or cloud state, idealized sensi-
 486 tivities (S) and those weighting factors (c). Applying this approach to Eqs. 6 and 7 yields
 487 the following formula for globally-averaged ERF over the SW and LW spectra:

$$\mathcal{E} = \Delta\tau_a \left[S_\tau^{\text{clear}} (1 - c_\tau) + S_\tau^{\text{cloudy}} c_\tau + \frac{dR}{dR_{\text{atm}}} \frac{dR_{\text{atm}}}{d\tau_a} \right] + \Delta \ln N_d [S_N c_N + S_{C,N} c_C + S_{\mathcal{L},N} c_{\mathcal{L}}] \quad (8)$$

488 The term representing \mathcal{F}_{ari} has been decomposed into cloud-free and cloudy contribu-
 489 tions to properly account for the masking or enhancement of ari by clouds, as discussed
 490 above. The sensitivity S_τ^{clear} is defined as $\frac{\partial R_{\text{clear}}}{\partial \tau_a}$. Similarly, S_τ^{cloudy} is defined as $\frac{\partial R_{\text{cloudy}}}{\partial \tau_a}$.
 491 Sensitivities that are a product of two partial derivatives, as defined by Eq. 7, are de-
 492 noted by a double subscript. For reference, Table 2 summarises the definitions of the vari-
 493 ables used in Eq. 8.
 494

495 An important and long standing objection to the approach embodied by Eq. 8 is
 496 that because aerosol perturbations are large and local, their effects are non-linear, and
 497 cannot be related to perturbations of the global aerosol state. However, such effects can
 498 be incorporated into the weighting factors. For instance, when applying the interpretive
 499 framework of Eq. 8 to the output from models that spatially and temporally resolve ari,
 500 it becomes possible to assess the extent to which differences arise from differences in how
 501 they represent the intrinsic sensitivity, S_τ , the magnitude of the perturbation, $\Delta\tau_a$, or
 502 the way in which local effects are scaled up globally, as measured by c_τ . To the extent
 503 that non-linearities are important – and often for global averages of very non-linear lo-
 504 cal processes they are not – it means that the weighting factors, c , may be situation-dependent,
 505 and their interpretation may be non-trivial.

506 The ari term of Eq. 8 has been assumed linear in $\Delta\tau_a$. This assumption is justi-
 507 fied by a series of arguments that starts at the source of the aerosol. For primary aerosols,
 508 aerosol number concentrations are linear in the emission rate. For secondary aerosols,
 509 linear relationships between emissions of gaseous precursor and RFari have been found
 510 at the global scale, including for precursors like dimethyl-sulfide (Rap et al., 2013). The
 511 aerosol population undergoes fast microphysical aging processes right after emission or
 512 nucleation (Jacobson & Seinfeld, 2004), changing its size, composition and mixing state.
 513 These microphysical processes grow anthropogenic nano-particles into sizes comparable
 514 to the wavelength of the radiation, where aerosols interact efficiently with radiation. Pre-
 515 existing aerosol particles act both as condensational sinks of gas-phase precursors and
 516 as seeds to efficiently grow semi-volatile aerosol precursors to ari-relevant sizes. The over-
 517 all scaling of secondary aerosol number concentrations from nucleation therefore depends
 518 on relative emission rates of primary and secondary aerosol precursors. Estimates from
 519 global microphysical aerosol models that include aerosol nucleation, condensation and
 520 coagulation confirm non-linear responses to the co-emission of primary carbonaceous aerosols
 521 and sulfur dioxide (SO₂, a precursor to sulfate aerosols), in particular near aerosol source
 522 regions (Stier et al., 2006). However, these deviations do not exceed 30% locally for ac-
 523 cumulation mode number concentrations and 15% for τ_a , sufficiently small to be assumed
 524 linear in the global mean context of this review. Further, ari scales fairly linearly with
 525 $\Delta\tau_a$ for a given single scattering albedo (SSA) (Boucher et al., 1998). The SSA of the
 526 aerosol population, which moderates the top-of-atmosphere ERF (see box), depends on
 527 the composition of aerosol sources, specifically the fraction of anthropogenic absorbing
 528 aerosols and notably black carbon (BC; also called soot (Bond et al., 2013)) aerosols. These
 529 factors affect the clear-sky albedo sensitivity S_τ and the atmospheric absorption efficiency
 530 $dR_{\text{atm}}/d\tau_a$.

531 Finally, Eq. 8 may require an additional term to represent changes in ice cloud prop-
 532 erties in response to changes in ice crystal number, but scientific understanding is not
 533 there yet to support a quantitative assessment of that term, as discussed in Section 9.

534 3.2 Lines of evidence

535 From a historical point of view, process-oriented studies at the relevant aerosol and
 536 cloud scales are the foundation of the conceptual thinking of aerosol RF. Observational
 537 and modeling tools have led to investigations that have helped refine process understand-
 538 ing and generate further lines of investigation with increasingly sharp tools.

539 For the purpose of this review, lines of evidence are grouped into three categories:
 540 estimation of sensitivities of radiation and clouds to aerosol changes; estimation of large-
 541 scale changes in the aerosol and cloud states over the industrial era; and inferences from
 542 observed changes in the overall Earth system.

543 3.2.1 Estimation of sensitivities

544 There are several methods with the potential to estimate sensitivities of radiation
 545 and clouds to aerosol changes:

- 546 • In situ observations using ground-based and airborne instruments;
- 547 • Remote sensing observations from ground-based networks, airborne and satellite
548 platforms;
- 549 • Process-based modeling at small scales using cloud-resolving models or large eddy
550 models.

551 Airborne measurements that combine cloud droplet size, droplet number, liquid wa-
 552 ter and cloud-reflected radiance (Brennguier et al., 2003; Werner et al., 2014) and high-
 553 quality ground-based measurements, for example from supersites, have provided strong,

554 quantitative evidence for aerosol effects on cloud microphysics (Twomey & Warner, 1967;
 555 Feingold et al., 2003; Garrett et al., 2003; Kim et al., 2003; Brenguier et al., 2003). How-
 556 ever, translating those effects to the radiative response and deriving sensitivities remains
 557 a challenge. For example, negative correlations between droplet size and aerosol concen-
 558 tration support the underlying theory proposed by Twomey (1977) but confound droplet
 559 size responses to aerosol with cloud water responses to the aerosol and its associated me-
 560 teorology (e.g. Brenguier et al., 2003) and thus make it difficult to unravel the net ra-
 561 diative response. Quantification of sensitivities has proven to be contingent on a vari-
 562 ety of factors, including choice of instrument, retrieval accuracy (Sena et al., 2016), ag-
 563 gregation scale (McComiskey & Feingold, 2012), and cloud regime. Drizzle is also a con-
 564 founding factor that obscures the relationships, reducing droplet number and increas-
 565 ing droplet size, as well as removing the aerosol (e.g. Feingold et al., 1996; Wood et al.,
 566 2012). In addition, in situ observations have thus far covered only a limited number of
 567 locations on the globe for varying duration and have sampled only a limited number of
 568 cloud regimes. The extent to which present understanding and estimates of \mathcal{F}_{aci} would
 569 be changed by future measurements is not known.

570 Satellite instruments provide the coverage in space and time necessary to evalu-
 571 ate sensitivities on the global scale. Aerosols and clouds are usually not retrieved in the
 572 same pixels, and there is some fuzziness in the distinction between thick haze and thin
 573 clouds. Satellite data are best used in conjunction with process understanding to factor
 574 out co-variabilities for which a causal influence by the aerosols may be difficult to
 575 ascertain. For example, aerosol and N_d may be simultaneously low simply because of
 576 precipitation, leading to aerosol removal, rather than because of aci affecting droplets.
 577 Relationships have been found between τ_a in cloud-free air and a variety of properties
 578 of nearby clouds: cloud droplet size (Nakajima et al., 2001; Sekiguchi et al., 2003), cloud
 579 fraction (Kaufman et al., 2005), cloud top pressure (Koren et al., 2005), shortwave ra-
 580 diative fluxes (N. G. Loeb & Schuster, 2008; Oreopoulos et al., 2016), precipitation (Lebsock
 581 et al., 2008) and lightning (Yuan, Remer, Pickering, & Yu, 2011). However, translating
 582 those relationships to physically meaningful sensitivities is difficult because variations
 583 in meteorological factors, such as humidity or atmospheric stability, affect both aerosol
 584 and cloud properties, generating correlations between them which are not necessarily causal
 585 in nature (Mauger & Norris, 2007; Boucher & Quaas, 2013). Constructs such as the albedo
 586 susceptibility (Platnick & Twomey, 1994) or precipitation susceptibility (Sorooshian et
 587 al., 2009) are useful in that they survey globally the regions of the Earth that have the
 588 potential to generate large responses to aerosol perturbations while controlling for key
 589 meteorologically driven variables. Progress in accounting for spurious correlations (i.e.
 590 correlations that do not imply a causal aerosol effect on the respective cloud property)
 591 has been made using statistical techniques (Gryspeerd et al., 2016), careful sampling
 592 (Christensen et al., 2017) and through combination with reanalysis data (Koren, Fein-
 593 gold, & Remer, 2010; McCoy, Bender, et al., 2018).

594 In addition to cloud albedo and cloud amount responses, fine-scale models have high-
 595 lighted other more nuanced, and potentially important aci processes like evaporative-
 596 entrainment feedbacks (S. Wang et al., 2003; A. S. Ackerman et al., 2004; Hill et al., 2009;
 597 Xue & Feingold, 2006), sedimentation-entrainment feedbacks (Bretherton et al., 2007),
 598 and boundary-layer decoupling (Sandu et al., 2008). The consequences for the ERF are
 599 complex. In some conditions, the aerosol-cloud system is resilient to perturbation (“buffered”)
 600 as a result of adjustments to the amount of cloud water (Stevens & Feingold, 2009) and
 601 sensitivities are small. In contrast, aerosol-mediated transitions between closed cellular
 602 convection and open cellular convection (Goren & Rosenfeld, 2012) are associated with
 603 large sensitivities, but as those transitions are likely contingent on meteorological state
 604 (Feingold et al., 2015), their global significance is not yet known.

605 **3.2.2 Estimation of large-scale changes**

606 Because unperturbed preindustrial aerosol and cloud distributions have not been
 607 observed, evaluation of $\Delta\tau_a$ and $\Delta\ln N_d$ requires large-scale modeling based on phys-
 608 ical parameterizations of key processes. Large-scale models, which are designed around
 609 the idea of integrating the essential processes of ari and aci at the global scale, could in
 610 principle be a useful tool to quantify aerosol ERF. This is in part because they are in-
 611 tended to physically account for energy exchanges through the Earth system and suited
 612 to analyzing the energy budget of the Earth, but also because they are built to trans-
 613 late hypotheses on preindustrial emissions into estimates of preindustrial aerosol and cloud
 614 distributions. But especially for aci, the more nuanced cloud responses to drop number
 615 perturbations described above are driven by processes that act at scales much smaller
 616 than General Circulation Model (GCM) resolutions. Consequently, they can be repre-
 617 sented in GCMs only by empirical, and thus inherently uncertain, parameterizations, and
 618 so their global applicability and importance are uncertain. GCMs therefore carry the un-
 619 certainties in forcing associated with less than ideal representation of aerosol and cloud
 620 processes. An important risk is therefore over-interpretation of model sensitivities to well-
 621 studied processes while neglecting other important processes that are poorly represented
 622 because they act at scales smaller than those resolved by large-scale models (Mülmenstädt
 623 & Feingold, 2018).

624 Nonetheless, when used correctly, large-scale models help constrain significant parts
 625 of the ari and aci problem, and are powerful tools for hypothesis testing about the im-
 626 pact of particular processes. Because of the uncertainties discussed above, global climate
 627 models (GCMs) produce a range of possible RFori (Myhre, Samset, et al., 2013) and ER-
 628 Faci (S. Ghan et al., 2016). Understanding the causes of differences among global mod-
 629 els has been one of the main objectives of the Aerosol Comparisons between Observa-
 630 tions and Models (AeroCom) initiative since its inception in 2003 (Textor et al., 2006;
 631 Schulz et al., 2006; Kinne et al., 2006). Diversity among models can result from struc-
 632 tural differences that arise from the use of different radiative transfer parameterizations,
 633 aerosol and cloud schemes, and surface albedo (Boucher et al., 1998; Halthore et al., 2005;
 634 J. E. Penner et al., 2009; Randles et al., 2013; Stier et al., 2013; S. Ghan et al., 2016; Fiedler
 635 et al., 2019). Diversity can result also from parametric differences, which arise from the
 636 imperfect knowledge of the parameters used in physical parameterizations as well as in
 637 boundary conditions like aerosol emissions. Parametric uncertainty can be quantified us-
 638 ing Perturbed Parameter Ensembles (PPEs) (L. A. Lee et al., 2011; Carslaw et al., 2013;
 639 Regayre et al., 2018). PPEs involve randomly perturbing model parameters within expert-
 640 elicited ranges to generate an ensemble that unfolds most of the uncertainty associated
 641 with the tuning-process of the original model. A PPE applied on the Hadley Centre cli-
 642 mate model by considering uncertainties in both the aerosol representation and the host
 643 physical climate model, found a 95% confidence interval for the parametric uncertainty,
 644 constrained by top-of-atmosphere radiative budget observations, of -2.3 to -0.6 W m^{-2}
 645 for aerosol ERF. This interval is shifted to more negative values compared to the expert
 646 judgment, guided by various observational and modelling considerations, of Boucher et
 647 al. (2013).

648 **3.2.3 Integral energy-balance inferences**

649 This distinct line of evidence, also called top-down approaches, builds inferences
 650 on radiative forcing and climate feedback and response (Eq. 1) based on the time evo-
 651 lution of, for example, surface temperature and surface radiative fluxes. An example of
 652 such a top-down inference is asserting that temperature changes and net forcing must
 653 have a common sign, so aerosol ERF must be less negative than total non-aerosol ERF.
 654 Those inferences are often interpreted with energy-balance models. This particular line
 655 of evidence is discussed in section 10.

4 Preindustrial to present-day change in aerosol optical depth

While present-day aerosol properties such as the aerosol optical depth (AOD), τ_a^{PD} , considered here at a wavelength of $0.55 \mu\text{m}$, can be measured directly by ground-based sun-photometers at certain locations or retrieved from satellite observations, the preindustrial (defined here as 1850) value, τ_a^{PI} , is not observable so $\Delta\tau_a = \tau_a^{\text{PD}} - \tau_a^{\text{PI}}$ can only be estimated.

Direct measurements of τ_a^{PD} come from the ground-based AErosol RObotic NETwork (AERONET) sun-photometer network (Holben et al., 1998; Smirnov et al., 2009), which provides near-global but sparsely sampled, cloud-free hourly τ_a^{PD} at accuracies better than 0.01 (Eck et al., 1999; Smirnov et al., 2000). With added information of their sky radiances samples, the AERONET sun-photometers also provide information on vertically integrated aerosol size and light absorption. However, continental and often near-urban locations lead to systematic biases (R. Wang et al., 2018). To supplement these measurements, long-term satellite remote sensing retrievals are also available, with more than 30 years of passive measurements, including almost two decades of Moderate Resolution Imaging Spectroradiometer (MODIS) aerosol retrievals; and more than a decade of active measurements using the Cloud-Aerosol Lidar with Orthogonal Polarization (CALIOP). Passive satellites retrieve an AOD from the measured radiance after carefully screening for clouds. Those AOD retrievals are based on radiative transfer calculations that take into account illumination and viewing geometry, extinction by Rayleigh scattering (with attendant assumption on aerosol height), surface reflectance, and aerosol properties (especially angular dependence of scattering and SSA). Levy et al. (2013) evaluate the uncertainty in global mean τ_a^{PD} from MODIS to about ± 0.03 , or 15 to 20%. Current satellite lidar retrieval of aerosol extinction requires the ratio of extinction to backscatter that depends on aerosol particle radius, sphericity, and SSA. An aerosol typing algorithm is used to choose from a set of default lidar ratio values, but this is a significant source of retrieval uncertainty. Globally-averaged clear-sky τ_a^{PD} at $0.55 \mu\text{m}$ from MODIS/Aqua Collection 6 is, at 0.17, about 30% larger than CALIOP Version 3 at about 0.12 (Winker et al., 2013). The true value is likely somewhere in between, because systematic errors in the MODIS retrieval, mostly driven by errors in surface albedo and cloud artifacts, tend to bias τ_a^{PD} high, whereas systematic CALIOP errors tend to bias τ_a^{PD} low (Kittaka et al., 2011). Watson-Parris et al. (submitted) obtained a range for τ_a^{PD} of 0.13 to 0.17 from 7 combinations of passive instruments and retrieval algorithms.

Most GCMs that simulate aerosol distributions routinely calculate τ_a for both present-day and preindustrial conditions. Figure 4 shows the relationship between $\Delta\tau_a$ and τ_a^{PD} in all of the CMIP5 (Taylor et al., 2012) models which participated in the sstClimAerosol experiment, the AeroCom Phase II (Myhre, Samset, et al., 2013) models and the density of 1 million emulated simulations of a PPE using the HadGEM3-UKCA model to sample uncertainties in 26 physical parameters relating to aerosol processes as well as present-day and preindustrial emissions (Watson-Parris et al., submitted; Yoshioka et al., 2019). While there is a large spread in the τ_a^{PD} (shown in the uppermost panel) in the unconstrained PPE, both multi-model ensembles (MMEs) peak between the lower and upper observational estimates. The MMEs simulate a relationship between τ_a^{PD} and $\Delta\tau_a$, which one would expect on physical grounds from a residence time argument, allowing the observational constraints on τ_a^{PD} of 0.13 to 0.17 to be translated into a range for $\Delta\tau_a$ of 0.03 to 0.04. Sampling only those PPE members which fall within the observational bounds, leads to a constraint on $\Delta\tau_a$ of 0.03 to 0.05. However, one needs to account for the high bias in the default τ_a^{PD} simulated by the PPE, and a possible high bias in observational estimates, so a range of 0.02 to 0.04 represents a more conservative assessment. By determining the anthropogenic contribution to τ_a^{PD} in the Monitoring Atmospheric Composition and Climate (MACC) Reanalysis (Benedetti et al., 2009), Bellouin, Quaas, et al. (2013) determine $\Delta\tau_a$ as 0.06. The Max Planck Institute Aerosol Climatology (MAC) (Kinne et al., 2013; Kinne, 2019) combines AERONET climatologies with

709 aerosol properties from AeroCom models (Kinne et al., 2006). They report $\Delta\tau_a$ as 0.03,
 710 which is within the range of the GCM estimates. It should, however, be noted that these
 711 estimates rely on the same industrial-era emissions datasets used in many of the GCM
 712 simulations. The larger spread in $\Delta\tau_a$ in the PPE is likely due to the fact that it sam-
 713 ples uncertainties in these emissions.

714 [INSERT FIGURE 4 HERE]

715 Relying on large-scale models to estimate $\Delta\tau_a$ implies that all preindustrial and
 716 present-day sources and sinks of anthropogenic aerosols are represented in these mod-
 717 els. There are several reasons that suggest that this is not the case. Potential underes-
 718 timates of $\Delta\tau_a$ come from many GCMs neglecting nitrate aerosols (Myhre, Samset, et
 719 al., 2013), which are partly anthropogenic, and having difficulties representing anthro-
 720 pogenic contributions to mineral dust aerosols (Evan et al., 2014). Potential overestimates
 721 of $\Delta\tau_a$ come from ignoring the possibility that preindustrial fires emitted carbonaceous
 722 aerosols at rates similar to present-day fires (Marlon et al., 2016). In addition, it remains
 723 unclear whether biogenic aerosols were more or less prevalent in the preindustrial atmo-
 724 sphere (Kirkby et al., 2016; Ding et al., 2008), and interactions between sulfate aerosol
 725 and organic aerosols of biogenic origin may be sizeable (Zhu et al., 2019).

726 Regarding mineral dust aerosols, their anthropogenic component is emitted directly
 727 by agriculture and indirectly by soils made more erodible and climate conditions made
 728 more erosive by human influence. Estimates of present-day anthropogenic dust fractions
 729 obtained by combining anthropogenic land-use data with mineral dust aerosol optical
 730 depth from satellite retrievals range from 8% in North Africa to about 75% in Australia
 731 (Ginoux et al., 2012) and China (X. Wang et al., 2018). On a global average, the present-
 732 day anthropogenic mineral dust fraction may be as large as 25% (Ginoux et al., 2010;
 733 Huang et al., 2015), translating to an increase in $\Delta\tau_a$ of about 0.007, or 15 to 30% of
 734 the range of 0.02 to 0.04 obtained above. However, uncertainties on these estimates are
 735 large. A few GCM studies yield a range of 10 to 60% for the global average in the an-
 736 thropogenic fraction of mineral dust for present-day (Mahowald & Luo, 2003; Tegen et
 737 al., 2004; Stanelle et al., 2014), although their simulated changes in anthropogenic min-
 738 eral dust aerosol disagree in both sign and magnitude (Webb & Pierre, 2018). This dis-
 739 agreement is at least in part caused by differences in simulated meteorological processes
 740 (Fiedler et al., 2016). There are uncertainties on mineral dust distributions in 1850 as
 741 well, which depend on how vegetation responds to climate changes (Mahowald, 2007).
 742 Considered together the contribution of anthropogenic mineral dust aerosols to ERF_{air}
 743 is expected to be smaller than for other anthropogenic aerosols, on the order of $-0.1 \pm$
 744 0.2 W m^{-2} (Boucher et al., 2013), owing to compensating contributions of SW scatter-
 745 ing and LW absorption. Indeed, Kok et al. (2018) showed that most models underesti-
 746 mate the size of mineral dust aerosols so the compensation between mineral dust SW
 747 and LW radiative effects may in fact be stronger than modelled. However, mineral dust
 748 aerosols are efficient ice nucleating particles (INPs) so anthropogenic mineral dust aerosol
 749 potentially alters the radiative properties and life cycle of ice clouds (Gettelman et al.,
 750 2012; Kuebbeler et al., 2014; J. E. Penner et al., 2018).

751 Regarding carbonaceous aerosols, emission inventories used by GCMs usually scale
 752 fire emissions back to preindustrial levels using historical population changes (e.g. Lamar-
 753 que et al., 2010), so obtain an increase through the industrial era. Paleoclimate records
 754 paint a more complex picture where preindustrial conditions might be more polluted,
 755 leading to a smaller $\Delta\tau_a$. The synthesis of sedimentary charcoal records by Marlon et
 756 al. (2016) suggests a sharp increase in biomass burning from 1800 to 1850, a period of
 757 high level of biomass burning from 1850 to 1970, a trough around the year 2000, followed
 758 by an abrupt increase up to 2010, although data density is highest in North America and
 759 Europe, so those trends may not be globally representative. Still, according to Marlon
 760 et al. (2016) present-day (2010) biomass burning appears larger, on a global scale and
 761 for the northern and southern hemispheres individually, than preindustrial if the prein-

dustrial reference year is set at 1750. But choosing a reference year of 1850 means that biomass burning levels were similar to present-day. In contrast, van Marle et al. (2017) derive, by merging the satellite record with several existing proxies, including the charcoal records, similar biomass-burning emissions between 1750 and 1850, and in their reconstruction, global biomass burning emissions increased only slightly over the full time period and peaked during the 1990s after which they decreased gradually. Hamilton et al. (2018) used significantly revised estimates of preindustrial fires in a single global model study and found an effect of only 10% on R_{Fari}. But the impact on CCN was larger, reducing the model’s R_{Faci} by 35 to 91% depending on the strength of preindustrial fire emissions.

In summary, a range of 0.02 to 0.04 for $\Delta\tau_a$ at 0.55 μm is supported by large-scale modeling and reanalyses. Combining the range for $\Delta\tau_a$ with the range of 0.13 to 0.17 for τ_a^{PD} yields a range of 0.14 to 0.29 for $\Delta\tau_a/\tau_a^{\text{PD}}$, meaning that human activities are likely to have increased globally-averaged τ_a by around 15 to 30% in 2005–2015 compared to the year 1850. The range for $\Delta\tau_a$ may be too narrow if a large contribution by anthropogenic mineral dust or nitrate aerosols has been overlooked by large-scale models, or too wide if the atmosphere in year 1850 was significantly more polluted by fire emissions than currently thought. Although those differences may not always affect globally-averaged ER_{Fari} on account of the absorbing properties of the aerosols involved, they could lead to sizable changes in ER_{Faci}.

5 Radiative forcing of aerosol-radiation interactions

As stated in Section 2.1, efficiency factors for scattering and absorption per unit AOD depend on a wide array of physical and chemical properties of the aerosols. In light of that complexity, the good agreement in clear-sky sensitivities $S_\tau^{\text{clear}} = \partial R_{\text{clear}}/\partial\tau_a$ among AeroCom models is remarkable, with Myhre, Samset, et al. (2013) reporting in their Table 3 a value of $-23.7 \pm 3.1 \text{ W m}^{-2} \tau_a^{-1}$ (neglecting an anomalous outlier because the causes for its very strong clear-sky R_{Fari} are not understood) or, if sensitivities are expressed in terms of planetary albedo, a range for S_τ^{clear} from 0.06 to 0.08 τ_a^{-1} . Clear-sky R_{Fari} against $\Delta\tau_a$ is shown in Fig. 5 for two multi-model ensembles and a large single-model PPE. While there is a large spread in the absolute values of R_{Fari}, particularly in the PPE which was designed to explore the full range of parametric uncertainty in HadGEM3 and is unconstrained by observations here, the slope, which is the sensitivity S_τ , is similar between the multi-model and perturbed parameter ensembles.

[INSERT FIGURE 5 HERE]

Uncertainties in the retrieval of τ_{abs} are much larger than for τ_a and contribute to the spread in S_τ^{clear} seen in Fig. 5. The absorption of seasalt and sulfate aerosols is well-constrained, but the absorption of mineral dust and carbonaceous aerosol is poorly characterized. Bond et al. (2013) noted that AeroCom models underestimate τ_{abs} compared to AERONET so they proposed increasing emissions of absorbing BC aerosols in response. They estimated that the present-day anthropogenic τ_{abs} from carbonaceous aerosols is about 0.007 at 0.55 μm . Bellouin, Quaas, et al. (2013) also used AERONET to prescribe aerosol absorption and reached a similar estimate based on a reanalysis of atmospheric composition. But more recent studies challenged the need for scaling of models and the suitability of AERONET constraints, instead improving modelled BC by increasing the model horizontal resolution (X. Wang et al., 2014), reducing BC lifetime (Samset et al., 2014) to reduce overestimations of BC concentrations in remote areas (Kipling et al., 2013), or accounting for AERONET τ_{abs} sampling errors (X. Wang et al., 2018) and possible high bias compared to in situ airborne absorption coefficients (E. Andrews et al., 2017). Compared to Kinne (2019), Bond et al. (2013) overestimated anthropogenic τ_{abs} because they underestimated the contribution of mineral dust aerosol to τ_{abs} and overestimated the anthropogenic fraction of BC aerosols. The revised calculation by Kinne (2019) there-

813 fore motivates a downward revision of τ_{abs} at $0.55 \mu\text{m}$, with a range of 0.0025 to 0.005.
 814 Rapid adjustments due to anthropogenic absorption are discussed in Section 7.

815 Extending S_{τ}^{clear} to all-sky conditions requires accounting for masking by clouds
 816 above aerosol but also aerosol absorption enhancement when clouds are below the aerosol
 817 (Fig 3). According to AeroCom models, those situations only contribute a small forcing
 818 on a global average, with a distribution centered around 0 W m^{-2} (Schulz et al., 2006).
 819 Studies based on CALIOP estimate a positive aerosol radiative effect above clouds (Oikawa
 820 et al., 2018; Chand et al., 2009; Kacenelenbogen et al., 2019), resulting from a partial
 821 compensation of a positive radiative effect by smoke aerosols with a negative radiative
 822 effect from mineral dust aerosols, although the anthropogenic fraction of those aerosols
 823 and the resulting cloudy-sky RFari is unknown. In addition, CALIOP underestimates
 824 aerosols at altitudes above 4 km (Watson-Parris et al., 2018). Although the regional cloudy-
 825 sky radiative effects of ari can be strongly positive (Keil & Haywood, 2003; de Graaf et
 826 al., 2014; Peers et al., 2015), a small globally-averaged cloudy-sky RFari is expected be-
 827 cause most of anthropogenic aerosols are located in the planetary boundary layer, where
 828 their RFari is masked by dense water clouds or partially masked by ice clouds. Indeed,
 829 GCMs tend to put too much aerosol mass aloft compared to CALIOP vertical aerosol
 830 extinction profiles (Koffi et al., 2016), so even the small cloudy-sky RFari reported by
 831 Schulz et al. (2006) may be an overestimate. Based on the results of Schulz et al. (2006),
 832 S_{τ}^{cloudy} may be as small as $\pm 0.02 \tau_{\text{a}}^{-1}$. That small efficiency coupled with the regional
 833 and seasonal nature of occurrences of anthropogenic aerosols above clouds suggest that
 834 all-sky S_{τ} is approximately equal to S_{τ}^{clear} weighted by an effective clear-sky fraction,
 835 and that cloudy-sky forcing only adds an uncertainty of $\pm 0.1 \text{ W m}^{-2}$ (Schulz et al., 2006).

836 This effective clear-sky fraction is the complement of the effective cloud fraction
 837 for ari, noted c_{τ} in equation 8. c_{τ} is the convolution of the cloud fraction \mathcal{C} and cloud
 838 optical depth, τ_{c} , to account for situations where clouds are too thin to completely mask
 839 the RFari of aerosols located below them, and $\Delta\tau_{\text{a}}$, to account for the different distri-
 840 butions of anthropogenic aerosols and low clouds. This gives

$$841 \quad c_{\tau} = \frac{\langle \tau_{\text{c}} \Delta\tau_{\text{a}} \mathcal{C} \rangle}{\langle \tau_{\text{c}} \Delta\tau_{\text{a}} \rangle} \quad (9)$$

842 where angle brackets denote global area-weighted temporal averaging. Stevens (2015)
 843 finds $c_{\tau} = 0.65$, which is close to the mean c_{τ} of 0.66 obtained by the 9 global aerosol-
 844 climate models that participated in H. Zhang et al. (2016) (Table 3). Those models give
 845 a standard deviation for c_{τ} of 0.06. Because large-scale models tend to have similar ge-
 846 ographical distributions of anthropogenic aerosols, differences primarily stems from dif-
 847 ferent liquid cloud climatologies in AeroCom models. GCMs are known to under-represent
 848 low-level cloudiness (Nam et al., 2012), so may underestimate c_{τ} by simulating the wrong
 849 spatial patterns of \mathcal{C} .

850 [INSERT TABLE 3 HERE]

851 In summary, the radiative forcing of ari, \mathcal{F}_{ari} , is computed as in Eq. 8, $\Delta\tau_{\text{a}} [S_{\tau}^{\text{clear}} (1 - c_{\tau}) + S_{\tau}^{\text{cloudy}} c_{\tau}]$
 852 where the last term represents the contribution of cloudy-sky ari. The ranges adopted
 853 for the terms of this equation are:

- 854 • 0.02 to 0.04 for $\Delta\tau_{\text{a}}$, as obtained by Section 4;
- 855 • -20 to $-27 \text{ W m}^{-2} \tau_{\text{a}}^{-1}$ for S_{τ}^{clear} , as simulated by AeroCom models used by Myhre,
 856 Samset, et al. (2013). S_{τ}^{clear} can also be expressed in terms of planetary albedo
 857 by dividing by the globally- and annually-averaged solar constant of 340 W m^{-2} :
 858 the range becomes 0.06 to $0.08 \tau_{\text{a}}^{-1}$;
- 859 • 0.59 to 0.71 for c_{τ} , as simulated by AeroCom models used by H. Zhang et al. (2016)
 860 (Table 3);
- 861 • $0.0 \pm 0.1 \text{ W m}^{-2}$ for the product $S_{\tau}^{\text{cloudy}} c_{\tau}$, as simulated by AeroCom models (Schulz
 862 et al., 2006).

863 Using the method described in section 2.2 to combine those ranges and compute the first
 864 term of Eq. 8 yields a range for \mathcal{F}_{ari} of -0.37 to -0.12 W m^{-2} . The rapid adjustments
 865 due to anthropogenic absorption are discussed separately in section 7.

866 6 Radiative forcing of aerosol-cloud interactions in liquid clouds

867 Since liquid clouds and ice clouds behave differently in several aspects, it is use-
 868 ful to distinguish between the two. Clouds with a cloud-top temperature warmer than
 869 0°C are liquid. Clouds colder than this behave in the same way in terms of the mech-
 870 anisms that determine R \mathcal{F}_{aci} if they consist of supercooled liquid water but behave dif-
 871 ferently when ice becomes present. The three key bulk quantities that describe the prop-
 872 erties of a liquid cloud are their liquid water path, \mathcal{L} , their cloud fraction, \mathcal{C} , and their
 873 droplet number concentration, N_{d} .

874 Cloud droplets are formed via adiabatic cooling of air parcels by updrafts that gen-
 875 erate supersaturation, and each droplet forms on an aerosol particle that serves as a CCN
 876 at the supersaturation determined by the cooling rate. Which aerosols are activated into
 877 cloud droplets depends on the size of the particles and their hygroscopicity (Köhler, 1936),
 878 as well as on the maximum supersaturation that is reached given the balance between
 879 adiabatic cooling due to the updraft that increases supersaturation, and condensation
 880 of vapor onto the droplets that reduces it (Twomey, 1959). In consequence, additional
 881 aerosol leads to further cloud droplets if they are large enough compared to the pre-existing
 882 aerosol population. On average, at the scale of an air parcel, an approximately logarith-
 883 mic scaling between aerosol concentration and N_{d} is obtained (Twomey, 1959). At the
 884 cloud scale, it is therefore sufficient to know the aerosol size distribution and hygroscop-
 885 icity, as well as the updraft distribution, to predict N_{d} as well as its sensitivity to the
 886 aerosol. A relative change of N_{d} in response to an aerosol, a , perturbation is thus

$$887 \beta_{\ln N_{\text{d}} - \ln a} = \frac{\partial \ln N_{\text{d}}}{\partial \ln a} \quad (10)$$

888 The aerosol metric a is left ambiguous here, since in different observations-based stud-
 889 ies, different choices are made. The optimal definition would be the CCN concentration
 890 at cloud base, but for many observations (e.g. remote sensing), this quantity is not ac-
 891 cessible. The sensitivity $\beta_{\ln N_{\text{d}} - \ln a}$ is often evaluated using linear regressions, with var-
 892 ious choices for the aerosol metric a (Feingold et al., 2003; McComiskey et al., 2009). For
 893 large updrafts and suitable aerosol, at relatively low background aerosol concentration,
 894 such as found for remote marine trade-wind cumulus, a sensitivity approximately equal
 895 to unity is observed with CCN as aerosol metric (Martin et al., 1994; Twohy et al., 2005;
 896 Werner et al., 2014). For more general situations, including smaller updraft speeds, higher
 897 CCN concentrations, and broader aerosol size distributions, the scaling between aerosol
 898 concentration and N_{d} is substantially lower (e.g., Boucher & Lohmann, 1995; Lu et al.,
 899 2009). McFiggans et al. (2006) explore the sensitivity from parcel modelling to obtain
 900 values between 0.7 and 0.9. Surface remote sensing statistics yield a range of 0.3 to 0.5
 901 for a coastal site (McComiskey et al., 2009), mid-latitude continental sites (Kim et al.,
 902 2008; Schmidt et al., 2015) and the Arctic (Garrett et al., 2004). Values can be larger
 903 - up to 0.75 - when sampling updraft conditions only (Schmidt et al., 2015). Painemal
 904 and Zuidema (2013) obtain values as large as 0.8 to 0.9 when combining in-situ aerosol
 905 observations with aircraft remote sensing for N_{d} over the South-East Pacific Ocean.

906 A wide range of observational evidence from ship tracks, trends in anthropogenic
 907 emissions, and degassing volcanic eruptions (Gassó, 2008; Christensen & Stephens, 2011;
 908 Yuan, Remer, Pickering, & Yu, 2011; Christensen et al., 2014; McCoy & Hartmann, 2015;
 909 Malavelle et al., 2017; Toll et al., 2017; McCoy, Field, et al., 2018; Li et al., 2018) and
 910 numerous field studies in different regions (Boucher & Lohmann, 1995; Lowenthal et al.,
 911 2004; Rosenfeld et al., 2008; Werner et al., 2014) support the theoretical argument that
 912 the impact of additional aerosols in the atmosphere is to increase N_{d} , and decrease the

913 cloud effective radius as the liquid water is spread among a larger number of droplets
 914 (Twomey, 1977). But quantifying those relationships is difficult and depends on cloud
 915 regime.

916 For global coverage, the sensitivity of N_d to aerosol can only be assessed from satel-
 917 lite retrievals (e.g. Nakajima et al., 2001; Lohmann & Lesins, 2002; Sekiguchi et al., 2003;
 918 Quaas et al., 2006). However, such assessments suffer from a number of problems.

- 919 1. Aerosol- and cloud quantities usually cannot be retrieved in the same column. It
 920 is thus unclear to what extent the aerosol retrieved in clear-sky pixels is represen-
 921 tative of the aerosol relevant for cloud droplet formation (e.g., Gryspeerdt et al.,
 922 2015). Even if in general, the horizontal scale of variance of the aerosol is large
 923 compared to that of clouds (Anderson, Charlson, Winker, et al., 2003), this as-
 924 sumption may be weak in the proximity of precipitating clouds. In addition, sam-
 925 pling the aerosol radiative properties in close vicinity to clouds leads to errors (Christensen
 926 et al., 2017) due to the humidity-swelling of the aerosol (Quaas et al., 2010) and
 927 misclassification of cloud as aerosols (J. Zhang et al., 2005).
- 928 2. The most straightforward remote sensing aerosol retrieval is the AOD, τ_a . How-
 929 ever, τ_a does not scale very well with the relevant CCN concentration at cloud base,
 930 because it is a column-integrated quantity, is affected by humidity, and by aerosols
 931 that may not act as CCN (Stier, 2016). Errors in retrieved τ_a are also largest at
 932 small values where cloud sensitivity may be largest (Ma et al., 2018). The aerosol
 933 index, calculated by multiplying τ_a by a measure of aerosol size, is often suggested
 934 as an approximate solution to provide a possibly better indicator of CCN concen-
 935 trations (J. E. Penner et al., 2011; Stier, 2016; Gryspeerdt et al., 2017), but at low
 936 aerosol loadings uncertainties in aerosol index are even larger than for τ_a .
- 937 3. Cloud droplet number concentration is derived from retrievals in a very indirect
 938 way, which relies on cloud-top quantities and assumptions to extrapolate down to
 939 cloud base where Eq. 10 applies. Depending in particular on cloud heterogeneity
 940 and solar zenith angle, retrievals may be strongly biased (Grosvenor et al., 2018).
 941 The retrieved N_d does not directly correspond to the activated droplet concen-
 942 tration near cloud base, but is the result of both cloud microphysical processes and
 943 cloud entrainment-mixing processes. Aggregation to relatively coarse retrieval scales
 944 reduces the representativeness of the sensitivity of N_d to the aerosol because im-
 945 portant process-level scales are not captured (McComiskey & Feingold, 2012).

946 From satellite remote sensing, thus, the sensitivity of N_d to aerosol is often estimated
 947 by evaluating Eq. 10 using τ_a as the aerosol metric. Most of the caveats listed above, ex-
 948 cept for the increased τ_a when considering retrievals within approximately 15 km of nearby
 949 clouds (Christensen et al., 2017), lead to too weak sensitivities when retrieving the N_d
 950 – τ_a relationship. Making use of satellite-based statistics to quantify $\beta_{\ln N - \ln \tau_a}$ usually
 951 yield much smaller values than those derived from airborne measurements (Nakajima
 952 & Schulz, 2009; McComiskey & Feingold, 2012; Schmidt et al., 2015; McCoy et al., 2017).
 953 The full range for $\beta_{\ln N - \ln a}$, using different aerosol quantities for a , compiled by those
 954 studies spans 0.14 to 1.00. However, local sensitivities need to be weighted globally to
 955 be relevant for the large-scale forcing. The newest compilation of large-scale sensitivi-
 956 ties by McCoy et al. (2017) obtains (their Fig. 3) a range of 0.3 to 0.8. It is difficult to
 957 rigorously assign confidence intervals, in particular because the physically meaningful
 958 range is bounded. Nevertheless, if one considers the full range of 0.14 to 1.00 from the
 959 four studies cited above as the 90% confidence interval, one obtains a $\pm\sigma$ interval of 0.52,
 960 which matches the interval obtained by McCoy et al. (2017).

961 Combining the range of 0.3 to 0.8 for $\beta_{\ln N_d - \ln \tau_a}$ with the ranges of 0.02 to 0.04
 962 for $\Delta\tau_a$ and 0.12 to 0.16 for τ_a obtained in Section 4 yields a range of 0.06 to 0.18 for
 963 $\Delta \ln N_d$, encompassing the estimate of 0.15 obtained by Charlson et al. (1992) and Stevens
 964 (2015).

The dependency of cloud reflectance on the bulk cloud properties N_d and \mathcal{L} is based on their relationship with cloud optical depth, τ_c , assuming adiabatic clouds (e.g., Bren-
guier et al., 2000):

$$\tau_c \propto \mathcal{L}^{\frac{5}{6}} N_d^{\frac{1}{3}} \quad (11)$$

$$d \ln \tau_c = \frac{5}{6} d \ln \mathcal{L} + \frac{1}{3} d \ln N_d \quad (12)$$

Further, variations in cloud albedo, α_c , are related to variations in τ_c approximately as (A. Ackerman et al., 2000)

$$d\alpha_c = \alpha_c (1 - \alpha_c) d \ln \tau_c = \alpha_c (1 - \alpha_c) \left(\frac{5}{6} d \ln \mathcal{L} + \frac{1}{3} d \ln N_d \right) \quad (13)$$

If $d \ln \mathcal{L}$ is set to zero, the radiative forcing of the Twomey effect, \mathcal{F}_{aci} , is isolated. Ac-
cording to Eq. 8, \mathcal{F}_{aci} is also:

$$\mathcal{F}_{\text{aci}} = \Delta \ln N_d S_N c_N \quad (14)$$

The anthropogenic perturbation of droplet number concentration is estimated from the sensitivity of N to aerosol perturbations, and the relative perturbation in aerosol, $\Delta \ln N_d = \beta_{\ln N - \ln a} \Delta \ln a$. If τ_a is chosen to quantify the aerosol, $\Delta N_d = \beta_{\ln N - \ln a} \frac{\Delta \tau_a}{\tau_a}$, leading to the equation:

$$\mathcal{F}_{\text{aci}} = \beta_{\ln N - \ln a} \frac{\Delta \tau_a}{\tau_a} S_N c_N \quad (15)$$

For reference, Table 2 summarises the definitions of the variables used in Eq. 15.

Since the Twomey effect has little impact on R_{LW}^\uparrow , S_N can be redefined for convenience as the sensitivity of the planetary albedo with respect to N_d perturbations:

$$S_N = \frac{\partial \alpha}{\partial \ln N_d} \quad (16)$$

Inserting Eq. 13 into Eq. 16 yields (Twomey, 1977):

$$S_N = \frac{1}{3} \alpha_c (1 - \alpha_c) \quad (17)$$

The global mean cloud albedo is quantified from the CERES SSF1deg Ed4A (N. Loeb et al., 2016) at $\alpha_c = 0.38 \pm 0.02$, evaluated as the planetary albedo at $1^\circ \times 1^\circ$ grid boxes where the fractional coverage by liquid-water clouds is larger than 95%. Propagating the uncertainty in α_c to S_N using Eq. 17 yields a range for S_N , as defined by Eq. 16, of 0.077 to 0.080. In Eqs. 6 and 14, c_N is an effective cloud fraction. It is “effective” because it is not just the fractional coverage by liquid water clouds, \mathcal{C}_{liq} , as retrieved from satellite data, that would be the relevant quantity at a given location in space and time (e.g., Quaas et al., 2008). Instead it also takes into account the spatial co-variability of the other terms relevant to deriving $\mathcal{R}_{\text{FacI}}$. c_N is needed because Eq. 13 is a global-mean equation. In essence, c_N is the spatio-temporally resolved \mathcal{F}_{aci} , normalised by the global-temporal averages of the first four terms on the right-hand side of Eq. 13:

$$c_N = \frac{\left\langle \mathcal{C}_{\text{liq}} \alpha_c (1 - \alpha_c) \beta_{\ln N - \ln \tau_a} \frac{\Delta \tau_a}{\tau_a} R_{\text{SW}}^\downarrow \right\rangle}{\left\langle \alpha_c (1 - \alpha_c) \right\rangle \left\langle \beta_{\ln N - \ln \tau_a} \right\rangle \left\langle \frac{\Delta \tau_a}{\tau_a} \right\rangle \left\langle R_{\text{SW}}^\downarrow \right\rangle} \quad (18)$$

where angle brackets denote global-area weighted temporal averaging of 2-dimensional distributions. In other words, it is the fractional coverage of liquid clouds weighted by:

- the sensitivity of cloud albedo to perturbations in N_d , S_N ;
- the local sensitivity of N_d to perturbations in aerosol, $\beta_{\ln N_d - \ln \tau_a}$
- the occurrence of anthropogenic perturbations to the aerosol, $\frac{\Delta \tau_a}{\tau_a}$; and
- the incoming solar radiation.

1006 The range in $\beta_{\ln N_d - \ln \tau_a}$, 0.3 to 0.8, is taken from McCoy et al. (2017) and the range for
 1007 $\Delta\tau_a$ is that spanned by Bellouin, Quaas, et al. (2013) and Kinne (2019).

1008 The local sensitivity $\beta_{\ln N_d - \ln \tau_a}$ is calculated using MODIS collection 6 cloud droplet
 1009 number concentration, sampled following Grosvenor et al. (2018) and the MODIS AOD
 1010 (Levy et al., 2013). The $\Delta\tau_a/\tau_a$ used are from Bellouin, Quaas, et al. (2013). Although
 1011 the magnitude of $\beta_{\ln N_d - \ln \tau_a}$ calculated using this method is an underestimate (J. E. Pen-
 1012 ner et al., 2011), C_N only depends on its spatial pattern. To obtain an uncertainty range
 1013 in C_N , alternative spatial distributions for $\beta_{\ln N_d - \ln \tau_a}$ are taken from McCoy et al. (2017)
 1014 and for $\Delta\tau_a/\tau_a$ from Kinne (2019), yielding a range for C_N of 0.19 to 0.29. The value
 1015 of 0.4 used in Stevens (2015) is therefore outside the 68% confidence interval obtained
 1016 here. Fig. 6 illustrates the geographical distribution of c_N as defined in Eq. 18 but av-
 1017 eraging the numerator only in time, not in space. Compared to C_{liq} , the distribution of
 1018 c_N emphasises low maritime clouds, and especially stratocumulus decks, which are most
 1019 sensitive to aerosol perturbations (Alterskjær et al., 2012; Oreopoulos & Platnick, 2008).

1020 [INSERT FIGURE 6 HERE]

1021 In summary, calculating $\Delta \ln N_d$ as $\Delta\tau_a/\tau_a^{PD} \beta_{\ln N_d - \ln \tau_a}$, where $\beta_{\ln N_d - \ln \tau_a} = \partial \ln N_d / \partial \ln \tau_a$,
 1022 yields a range of 0.06 to 0.18, based on the ranges of:

- 1023 • 0.02 to 0.04 for $\Delta\tau_a$ and 0.12 to 0.16 for τ_a^{PD} , following Section 4;
- 1024 • 0.3 to 0.8 for $\beta_{\ln N_d - \ln \tau_a}$, following McCoy et al. (2017);

1025 Note that McCoy et al. (2017) infer the sensitivity from sulfate mass concentration rather
 1026 than AOD. Their sensitivity is therefore used here by assuming that the relative pertur-
 1027 bation in anthropogenic AOD is proportional to the perturbation in anthropogenic sul-
 1028 fate mass concentration.

1029 The range for $\Delta \ln N_d$ means that human activities are likely to have increased globally-
 1030 averaged cloud droplet number concentrations by 6 to 18% in 2005–2015 compared to
 1031 the year 1850. The radiative forcing of aci, \mathcal{F}_{aci} , is computed following Eq. 14. The ranges
 1032 adopted for the terms of this equation are:

- 1033 • 0.06 to 0.18 for $\Delta \ln N_d$, as above;
- 1034 • 0.077 to 0.080 for S_N , based on uncertainties in α_c from CERES. That range con-
 1035 verts to a range of -26 to -27 W m^{-2} in terms of top-of-atmosphere radiation:
 1036 the conversion is done by multiplying by the global, annual mean incoming solar
 1037 radiation of 340 W m^{-2} ;
- 1038 • the range of 0.19 to 0.29 for c_N .

1039 Using the method described in section 2.2 to combine those ranges and solve Eq. 15, the
 1040 range for \mathcal{F}_{aci} is -1.20 to -0.35 W m^{-2} . Rapid adjustments to aci are quantified sep-
 1041 arately in section 8.

1042 7 Rapid adjustments to aerosol-radiation interactions

1043 Both dR/dR_{atm} and $dR_{atm}/d\tau_a$ of Eq. 8 have been found to depend on the amount
 1044 and altitude of absorbing aerosols and the location of those aerosols relative to the clouds
 1045 by large-eddy simulations (B. T. Johnson et al., 2004), global modelling (J. E. Penner
 1046 et al., 2003; J. Hansen et al., 2005), and observations (Koren et al., 2004). These find-
 1047 ings were summarised into frameworks where the sign of the adjustments depends on the
 1048 cloud regime and whether aerosols are below, in, or above the clouds (Koch & Del Gen-
 1049 io, 2010; Bond et al., 2013), although only a handful of studies were available to illus-
 1050 trate each case. When absorbing aerosol lies within the boundary layer, the RF is pos-
 1051 itive while when it lies above the boundary layer it is negative. Assessments based on

1052 large-scale modeling, like Boucher et al. (2013), conclude that the rapid adjustments to
 1053 ari operating via changes in cloud properties exert a negative RF on a global average,
 1054 of the order of -0.1 W m^{-2} , suggesting a dominance of absorbing aerosol above clouds.
 1055 LES modeling of semi-direct effects suggests a positive RF from convective cloud sup-
 1056 pression when absorbing aerosol lies within the boundary layer (Feingold et al., 2005)
 1057 and positive again when absorbing aerosol lies above stratocumulus clouds (Yamaguchi
 1058 et al., 2015). The latter study showed a delay of the stratocumulus to cumulus transi-
 1059 tion, complementing observations by Adebiyi et al. (2015). That delay could be asso-
 1060 ciated with a locally large negative RF. But as discussed in Section 3.2.1, scaling those
 1061 results to a global radiative sensitivity is challenging.

1062 In contrast to RFari, a substantial fraction of the rapid adjustments happens in the
 1063 LW spectrum (J. E. Penner et al., 2003). The Precipitation Driver Response Model In-
 1064 tercomparison Project (PDRMIP) (Myhre et al., 2017) focused again on rapid adjust-
 1065 ments in clouds, but also on the contribution stemming from altered tropospheric tem-
 1066 perature and water vapor profiles. Smith et al. (2018) found that rapid adjustments as-
 1067 sociated with temperature changes in the troposphere and stratosphere and those due
 1068 to water vapor changes are comparable in magnitude to the rapid adjustments in clouds.
 1069 Again, most of the rapid adjustments occur in the LW spectrum. The PDRMIP results
 1070 indicate that the total rapid adjustment represents about half of the strength of the RFari
 1071 by BC aerosols. Scaling the PDRMIP results to current estimate of global anthropogenic
 1072 emission of BC (Hoesly et al., 2018) would give total rapid adjustment due to BC of about
 1073 -0.2 W m^{-2} . However, the PDRMIP results are based on global models that may over-
 1074 estimate the lifetime of BC aerosols and their concentrations aloft. A shorter BC life-
 1075 time, in better agreement with observations in the middle and upper troposphere, would
 1076 reduce the magnitude of the rapid adjustment but would also reduce the BC RFari (Hodnebrog
 1077 et al., 2014).

1078 PDRMIP models find a total rapid adjustment of -1.3 W m^{-2} for an instantaneous
 1079 change in atmospheric absorption of $+6.1 \text{ W m}^{-2}$ (Supplementary Tables 1 and 2 of Myhre
 1080 et al., 2018), leading to a mean $dR/dR_{\text{atm}} = -0.2$, with a standard deviation of 0.09.
 1081 The radiative forcing exerted within the atmosphere per unit anthropogenic τ_a is gen-
 1082 erally small, except over regions and during seasons where the amount of absorbing aerosol
 1083 is large. On a global, annual average basis, Bellouin, Quaas, et al. (2013) find $dR_{\text{atm}}/d\tau_a =$
 1084 $+41 \text{ W m}^{-2} \tau_a^{-1}$. This is at the higher end of the range obtained by AeroCom models,
 1085 which span $+13$ to $+47 \text{ W m}^{-2} \tau_a^{-1}$, with a median of $+26 \text{ W m}^{-2} \tau_a^{-1}$ and a standard
 1086 deviation of $9 \text{ W m}^{-2} \tau_a^{-1}$ (Myhre, Samset, et al., 2013).

1087 In summary, rapid adjustments of ari are computed using the second term of Eq. 8,
 1088 $\Delta\tau_a dR/dR_{\text{atm}} dR_{\text{atm}}/d\tau_a$. The ranges adopted for the terms of this equation are:

- 1089 • 0.02 to 0.04 for $\Delta\tau_a$, as obtained by Section 4;
- 1090 • -0.1 to -0.3 for dR/dR_{atm} based on PDRMIP simulations reported by Myhre
 1091 et al. (2018);
- 1092 • 17 to $35 \text{ W m}^{-2} \tau_a^{-1}$ for $dR_{\text{atm}}/d\tau_a$, based on AeroCom simulations reported by
 1093 Myhre, Samset, et al. (2013).

1094 Using the method described in section 2.2 to combine those ranges yields a range for the
 1095 rapid adjustments to ari of -0.05 to -0.25 W m^{-2} . The range for $\mathcal{E}\text{ari}$ is obtained by
 1096 adding, with the method described in section 2.2 again, the range for rapid adjustments
 1097 to the range of -0.12 to -0.37 W m^{-2} obtained for $\mathcal{F}\text{ari}$ in Section 5. Doing so yields
 1098 a range of -0.23 to -0.58 W m^{-2} for $\mathcal{E}\text{ari}$. Note that $\mathcal{F}\text{ari}$ and its rapid adjustments
 1099 are correlated, at least in the framework of Eq. 8, through $\Delta\tau_a$.

1100 8 Rapid adjustments to aerosol-cloud interactions

1101 The change in N_d due to aerosols that drives the Twomey effect may also impact
 1102 cloud droplet size and so modify cloud processes (Albrecht, 1989; A. S. Ackerman et al.,
 1103 2004). While the radiative forcing of the Twomey effect is formulated in terms of a con-
 1104 stant \mathcal{L} , a change to cloud processes may be able to modify \mathcal{L} and \mathcal{C} , possibly generat-
 1105 ing a significant radiative forcing (Albrecht, 1989; Pincus & Baker, 1994). This section
 1106 concentrates on liquid cloud adjustments. Similar rapid adjustments in response to aerosol
 1107 perturbations in mixed-phase and ice clouds may also produce a sizable radiative forc-
 1108 ing (Lohmann, 2002; Storelvmo et al., 2008; Lohmann, 2017; Storelvmo, 2017) but are
 1109 covered by Section 9 because different processes are involved and the level of scientific
 1110 inquiry is less advanced. The present section also considers constraints on rapid adjust-
 1111 ments in \mathcal{L} and \mathcal{C} separately, following Eq. 8. This separation allows a better compar-
 1112 ison with the observational studies that adopted an approach where a system-wide vari-
 1113 able, the cloud radiative effect, is used to compute ERF_{aci}. Those studies treat “intrinsic”
 1114 (changes in cloud albedo), and “extrinsic” (changes in \mathcal{C}) effects separately (e.g., Chen
 1115 et al., 2014). Doing so reduces the number of free parameters to just a few (e.g., \mathcal{C} , α_c ,
 1116 and τ_a) in which the observational uncertainties are better known than for N_d and \mathcal{L} .
 1117 It also has a closer correspondance to the internal structure of many GCMs, where \mathcal{L} and
 1118 \mathcal{C} are treated by different parametrisations, even though the liquid cloud adjustments
 1119 are usually parameterised through modification of the autoconversion rate (e.g. Khairout-
 1120 dinov & Kogan, 2000), which is the rate at which cloud water becomes rain water. The
 1121 intrinsic/extrinsic methodology closely agrees with earlier methods (e.g Quaas et al., 2008),
 1122 as shown by Amiri-Farahani et al. (2017) and Christensen et al. (2017).

1123 8.1 Adjustments in liquid water path \mathcal{L}

1124 The sensitivity of \mathcal{L} to N_d varies regionally (Han et al., 2002) and is expected to
 1125 depend on the relative magnitude of two key processes (Lohmann & Feichter, 2001). The
 1126 suppression of precipitation from a reduction in droplet size could increase \mathcal{L} (Albrecht,
 1127 1989), while radiation, evaporation, and sedimentation enhance cloud-top turbulence and
 1128 increase cloud top cooling, enhancing the entrainment of dry air, resulting in a reduc-
 1129 tion in \mathcal{L} in polluted regions (S. Wang et al., 2003; A. S. Ackerman et al., 2004; Brether-
 1130 ton et al., 2007). The overall sensitivity of \mathcal{L} to aerosol is strongly modulated by mete-
 1131 orology, affecting the relative importance of each process (Chen et al., 2014; Michibata
 1132 et al., 2016; Christensen et al., 2017; Neubauer et al., 2017; Gryspeerd, Goren, et al.,
 1133 2019), which will be different in different cloud regimes.

1134 Satellite studies have shown a close relationship between cloud droplet size and pre-
 1135 cipitation in warm clouds, with smaller droplets inhibiting precipitation formation (Rosenfeld
 1136 & Ulbrich, 2003; Suzuki et al., 2013). A strong positive $\beta_{\ln \mathcal{L} - \ln N_d}$ ($=\partial \ln \mathcal{L} / \partial \ln N_d$ fol-
 1137 lowing the definition of $\beta_{\ln N_d - \ln \tau_a}$) is found in precipitating clouds (Chen et al., 2014),
 1138 suggesting that precipitation suppression can increase \mathcal{L} . With a parametrised impact
 1139 of N_d on only the autoconversion rate, many GCMs produce an increase in \mathcal{L} with in-
 1140 creasing aerosol (Quaas et al., 2009), resulting in a negative radiative forcing that en-
 1141 hances the overall ERF_{aci}[liquid] in some models by around 30% (Gettelman, 2015). How-
 1142 ever, comparisons of GCM results to cloud perturbations due to shipping and volcanic
 1143 aerosol support a weaker \mathcal{L} adjustment on a global average (Malavelle et al., 2017; Toll
 1144 et al., 2017).

1145 The tendency of GCMs to form light precipitation too frequently may lead to an
 1146 overly strong impact of precipitation suppression (Stephens et al., 2010; M. Wang et al.,
 1147 2012), as aerosols cannot suppress precipitation from a non-precipitating cloud (Sorooshian
 1148 et al., 2009). Precipitation processes in GCMs have been shown to be less sensitive to
 1149 aerosol than in observations (Jing & Suzuki, 2018), although observations can easily con-
 1150 fuse cause and effect, so that scavenging may in fact not be sufficiently active in GCMs.

1151 In any case, the size of the \mathcal{L} - N_d sensitivity component driven by precipitation suppression is still uncertain. Despite this, GCMs rarely produce an enhancement of the RFaci
 1152 larger than 50% due to changes in \mathcal{L} (Gryspeerd, Mülmenstädt, et al., 2019).
 1153

1154 Satellites often observe a strong negative $\beta_{\ln \mathcal{L} - \ln N_d}$, particularly in regions of low
 1155 cloud-top humidity (Chen et al., 2014; Michibata et al., 2016), which may be driven by
 1156 aerosol-dependent cloud-top entrainment, and might also not respect assumptions made
 1157 by the retrievals on the adiabatic nature of the clouds. It might also be a manifestation
 1158 of reductions in N_d due to precipitation formation in clouds with elevated \mathcal{L} . The re-
 1159 lationship is reproduced by global cloud-resolving simulations (Sato et al., 2018). The
 1160 possible decrease in \mathcal{L} due to this effect is therefore not well constrained and generally
 1161 not included in the GCM studies cited above. Gryspeerd, Goren, et al. (2019) find val-
 1162 ues of $\beta_{\ln \mathcal{L} - \ln N_d}$ as negative as -0.4 , but note that this is likely an overestimate due to
 1163 the impact of meteorological covariations, with a value closer to -0.1 being in better agree-
 1164 ment with A. S. Ackerman et al. (2004) and results from natural experiments. The lower
 1165 bound for this adjustment is thus taken at -0.1 . Toll et al. (2017) find a value of -0.011 ,
 1166 which is the least negative number that is based on large-scale aggregate observations
 1167 with plausible evidence for causality in the $\mathcal{L} - N_d$ relationship. It is thus taken as an
 1168 upper bound for this adjustment, since positive values, although possible in individual
 1169 clouds, are unlikely to hold on average according to the analyses of ship, volcano, and
 1170 pollution tracks by Toll et al. (2017, 2019).

1171 8.2 Adjustments in cloud cover \mathcal{C}

1172 The suppression of precipitation may also lead to a change in \mathcal{C} , either via increases
 1173 in cloud lifetime (Albrecht, 1989) or by affecting the transition between closed- and open-
 1174 celled stratocumulus (Rosenfeld, 2006). Many studies have observed links between \mathcal{C} and
 1175 aerosol radiative properties, especially τ_a , finding both increases and decreases in \mathcal{C} with
 1176 increasing aerosol (Sekiguchi et al., 2003; Kaufman et al., 2005; Kaufman & Koren, 2006;
 1177 N. G. Loeb & Schuster, 2008; Small et al., 2011; Dey et al., 2011; Yuan, Remer, & Yu,
 1178 2011; Gryspeerd, Stier, & Partridge, 2014b). However, it has proved challenging to sepa-
 1179 rate the role of aerosols from the impact of retrieval biases (Brennan et al., 2005; Várnai
 1180 & Marshak, 2009) and meteorological covariations (Quaas et al., 2010; Chand et al., 2012;
 1181 Grandey et al., 2013).

1182 GCMs typically show an increase in \mathcal{C} and a corresponding negative rapid adjust-
 1183 ment in response to aerosol (Zelinka et al., 2014; S. Ghan et al., 2016), due to the aerosol
 1184 impact depending indirectly on the aerosol-driven reduction in autoconversion. Simu-
 1185 lating a more complex array of processes, LES studies have found decreases in \mathcal{C} in re-
 1186 sponse to N_d increases, although there is often a compensating effect over the cloud life-
 1187 time (Xue & Feingold, 2006; Seifert et al., 2015), leading to a small overall $\beta_{\mathcal{C} - \ln N_d} =$
 1188 $\partial \mathcal{C} / \partial \ln N_d$, suggesting a lower bound on $\beta_{\mathcal{C} - \ln N_d}$ of 0.

1189 Recent studies have applied a number of different methods to disentangle the role
 1190 of meteorology from the impact of aerosols on \mathcal{C} in observations. Three methods, based
 1191 on a statistical accounting for confounders (Gryspeerd et al., 2016), careful sampling
 1192 (Christensen et al., 2017) and a neural network (Andersen et al., 2017), find rapid ad-
 1193 justments via \mathcal{C} changes of between 130 to 200% of the radiative forcing of the Twomey
 1194 effect. The agreement between these observational methods provides a measure of con-
 1195 fidence in this estimate, but these methods are all based on snapshots of the aerosol-cloud
 1196 field. The inherently time-dependent nature of cloud adjustments means that this may
 1197 lead to an overestimate of the effect, or an underestimate due to undetected aerosol per-
 1198 turbations (Possner et al., 2018) where similarly strong rapid adjustments via \mathcal{C} were found.

1199

8.3 Radiative sensitivities and effective cloud fractions

1200

Following Eq. 13, the change in cloud albedo due to changes in \mathcal{L} is given by:

1201

$$d\alpha_c = \frac{5}{6} \alpha_c (1 - \alpha_c) d \ln \mathcal{L} \iff S_{\mathcal{L},N} = \frac{5}{6} \alpha_c (1 - \alpha_c) \quad (19)$$

1202

1203

The planetary albedo α can be expressed as the sum of cloudy-sky albedo, α_c , weighted by cloud fraction, \mathcal{C} , and clear-sky albedo, α_{clear} , weighted by the complement:

1204

$$\alpha = \mathcal{C} \alpha_c + (1 - \mathcal{C}) \alpha_{\text{clear}} = \mathcal{C} (\alpha_c - \alpha_{\text{clear}}) + \alpha_{\text{clear}} \quad (20)$$

1205

Thus, α scales with \mathcal{C} with $(\alpha_c - \alpha_{\text{clear}})$ as scaling factor:

1206

$$S_{\mathcal{C},N} = \alpha_c - \alpha_{\text{clear}} \quad (21)$$

1207

1208

1209

1210

1211

Although α_c varies due to aerosol impacts on N_d and \mathcal{L} , these changes are a small fraction of α_c so are ignored here. From observations, the scaling factor takes values of 0.3 to 0.5 for marine boundary-layer clouds (Bender et al., 2011). The linear scaling is appropriate for stratocumulus clouds where clouds are capped by the inversion and therefore deepen relatively little as they widen (Feingold et al., 2017).

1212

1213

Like RFacI, rapid adjustments in \mathcal{L} act on cloudy regions only, such that by analogy with Eq. 18, the effective cloud fraction $c_{\mathcal{L}}$ can be written as

1214

$$c_{\mathcal{L}} = \frac{\left\langle \mathcal{C}_{\text{liq}} \alpha_c (1 - \alpha_c) \beta_{\ln \mathcal{L} - \ln N_d} \beta_{\ln N_d - \ln \tau_a} \frac{\Delta \tau_a}{\tau_a} R_{\text{SW}}^{\downarrow} \right\rangle}{\langle \alpha_c (1 - \alpha_c) \rangle \langle \beta_{\ln \mathcal{L} - \ln N_d} \rangle \langle \beta_{\ln N_d - \ln \tau_a} \rangle \left\langle \frac{\Delta \tau_a}{\tau_a} \right\rangle \left\langle R_{\text{SW}}^{\downarrow} \right\rangle} \quad (22)$$

1215

1216

1217

1218

1219

1220

1221

1222

1223

1224

Differing only through an introduction of the $\beta_{\ln \mathcal{L} - \ln N_d}$ term, $c_{\mathcal{L}}$ is very similar to c_N given by Eq. 18 and is calculated in a similar manner. $\beta_{\ln \mathcal{L} - \ln N_d}$ is calculated using MODIS cloud retrievals at a $1^\circ \times 1^\circ$ resolution, with the sensitivities calculated using linear regressions on the log variables. Using CERES SSF 1deg Ed4 data (Wielicki et al., 1996) for the radiative sensitivities, gives $c_{\mathcal{L}}$ as 0.27, an increase over \mathcal{C}_{liq} (0.22), with a similar spatial pattern (Fig. 6c). This increase in the magnitude of the effective cloud fraction is expected due to spatial correlations between \mathcal{C}_{liq} and $\beta_{\ln N - \ln \tau_a}$ (Gryspeerdt & Stier, 2012). This similarity in $c_{\mathcal{L}}$ and c_N is supported by the resemblance of the patterns of the ERFaci[LWP] and the RFacI in observational (Gryspeerdt, Goren, et al., 2019) and modelling (Mülmenstädt et al., 2019) studies, due to the dominating influence of \mathcal{C}_{liq} .

1225

1226

1227

1228

1229

1230

1231

1232

1233

1234

The effective cloud fraction for adjustments in \mathcal{C} is less obvious, as it acts by changing the cloud fraction. The RFacI and the \mathcal{L} adjustment only act by changing cloud properties, such that the area over which they act is the liquid cloud fraction. In contrast, the area over which the \mathcal{C} adjustment can operate is any region not obscured by overlying ice cloud, leading to $(1 - \mathcal{C}_{\text{ice}})$ as the initial cloud fraction (Gryspeerdt et al., 2016). \mathcal{C}_{ice} has to be weighted by the optical depth of the ice clouds, which determines the radiative impact of the underlying liquid clouds. This is approximated in observation-based studies, with detected ice clouds assumed to be opaque and those below the detection limit, an optical depth of around 0.4 for MODIS (S. A. Ackerman et al., 2008), assumed transparent. The effective cloud fraction $c_{\mathcal{C}}$ is:

1235

$$c_{\mathcal{C}} = \frac{\left\langle (1 - \mathcal{C}_{\text{ice}}) (\alpha_c - \alpha_{\text{clear}}) \beta_{\mathcal{C} - \ln N} \beta_{\ln N - \ln \tau_a} \frac{\Delta \tau_a}{\tau_a} R_{\text{SW}}^{\downarrow} \right\rangle}{\langle (\alpha_c - \alpha_{\text{clear}}) \rangle \langle \beta_{\mathcal{C} - \ln N} \rangle \langle \beta_{\ln N - \ln \tau_a} \rangle \left\langle \frac{\Delta \tau_a}{\tau_a} \right\rangle \left\langle R_{\text{SW}}^{\downarrow} \right\rangle} \quad (23)$$

1236

1237

The calculation of $c_{\mathcal{C}}$ follows $c_{\mathcal{L}}$ (Eq. 22), using MODIS cloud and AOD retrievals to calculate $\beta_{\mathcal{C} - \ln N}$ and $\beta_{\ln N - \ln \tau_a}$ and CERES data for the radiative sensitivities. As

1238 for $\beta_{\ln \mathcal{L} - \ln N}$, $\beta_{\mathcal{C} - \ln N}$ is calculated with a linear regression within each $1^\circ \times 1^\circ$ gridbox.
 1239 This gives $c_{\mathcal{C}}$ as 0.59 (Fig. 6d), a decrease compared to $1 - \mathcal{C}_{ice}$ (0.68). Note that $c_{\mathcal{C}}$ can
 1240 be greater than 1, as it is not a true cloud fraction and incorporates the covariation be-
 1241 tween the components of Eq.8. The uncertainty in $c_{\mathcal{L}}$ and $c_{\mathcal{C}}$ depends only on the spa-
 1242 tial pattern of the individual terms in their equations (except for \mathcal{C}_{liq} and \mathcal{C}_{ice}). As with
 1243 c_N , the uncertainty in $c_{\mathcal{L}}$ and $c_{\mathcal{C}}$ is estimated using the spatial distributions of $\beta_{\ln N - \ln \tau_a}$
 1244 and $\Delta \ln \tau_a$ from McCoy et al. (2017), giving $c_{\mathcal{L}}$ and $c_{\mathcal{C}}$ of 0.21 and 1.07, respectively.
 1245 Using the distributions of $\Delta \ln \tau_a$ from Kinne (2019) produces values of 0.29 and 0.76,
 1246 respectively.

1247 8.4 Summary

1248 In summary, the contribution of rapid adjustments to globally-averaged RFaci is
 1249 calculated in a similar way to Eq. 14, as:

$$1250 \Delta \ln N_d [\beta_{\ln \mathcal{L} - \ln N_d} S_{\mathcal{L},N} c_{\mathcal{L}} + \beta_{\ln \mathcal{C} - \ln N_d} S_{\mathcal{C},N} c_{\mathcal{C}}] \quad (24)$$

1251 For reference, Table 2 summarises the definitions of the variables used in Eq. 24. The
 1252 ranges adopted for the terms of this equation are:

- 1253 • 0.06 to 0.18 for $\Delta \ln N_d$, following Section 6;
- 1254 • -0.3 to -0.011 for $\beta_{\ln \mathcal{L} - \ln N_d}$ based on the satellite analyses of Gryspeerdt et al.
 1255 (2018) and Toll et al. (2017);
- 1256 • -54 to -56 W m^{-2} for $S_{\mathcal{L},N}$. This range is obtained by multiplying $S_{\mathcal{L},N}$ expressed
 1257 in terms of planetary albedo, i.e. from 0.177 to 0.184 based on propagating CERES
 1258 albedo uncertainties using Eq. 19, by the solar constant 340 W m^{-2} . The result
 1259 is then multiplied by 0.9 to account for an offsetting contribution of 10% coming
 1260 from the terrestrial spectrum, as calculated by GCMs (Zelinka et al., 2014; Heyn
 1261 et al., 2017);
- 1262 • 0.21 to 0.29 for $c_{\mathcal{L}}$, based on satellite retrievals of cloud properties and planetary
 1263 albedo;
- 1264 • 0 to 0.1 for $\beta_{\ln \mathcal{C} - \ln N_d}$ based on GCMs and large-eddy simulations;
- 1265 • -91 to -153 W m^{-2} for $S_{\mathcal{C},N}$. This range is obtained from Bender et al. (2011)
 1266 and converted to top-of-atmosphere radiance sensitivities using the same method
 1267 as for $S_{\mathcal{L},N}$ above;
- 1268 • 0.76 to 1.07 for $c_{\mathcal{C}}$, based on satellite retrievals of cloud properties and planetary
 1269 albedo;

1270 Using the method described in section 2.2 to combine those ranges and solve Eq. 24, rapid
 1271 adjustments in \mathcal{L} contribute from 0 to $+0.50 \text{ W m}^{-2}$ and rapid adjustments in \mathcal{C} con-
 1272 tribute from -1.35 to 0 W m^{-2} . To obtain ERFaci, the range of -1.20 to -0.35 W m^{-2}
 1273 obtained for $\mathcal{F}aci$ in Section 6 is added to those rapid adjustments using the method de-
 1274 scribed in section 2.2 to yield a range of -2.0 to -0.3 W m^{-2} for $\mathcal{E}aci$. Note that $\mathcal{F}aci$
 1275 and its rapid adjustments are correlated, at least in the framework of Eqs. 15 and 24,
 1276 through the term $\Delta \ln N_d = \beta_{\ln N - \ln a} \Delta \tau_a / \tau_a$.

1277 Based on this potential correlation, an alternative way to bound ERFaci would be
 1278 to directly scale rapid adjustments according to $\mathcal{F}aci$. For rapid adjustments in \mathcal{L} , Lebsack
 1279 et al. (2008) and Christensen et al. (2017) find they do not completely offset RFaci, with
 1280 the reduction likely less than 60% (Gryspeerdt, Goren, et al., 2019). But they may also
 1281 enhance RFaci. The implementation of microphysical adjustments to aci by only one mech-
 1282 anism – precipitation suppression – in GCMs is sub-optimal, but rarely gives an enhance-
 1283 ment of the RFaci larger than 50% (Gryspeerdt, Mülmenstädt, et al., 2019). For rapid
 1284 adjustments in \mathcal{C} , satellite-based studies that account for biases and confounding factors
 1285 produce around a 150% enhancement to the RFaci (Gryspeerdt et al., 2016; Christensen
 1286 et al., 2017; Andersen et al., 2017; Possner et al., 2018). Some high-resolution simula-

1287 tions find a small change to \mathcal{C} as a function of aerosol (Seifert et al., 2015), producing
 1288 an upper bound of a 0% enhancement of the RFaci. Scaling rapid adjustments based on
 1289 \mathcal{F} aci is however only an advantage if the uncertainty in \mathcal{F} aci is sufficiently small.

1290 9 Aerosol interactions with ice clouds

1291 Ice clouds are also affected by aerosol, although the impact of aerosol depends on
 1292 the aerosol type and the dominant ice nucleation mode. Sulfate aerosols facilitates ho-
 1293 mogeneous freezing of haze drops in the upper troposphere at cirrus temperatures (lower
 1294 than about -38°C). Thus the increase in sulfate concentrations due to anthropogenic
 1295 precursor emissions leads to an increase in ice crystal number, N_i . This effect implies cir-
 1296 rus clouds with higher emissivity (less LW radiation emitted to space) and reflectivity
 1297 (more SW reflected back to space), with RFs of opposite sign. Studies using satellite re-
 1298 trievals of N_i provide some observational evidence for an enhancement from aerosol (Sourdeval
 1299 et al., 2018; Gryspeerdt et al., 2018; D. L. Mitchell et al., 2018) in regions of strong up-
 1300 drafts, although theoretical studies suggest that the overall magnitude of this effect is
 1301 small because the primary control on the homogeneous nucleation rate is the in-cloud
 1302 updraft (DeMott et al., 1997; Lohmann & Kärcher, 2002; Kay & Wood, 2008; Jensen
 1303 et al., 2013, 2016; Krämer et al., 2016).

1304 Some aerosol types are effective heterogeneous INPs. Mineral dust (particularly feldspars;
 1305 Atkinson et al., 2013) has been shown to be an effective INP in laboratory studies (Hoose
 1306 & Möhler, 2012) and is correlated to the occurrence of glaciated clouds (Choi et al., 2010;
 1307 Tan et al., 2014), so anthropogenic changes to mineral dust aerosols may change INP
 1308 distributions (see Section 4). The internal mixing of dust and soluble aerosol has been
 1309 shown to suppress the INP activity of dust, such that anthropogenic emissions of liquid
 1310 aerosol may also impact INP distributions (e.g. Cziczo et al., 2009). The ability of BC
 1311 to act as an INP depends on its physical characteristics and mixing state, with parti-
 1312 cles containing macropores being observed to nucleate ice at cirrus temperatures (Mahrt
 1313 et al., 2018), but there is increasing evidence that it is a poor INP at warmer temper-
 1314 atures (Kanji et al., 2017). In a situation dominated by heterogeneous nucleation, in-
 1315 creasing INP would increase N_i . In contrast, in situations dominated by homogeneous
 1316 nucleation, increasing INP can reduce the available supersaturation below the homoge-
 1317 neous nucleation threshold, reducing N_i (Kärcher & Lohmann, 2003). Similarly, there
 1318 is some evidence from satellite retrievals for a suppression of homogeneous nucleation
 1319 and N_i by INP (Chylek et al., 2006; Zhao et al., 2018; Gryspeerdt et al., 2018), but the
 1320 sparse nature of INP measurements makes these results uncertain. Furthermore, Christensen
 1321 et al. (2014) found by studying CALIOP lidar observations of over 200 ship tracks in mixed-
 1322 phase stratocumulus clouds that increased aerosols enhance the occurrence of ice and
 1323 decreased total water path in polluted clouds.

1324 The only global estimates of RFaci[ice] and ERFac[ice] that currently exist are pro-
 1325 duced using GCMs and mostly focus on cirrus. It is not always possible to separate the
 1326 instantaneous radiative forcing from its rapid adjustments in the literature and it is not
 1327 clear whether the ERFac[ice] would scale with the RFaci in a similar fashion to the ER-
 1328 Fac[liq]. Gettelman et al. (2012) found a positive RFaci[ice] of $+0.3 \text{ W m}^{-2}$, or about
 1329 a 20% offset of RFaci[liquid]. The importance of the the fraction of particles acting as
 1330 INP was highlighted by J. E. Penner et al. (2009), who found a negative RFaci[ice] of
 1331 -0.3 to -0.4 W m^{-2} with a lower preindustrial INP population. Similarly, the INP ef-
 1332 ficiency of BC has a large effect on the simulated N_i and RFari (J. E. Penner et al., 2009).
 1333 The uncertainty in these factors is reflected in the wide range of estimates of ERFac[ice]
 1334 (Heyn et al., 2017). In general, aerosol interactions with ice clouds are likely N_i depen-
 1335 dent and slightly larger for those states with less homogeneous nucleation and lower ice
 1336 number concentration in the base state. The uncertainty regarding the balance of ho-
 1337 mogeneous and heterogeneous nucleation for ice clouds (Gasparini & Lohmann, 2016)
 1338 and the lack of observations to constrain globally cirrus INP or N_i limit how accurately

1339 the aerosol effect on ice clouds can be constrained. On balance, it seems like effects may
1340 be small and positive: by increasing ice crystal numbers, cirrus LW increases faster than
1341 SW cooling. However, as laboratory measurements have shown that BC is not as effi-
1342 cient an INP as previously thought and does not affect homogeneous nucleation, a large
1343 RFaci[ice] is less likely than in the past. Combined with the second order effect of aerosol
1344 on homogeneous nucleation, this suggests the resulting RFaci[ice] may be on the order
1345 of a small fraction of the total anthropogenic ERFaci, but cannot be bounded yet be-
1346 cause of the large uncertainty in the present and preindustrial states of ice cloud nucle-
1347 ation pathways and INP populations.

1348 There is no observational evidence for strong adjustments in mixed-phase and ice
1349 clouds. Christensen et al. (2016) presents some evidence for a modest aerosol radiative
1350 warming by deep convective cores without anvil spreading, identified from CloudSat radar
1351 observations. The ability of INP to glaciate supercooled liquid clouds in the tempera-
1352 ture range of -38°C to 0°C is well established theoretically and supported by observed
1353 relationships between aerosol and cloud glaciation (Hu et al., 2010; Choi et al., 2010; Kanitz
1354 et al., 2011; Tan et al., 2014) at a global scale. An increase in cloud ice through an in-
1355 crease in the number of INPs might be expected to increase precipitation rates (Lohmann,
1356 2002; Field & Heymsfield, 2015), but the resulting impact on cloud water and amount
1357 along with the corresponding radiative effect of anthropogenic aerosols is currently not
1358 well constrained, with GCM studies suggesting the net overall effect to be small (Lohmann,
1359 2002; Hoose et al., 2008). Models that include explicit treatment of INP sources and cloud
1360 microphysics at high resolution suggest a strong link between \mathcal{L} (and reflected SW ra-
1361 diation) and INP driven by changes in precipitation (Vergara-Temprado, Holden, et al.,
1362 2018).

1363 There is some observational evidence of aerosols impacting convective clouds, with
1364 many possible mechanisms proposed (Williams et al., 2002; Fan et al., 2013; Rosenfeld
1365 et al., 2008). However, interpreting those results based on high resolution simulations
1366 of deep convective clouds that often last a few hours only may overemphasize the im-
1367 portance of microphysical perturbations that may not matter for longer climate-relevant
1368 systems. While changes in cloud top height have proved difficult to isolate from mete-
1369 orological covariations (Gryspeerd, Stier, & Grandey, 2014), studies have found an en-
1370 hancement of lightning in regions of enhanced aerosol (Yuan, Remer, Pickering, & Yu,
1371 2011; Gryspeerd, Stier, & Partridge, 2014a; Thornton et al., 2017) and increases in cloud
1372 top height downwind of volcanoes (Yuan, Remer, & Yu, 2011; Mace & Abernathy, 2016),
1373 suggestive of an aerosol impact. The radiative effect of an aerosol impact on convective
1374 clouds is unclear. It is possible that an increase in thin anvil cirrus might act as a warm-
1375 ing effect (Koren, Remer, et al., 2010), but there are no strong observational constraints
1376 on this process and it may be small globally due to the tendency of LW and SW effects
1377 to cancel each other (Lohmann, 2008; Heyn et al., 2017) in deep convective clouds. Lo-
1378 cal circulation changes associated with aerosol gradients could however be important.
1379 For example, Blossey et al. (2018) found by modeling shipping lanes that the gradient
1380 between polluted shipping lane clouds and their cleaner surroundings may strengthens
1381 updrafts in the lane.

1382 In summary, there is clear evidence of aerosols influencing the cloud phase but un-
1383 certainties remain too large to provide robust assessments. Estimates of the ERFaci[ice]
1384 are currently sparse and the uncertainty from cloud microphysics schemes tends to ri-
1385 val potential aerosol effects (White et al., 2017). RFaci[ice] from cirrus would tend to
1386 be positive because of anthropogenic aerosols inducing more small ice crystals and higher
1387 ice mass through an increase in homogeneous freezing (Gettelman et al., 2012). This re-
1388 sponse might not occur depending on details of the balance of heterogeneous and homo-
1389 geneous freezing (Zhou & Penner, 2014; J. E. Penner et al., 2018), and the ice nuclei pop-
1390 ulation, but evidence currently supports a positive RFaci[ice] from cirrus of a few tenths
1391 of a W m^{-2} . For shallow mixed-phase clouds the effect of changes in CCN appears to

1392 be smaller than for liquid clouds (Christensen et al., 2014), but there is likely to be a posi-
 1393 tive RF in response to increases in INP, driven by increases in precipitation (Vergara-
 1394 Temprado, Miltenberger, et al., 2018).

1395 The current lack of observational constraints on ice phase processes limits the ac-
 1396 curacy with which the ERF_{ice} can be constrained, so it is not bounded in this re-
 1397 view. Observational constraints on the size of anthropogenic perturbation in N_i would
 1398 allow further progress. In addition, studies providing estimates for sensitivities of ice cloud
 1399 albedo, ice water path, and ice cloud fraction, as well as cloud top height, to anthropogenic
 1400 aerosol changes would allow the decomposition of the ice as well as mixed-phase and LW
 1401 terms of Eq. 8 in a way similar to liquid clouds.

1402 10 Inferences based on observed changes in temperature and radia- 1403 tion

1404 The temperature of Earth’s surface has increased by $1.0 \pm 0.2^\circ\text{C}$ since preindus-
 1405 trial times (Allen et al., 2018), and except for periods lasting less than a few decades,
 1406 this increase in temperature occurred since 1850 (Hartmann et al., 2013). This increase
 1407 in temperature is attributed mainly to anthropogenic forcing, primarily the ERFs due
 1408 to increases in abundance of the greenhouse gases (GHG; positive, warming influence)
 1409 minus the effective forcings due to increases in abundance of aerosols (negative, cooling
 1410 influence) (Myhre, Shindell, et al., 2013; Bindoff et al., 2013). Here arguments are pre-
 1411 sented that the increase in global temperature together with knowledge of the GHG forc-
 1412 ing can usefully constrain the aerosol forcing.

1413 [INSERT FIGURE 7 HERE]

1414 Under the assumption that the increase in global temperature is a response to forc-
 1415 ing, the continuous increase in Earth’s temperature implies that the net average forc-
 1416 ing has been positive throughout the period, except for short periods e.g. after volcanic
 1417 eruptions (Stevens, 2015). Knowledge of greenhouse gas ERF provides a constraint on
 1418 the magnitude of the total ERF: the total ERF in the year 2011 with respect to year 1750,
 1419 excluding the aerosol ERF, is estimated as $+3.1 \pm 0.4 \text{ W m}^{-2}$ (Myhre, Shindell, et al., 2013)
 1420 (uncertainty converted to $\pm 1\sigma$), implying within the stated assumption that the 2011
 1421 aerosol ERF was less negative than -3.5 W m^{-2} . Rotstayn et al. (2015) analysed the re-
 1422 lationship between the simulated aerosol ERF (2010 vs. 1765) and the simulated change
 1423 in global-mean surface temperature 2000 vs. 1860 in the CMIP5 multi-model ensemble
 1424 (Fig. 7a). They also cite the average temperature increase over the same period from five
 1425 observational datasets at 0.6 K. The emergent constraint (Klein & Hall, 2015) constructed
 1426 by Rotstayn et al. (2015) from surface temperature change suggests values of aerosol ERF
 1427 around -1.0 W m^{-2} .

1428 Stevens (2015) proposed that it is possible to draw a tighter constraint on the aerosol
 1429 ERF by considering an earlier part of the industrial period, when the relative importance
 1430 of the aerosol ERF would be expected to have been greater due to the assumed sub-linearity
 1431 of the aerosol ERF. He further argued that the constraint is still tighter when assum-
 1432 ing that increasing temperatures in the Northern Hemisphere (NH) can be linked to a
 1433 net positive hemispheric ERF. The suggestion, based on a simple model for the hemispheric-
 1434 mean forcing, led to the conclusion that the present global aerosol ERF is unlikely to
 1435 be more negative than -1.0 W m^{-2} . However, slightly more comprehensive energy bal-
 1436 ance models (Booth et al., 2018) and general circulation models (Kretzschmar et al., 2017)
 1437 find that global mean aerosol ERFs as negative as -2 W m^{-2} are still consistent with
 1438 the observed NH temperature increase. It is plausible that restricting the analysis in the
 1439 original study by Stevens (2015) to the Northern hemispheric energy balance is hampered
 1440 by the existence of and the uncertainty in the cross-equatorial energy transports. Re-
 1441 quiring instead that each decade during the second half of 20th century has non-negative

total anthropogenic and natural ERF, taking into account a low efficacy of volcanic forcing (Gregory et al., 2016), shows that it is unlikely that the aerosol forcing is more negative than -1.7 W m^{-2} . It is noteworthy that the GCMs in the CMIP5 ensemble with the most negative aerosol ERFs exhibit behavior that calls their fidelity into question, such as a much smaller warming than observed for many time periods of the 20th century (Golaz et al., 2013) or unrealistic pattern in aerosol radiative effects (Stevens & Fiedler, 2017). The globally-averaged emission rate of sulfate aerosols has been approximately stable since the mid-1970s (Hoesly et al., 2018) although the geographical distribution has moved equatorward to different cloud regimes. This allows for a tighter constraint when considering only the more recent past, and increasingly tight constraints may be possible in the future if aerosol ERF weakens and CO₂ ERF increasingly dominates the overall anthropogenic ERF (Myhre et al., 2015). It is noteworthy that energy balance calculations with zero aerosol ERF can yield global mean temperature evolutions that are consistent with the instrumental record, albeit requiring low sensitivity. Schwartz (2018) showed that the observed temperature record over the period 1850 to 2011 is consistent with aerosol forcing throughout the IPCC 5-95% uncertainty range, but requiring low transient sensitivity (1.0 K) for low-magnitude present aerosol forcing (-0.09 W m^{-2}) and high transient sensitivity (2.0 K) for high-magnitude present aerosol forcing (-1.88 W m^{-2}).

A stronger constraint could be obtained if transient climate sensitivity, the ratio of global temperature increase to global mean net forcing, were known to a good accuracy (Schwartz & Andreae, 1996; Knutti et al., 2002; Anderson, Charlson, Schwartz, et al., 2003). Fig. 7b displays the hyperbolic inverse relationship between the transient climate response and aerosol ERF shown here for a large ensemble from a simple climate model, and from an energy balance model. The ensemble by Smith et al. (2018) has a 16-84% confidence interval for transient climate response of 1.3 to 2.0 K, which translates into a $\pm 1\sigma$ confidence interval for aerosol ERF of -1.2 to -0.6 W m^{-2} . Skeie et al. (2018) obtain a quantitatively similar relationship between aerosol ERF and transient climate response using an energy balance model.

Beyond surface temperature, observations of the radiation budget may be exploited to infer clues about aerosol ERF. Murphy et al. (2009) analyse satellite retrievals of the top-of-atmosphere radiation budget. They find a likely range for aerosol ERF of about -0.6 to -1.5 W m^{-2} . Cherian et al. (2014) explore the observations of surface solar radiation over Europe for the 1980–2005 period, in comparison to GCMs. They relate regional surface solar radiation trends simulated by the GCMs in the CMIP5 multi-climate model ensemble and simulated global-mean aerosol ERF. The observed surface solar radiation trend for the 1980–2005 period over Europe, together with the GCM emergent constraint suggested a plausible range of aerosol ERF of -0.9 to -1.5 W m^{-2} . In turn, Storelvmo et al. (2018) analyzed multiple surface solar radiation measurement stations across the globe with varying record lengths in comparison to the CMIP5 multi-model ensemble. They concluded that all GCMs exhibit much weaker trends in surface solar radiation than the observations they assessed, since the mid-20th century. However, the simulated temperature trends by the GCMs are consistent with the observed temperature changes. Their result might be indicative of the possibility of a very strong aerosol ERF in the SW spectrum, but does not consider LW components.

In summary, there are two conclusions from the assessment of the climate responses: (i) the fact that surface SW radiation responded to aerosol emission changes as observed, combined with the conclusion by Section 4 that anthropogenic aerosols are relatively weakly absorbing on a global average, establishes that the SW component of the aerosol ERF is negative, and (ii) different studies based on observed global temperature changes conclude that an ERF more negative than -1.2 to -2.0 W m^{-2} , depending on the study, is outside the likely range considered in this assessment. On balance, -1.6 W m^{-2} is adopted here for the lower bound of the $\pm 1\sigma$ confidence interval.

1494 **11 Synthesis and challenges**

1495 Based on the conceptual model of aerosol instantaneous RF and rapid adjustments
 1496 represented by Eq. 8, this review has considered several lines of evidence, including mod-
 1497 eling and observations at various scales, on the likely strength of aerosol ERF, defined
 1498 with respect to year 1850. Of all the components of aerosol ERF quantified in this re-
 1499 view, and for which different lines of evidence support the existence of an effect, rapid
 1500 adjustments to aci are most difficult to bound based on current literature, because it is
 1501 challenging to properly average globally the many possible cloud responses to aerosol per-
 1502 turbations. The dominant uncertainties are however the industrial-era changes in aerosol
 1503 optical depth, $\Delta\tau_a$, and in cloud droplet number concentration, ΔN_d , because they ef-
 1504 fectively cascade through to each ERF component under the framework of this review
 1505 and its assumptions. Based on a combination of large-scale modeling and satellite re-
 1506 trievals, human activities are likely to have increased aerosol optical depth by 14 to 29%
 1507 and cloud droplet number concentration by 6 to 18% in 2005–2015 compared to the year
 1508 1850. Table 4 gives ranges in the 16-84% confidence interval for each term of Eq. 8. The
 1509 table also lists the main lines of evidence used in this review to obtain each range. Global
 1510 modeling and satellite analyses are the main lines of evidence used. Although small-scale
 1511 modeling and observation studies should in theory be the most accurate sources for the
 1512 radiative sensitivities of Eq. 8, the current lack of a strategy for scaling their results to
 1513 the global average limits their use.

1514 [INSERT TABLE 4 HERE]

1515 Adding the ranges for ERFari (-0.58 to -0.23 W m^{-2}) and ERFaci (-2.00 to -0.30 W m^{-2})
 1516 together using the Monte-Carlo approach described in section 2.2 yields a range for to-
 1517 tal aerosol ERF of -2.50 to -0.65 W m^{-2} at the 16 to 84% confidence level. This range
 1518 is similar to that obtained from a single-model PPE, constrained by observations, which
 1519 covers -2.2 to -0.7 W m^{-2} (Regayre et al., 2018). In other words, process-based attempts
 1520 to quantify aerosol ERF do not constrain the more negative bound. As discussed in sec-
 1521 tion 10, inferences based on observed climate changes provide additional constraints that
 1522 narrow the distribution by making an aerosol ERF more negative than -1.6 W m^{-2} un-
 1523 likely. The upper bound is not constrained further by those inferences. Consequently,
 1524 the likely range of aerosol ERF obtained by this review spans -1.6 to -0.65 W m^{-2} ($\pm 1\sigma$
 1525 range).

1526 This review estimates all uncertainty ranges at the 16 to 84% confidence level, as
 1527 discussed in Section 2.2. IPCC Assessment Reports make a different choice, reporting
 1528 at the 5 to 95% confidence level. To facilitate comparisons, Table 5 translates the ranges
 1529 given by this review to the 5 to 95% confidence level. However, those latter ranges are
 1530 more dependent on the assumed shapes of the distributions given in Table 4, which are
 1531 difficult to assess from the literature. Comparing Tables 1 and 5 suggests that working
 1532 through traceable and arguable lines of evidence, as done in this review, produces un-
 1533 certainty ranges that are similar to the expert judgment of IPCC AR5, albeit shifted to-
 1534 wards more negative ERFs.

1535 [INSERT TABLE 5 HERE]

1536 The full probability distribution functions (PDFs) for aerosol ERF and its com-
 1537 ponents are shown in Figure 8. Also shown are the PDFs obtained for total aerosol ERF
 1538 by the IPCC 5th Assessment Report (Myhre, Shindell, et al., 2013). The Figure illus-
 1539 trates the reduction in the range for ERFari, which is due to a reduction of the likeli-
 1540 hood of strong rapid adjustments to ari. The range for ERFaci is much wider in this re-
 1541 view than in Myhre, Shindell, et al. (2013), the long tail coming from this review’s wider
 1542 assessment of rapid adjustments of aerosol-cloud interactions in liquid clouds. Conse-
 1543 quently, the range for total aerosol ERF is also much wider. This review however decreases
 1544 the likelihood of an aerosol ERF more positive than -0.4 W m^{-2} . In addition, recall that

1545 total aerosol ERF more negative than -2.0 W m^{-2} rely on more speculative aerosol-driven
 1546 cloud changes, and are not consistent with observed temperature and surface radiation
 1547 changes, as discussed in Section 10.

1548 [INSERT FIGURE 8 HERE]

1549 There are a number of challenges to overcome to narrow the range of aerosol ERF
 1550 further. This review has already discussed the challenges associated with the imperfect
 1551 knowledge of changes in aerosols over the industrial period (Carslaw et al., 2013), which
 1552 in this review were encapsulated in $\Delta\tau_a$ (Section 4), and with aerosol interactions with
 1553 ice clouds (Section 9), which are not yet characterised sufficiently well to allow a global
 1554 assessment of sensitivities. But other outstanding challenges should be highlighted:

- 1555 • The lack of resolution of small scales by large-scale models means that their in-
 1556 tegration of local processes into a globally-averaged number is imperfect. For ari,
 1557 small scales contribute significantly to spatial variability of relative humidity and
 1558 unresolved aerosol amount/composition, which together determine hygroscopic growth
 1559 and the amount of light scattered. Because aerosol growth factors are super-linear,
 1560 application of a spatially averaged aerosol growth factor could significantly un-
 1561 derestimate the average of the local growth factors, particularly at relative humiditi-
 1562 ties above 85% (Nemesure et al., 1995; J. M. Haywood et al., 1997; Petersik et al.,
 1563 2018). For aci, unresolved cloud-scale vertical motion and turbulent mixing, and
 1564 coarsely parameterised cloud- and precipitation-, as well as aerosol sink processes,
 1565 lead to poor representations of cloud and aerosol fields, their spatio-temporal col-
 1566 location, and regime-dependent small- to meso-scale interactions of processes. The
 1567 emergence of global storm resolving models (Satoh et al., 2018) and the ability
 1568 to perform global LES for a few days would add substantially to our ability to bet-
 1569 ter quantify these processes.
- 1570 • The co-variability of aerosol, clouds and meteorological conditions implies scale
 1571 effects. The fidelity of a modelled ERF_{aci} or ERF_{ari} is dependent not only on the
 1572 ability of the model to generate realistic clouds on average, but also to capture
 1573 their co-variability at smaller spatio-temporal scales. As shown by various stud-
 1574 ies, the composite response does not equal the local responses averaged up to the
 1575 composite scale. In reality local data typically comprise relatively small aerosol
 1576 ranges and small albedo, N_d , or effective radius responses. If aci metrics or ERFs
 1577 are based on aggregation of many such scenes they will tend to bias the relation-
 1578 ships by (i) extending the range of conditions beyond the natural local fluctua-
 1579 tions; and (ii) removing the small-scale co-variability between meteorology and
 1580 aerosol. The magnitude of these biases is poorly known.
- 1581 • The frequency of occurrence of aerosol perturbations to planetary albedo in gen-
 1582 eral, and to clouds in particular, has not yet been quantified at the global scale.
 1583 For example, ship tracks are often cited as evidence that tremendous radiative ef-
 1584 fects can be generated by anthropogenic aerosol emissions, yet merely 0.002% of
 1585 the world’s commercial ocean-going fleet are expected to generate a ship track in
 1586 their wake at any given time (Campmany et al., 2009). So, while evidence exists
 1587 to support large contributions of rapid adjustments to ERF_{aci}, these events seem
 1588 infrequent. The challenge is that large-scale attribution of changes in cloud prop-
 1589 erties to aerosol perturbations is complicated by co-variability between meteorol-
 1590 ological drivers and aerosols, discussed above, and the high degree of natural vari-
 1591 ability within the cloud deck itself, which can span orders of magnitudes in cloud-
 1592 radiative properties (Wood et al., 2018).
- 1593 • Models of all scales include a very large number of imprecisely known parameters.
 1594 In such complex model systems with compensating effects of imperfectly known
 1595 processes, even tight observational constraint of any model variables can leave open
 1596 wide ranges of aerosol RFs (J. S. Johnson et al., 2018) so understanding why some

1597 models do well against multiple constraints is important (J. Penner, 2019). This
 1598 model constraint limitation has become known as equifinality (Beven & Freer, 2001).
 1599 • Although this review has taken a global perspective in its assessment of aerosol
 1600 ERF, geographical considerations remain important. For example, it is possible
 1601 that the radiative sensitivities in Eq. 8 vary in time when aerosol and/or cloud pat-
 1602 terns change in response to changes in emissions and climate. In addition, assum-
 1603 ing that aci are saturated in the more polluted regions, then any additional an-
 1604 thropogenic aerosols would need to reach pristine regions in order to exert an ER-
 1605 Faci. More observational evidence is needed to constrain the magnitude with which
 1606 anthropogenic aerosols affect pristine regions like the Southern Ocean and ocean
 1607 cloud decks adjacent to continents in the eastern Pacific and eastern Atlantic oceans.

1608 The lack of evidence to support some of the hypotheses discussed in this review points
 1609 to the need for improving scientific understanding of aerosol ERF processes and occur-
 1610 rences in the atmosphere. The review has identified a few critical next steps. Firstly, scale
 1611 effects are increasingly being considered among hierarchies of models and must inform
 1612 global aerosol model development to ensure a more exhaustive representation of aerosol
 1613 forcing and rapid adjustment mechanisms. Secondly, volcanic eruptions and ship tracks
 1614 have provided important insights into cloud adjustments to aerosol perturbations, and
 1615 may provide opportunities to improve understanding of potential cloud phase shifts and
 1616 ice cloud responses. Thirdly, the strength of the constraints on aerosol ERF bounds pro-
 1617 vided by inferences based on observed climate changes is diminished by an incomplete
 1618 understanding of the uncertainties affecting those methods. “Perfect model” compar-
 1619 isons, where top-down methods are applied to synthetic data of known equilibrium cli-
 1620 mate sensitivity and aerosol ERF, would strengthen that important line of evidence. Fourthly,
 1621 statistical methods to thoroughly explore causes of model uncertainty are now being more
 1622 widely adopted, and are being combined with traditional multi-model ensembles to more
 1623 rigorously understand the effectiveness of observational constraints. Finally, global large-
 1624 eddy simulations hold promise to substantially improve the quantification of aerosol-cloud
 1625 interactions.

1626 Glossary

1627 **Aerosol** Solid and liquid particulates in suspension in the atmosphere, with the excep-
 1628 tion of cloud droplets and ice crystals.

1629 **Albedo** Ratio of reflected to incident irradiance.

1630 **Cloud Condensation Nuclei** Subset of the aerosol population that serves as sites where
 1631 water vapor condenses to form cloud droplets.

1632 **Effective Radiative Forcing** The sum of radiative forcing and rapid adjustments (see
 1633 those terms).

1634 **General Circulation Model** Numerical model that solves fluid mechanics equations
 1635 to simulate the 3-dimensional dynamics of the moist atmosphere. Those models
 1636 also include parametrizations of radiation, clouds, and, increasingly, aerosols.

1637 **Ice Nucleating Particle** Subset of the aerosol population that facilitate cloud ice crys-
 1638 tal formation.

1639 **Large Eddy Simulation** Category of numerical models that solve the fluid dynam-
 1640 ics equations by computing the large scale motion of turbulent flow.

1641 **Liquid Water Path** Column-integrated cloud liquid water content, i.e. mass of cloud
 1642 liquid water per unit surface area.

1643 **Optical depth** Column-integrated extinction cross section. Can be defined for any source
 1644 of extinction in the atmosphere, including aerosols and clouds.

1645 **Primary aerosol** Aerosols that are emitted into the atmosphere directly as solid or liq-
 1646 uid particulates.

- 1647 **Radiative Forcing** Imbalance in the Earth's energy budget caused by human activ-
 1648 ities or volcanic eruptions, or changes in the output of the Sun or the orbital pa-
 1649 rameters of the Earth.
- 1650 **Rapid Adjustments** Subset of the responses of the atmosphere-land-cryosphere sys-
 1651 tem to radiative forcing, which happened independently of the much slower changes
 1652 in sea surface temperature.
- 1653 **Secondary aerosol** Aerosols formed by atmospheric chemistry from gaseous precu-
 1654 sors.
- 1655 **Single scattering albedo** Ratio of scattering efficiency to extinction efficiency, where
 1656 extinction is the sum of scattering and absorbing. A purely scattering particle has
 1657 a single-scattering albedo of 1, and that value decreases with increasing absorp-
 1658 tion.
- 1659 **Twomey effect** Increase in cloud albedo caused by an increase in cloud condensation
 1660 nuclei for a fixed water content. Named after the late Sean Twomey, following Twomey
 1661 (1974).

1662 Acronyms

- 1663 **AeroCom** Aerosol Comparisons between Observations and Models
- 1664 **AERONET** AErosol RObotic NETwork
- 1665 **aci** Aerosol-cloud interactions
- 1666 **ari** Aerosol-radiation interactions
- 1667 **AOD** Aerosol Optical Depth
- 1668 **BC** Black Carbon
- 1669 **CALIOP** Cloud-Aerosol Lidar with Orthogonal Polarization
- 1670 **CCN** Cloud Condensation Nuclei
- 1671 **CERES** Clouds and the Earth's Radiant Energy System
- 1672 **CF** Cloud Fraction
- 1673 **CMIP** Climate Model Intercomparison Project
- 1674 **ERF** Effective Radiative Forcing
- 1675 **ERFaci** Effective Radiative Forcing of Aerosol-Cloud Interactions
- 1676 **ERFari** Effective Radiative Forcing of Aerosol-Radiation Interactions
- 1677 **GCM** General Circulation Model
- 1678 **GHG** Greenhouse Gas
- 1679 **IPCC** Intergovernmental Panel on Climate Change
- 1680 **IPCC AR5** 5th Assessment Report of the IPCC
- 1681 **LES** Large Eddy Simulation
- 1682 **LWP** Liquid Water Path
- 1683 **MAC** Max Planck Institute Aerosol Climatology
- 1684 **MACC** Monitoring Atmospheric Composition and Climate
- 1685 **MODIS** Moderate Resolution Imaging Spectroradiometer
- 1686 **PDRMIP** Precipitation Driver Response Model Intercomparison Project
- 1687 **PPE** Perturbed Parameter Ensemble
- 1688 **RF** Radiative Forcing
- 1689 **RFaci** Radiative Forcing of Aerosol-Cloud Interactions
- 1690 **RFari** Radiative Forcing of Aerosol-Radiation Interactions

1691 Acknowledgments

1692 The authors thank Chris Forest, Norman Loeb, and Brian Soden for fruitful discussions
 1693 at the World Climate Research Programme Grand Challenge Workshop: Bounding Aerosol

1694 Effective Radiative Forcing at Schloss Ringberg in February 2018. The authors thank
 1695 Masaru Yoshioka, Leighton Regayre, and Kirsty Pringle for sharing the Perturbed Pa-
 1696 rameter Ensemble data used in this review. The CALIOP data were obtained from the
 1697 NASA Langley Research Center Atmospheric Science Data Center (ASDC). The work-
 1698 shop was supported by the Max Planck Society and the Deutsche Forschungsgemeinschaft
 1699 (DFG, reference QU 311/18-1). The Ringberg workshop organisers acknowledge partial
 1700 funding from the European Union’s Seventh Framework Programme (FP7/2007-2013)
 1701 project BACCHUS under grant agreement no. 603445 and from the Swiss National Sci-
 1702 ence Foundation (project number 200021_160177). AG acknowledges support from the
 1703 U.S. National Science Foundation. ALD acknowledges PAGES for supporting the Global
 1704 Paleofire Working Group (GPWG). DTM acknowledges support from the PRIMAVERA
 1705 project, funded by the European Union’s Horizon 2020 programme, Grant Agreement
 1706 no. 641727. DW-P, JMH and NB acknowledge support from the NERC CLouds and Aerosol
 1707 Radiative Impacts and Forcing: Year 2016 (CLARIFY-2016, NE/L013746/1) project.
 1708 FM acknowledges support from the UK Natural Environment Research Council (NERC)
 1709 South West Asian Aerosol Monsoon Interactions project (SWAAMI, NE/L013886/1).
 1710 KC acknowledges support from the NERC Global Aerosol Synthesis and Science project
 1711 (GASSP, NE/J024252/1) and the Aerosol-Climate Uncertainty Reduction project (ACURE,
 1712 NE/P013406/1). MS acknowledges funding from the European Union’s Horizon 2020 re-
 1713 search and innovation programme under grant agreement No 641816 (CRESCENDO).
 1714 PMF acknowledges financial support from the NERC under grant NE/N006038/1 (Se-
 1715 curing Multidisciplinary UndeRstanding and Prediction of Hiatus and Surge events). PS
 1716 acknowledges support from the European Research Council (ERC) project constRain-
 1717 ing the EffeCts of Aerosols on Precipitation (RECAP) under the European Union’s Hori-
 1718 zon 2020 research and innovation programme with grant agreement No 724602 and from
 1719 the Alexander von Humboldt Foundation. SES was supported by the Atmospheric Sys-
 1720 tem Research Program, U.S. Department of Energy, Contract No. DE-SC0012704. TM
 1721 acknowledges support from the European Research Council (ERC) Consolidator Grant
 1722 770765. VT acknowledges support from the Estonian Research Council grant PSG202.
 1723 YS acknowledges support from the JSPS Grant-in-Aid for Young Scientists (B), with grant
 1724 number 15K17766. Data availability: The MODIS data are from the NASA Goddard
 1725 Space Flight Center (<https://ladsweb.modaps.eosdis.nasa.gov/>). The AMSR-E data
 1726 are obtained from the National Snow and Ice Data Center (<https://nsidc.org>) and
 1727 the CERES data are from the NASA Langley Atmospheric Research Center ([https://](https://ceres.larc.nasa.gov)
 1728 ceres.larc.nasa.gov). MACv2 distributions are accessible at [ftp://ftp-projects](ftp://ftp-projects.zmaw.de/aerocom/climatology/MACv2_2018/)
 1729 [.zmaw.de/aerocom/climatology/MACv2_2018/](ftp://ftp-projects.zmaw.de/aerocom/climatology/MACv2_2018/). MACC distributions can be downloaded
 1730 from <https://apps.ecmwf.int/datasets/data/cams-climate-forcings/>.

1731 References

- 1732 Ackerman, A., Toon, O., Taylor, J., Johnson, D., Hobbs, P., & Ferek, R. (2000).
 1733 Effects of aerosols on cloud albedo: Evaluation of Twomey’s parameterization
 1734 of cloud susceptibility using measurements of ship tracks. *J. Atmos. Sci.*, *57*,
 1735 2684-2695. doi: 10.1175/1520-0469(2000)057<2684:EOAOCA>2.0.CO;2
- 1736 Ackerman, A. S., Kirkpatrick, M. P., Stevens, D. E., & Toon, O. B. (2004, 12). The
 1737 impact of humidity above stratiform clouds on indirect aerosol climate forcing.
 1738 *Nature*, *432*, 1014. doi: 10.1038/nature03174
- 1739 Ackerman, S. A., Holz, R. E., Frey, R., Eloranta, E. W., Maddux, B. C., & McGill,
 1740 M. (2008). Cloud detection with MODIS. part II: Validation. *J Atmos Ocean*
 1741 *Tech*, *25*(7), 1073-1086. doi: 10.1175/2007JTECHA1053.1
- 1742 Adebisi, A. A., Zuidema, P., & Abel, S. J. (2015). The convolution of dynamics and
 1743 moisture with the presence of shortwave absorbing aerosols over the southeast
 1744 Atlantic. *Journal of Climate*, *28*(5), 1997-2024. Retrieved from [https://](https://doi.org/10.1175/JCLI-D-14-00352.1)
 1745 doi.org/10.1175/JCLI-D-14-00352.1 doi: 10.1175/JCLI-D-14-00352.1
- 1746 Aitken, J. (1880). On dust, fogs, and clouds. *Proceedings of the Royal Society of Ed-*

- 1747 *inburgh*, 11(108), 122–126.
- 1748 Albrecht, B. A. (1989, 1). Aerosols, cloud microphysics, and fractional cloudiness.
1749 *Science*, 245(4923), 1227–1230. doi: 10.1126/science.245.4923.1227
- 1750 Allen, M. R., Dube, O. P., Solecki, W., Aragón-Durand, F., Cramer, W.,
1751 Humphreys, S., . . . Zickfeld, K. (2018). Framing and context. In V. Masson-
1752 Delmotte et al. (Eds.), *Global warming of 1.5°c* (chap. 1). Cambridge, United
1753 Kingdom and New York, NY, USA: Cambridge University Press.
- 1754 Alterskjær, K., Kristjánsson, J. E., & Seland, Ø. (2012). Sensitivity to deliber-
1755 ate sea salt seeding of marine clouds – observations and model simulations. *At-
1756 mospheric Chemistry and Physics*, 12(5), 2795–2807. Retrieved from [https://
1757 www.atmos-chem-phys.net/12/2795/2012/](https://www.atmos-chem-phys.net/12/2795/2012/) doi: 10.5194/acp-12-2795-2012
- 1758 Amiri-Farahani, A., Allen, R. J., Neubauer, D., & Lohmann, U. (2017). Impact
1759 of saharan dust on north atlantic marine stratocumulus clouds: importance
1760 of the semidirect effect. *Atmos. Chem. Phys.*, 17(10), 6305–6322. Re-
1761 trieved from <https://www.atmos-chem-phys.net/17/6305/2017/> doi:
1762 10.5194/acp-17-6305-2017
- 1763 Andersen, H., Cermak, J., Fuchs, J., Knutti, R., & Lohmann, U. (2017, 1). Under-
1764 standing the drivers of marine liquid-water cloud occurrence and properties
1765 with global observations using neural networks. *Atmos. Chem. Phys.*, 17(15),
1766 9535–9546. doi: 10.5194/acp-17-9535-2017
- 1767 Anderson, T. L., Charlson, R. J., Schwartz, S. E., Knutti, R., Boucher, O., Rodhe,
1768 H., & Heintzenberg, J. (2003). Climate forcing by aerosols—a hazy picture.
1769 *Science*, 300(5622), 1103–1104. Retrieved from [http://science.sciencemag
1770 .org/content/300/5622/1103](http://science.sciencemag.org/content/300/5622/1103) doi: 10.1126/science.1084777
- 1771 Anderson, T. L., Charlson, R. J., Winker, D. M., Ogren, J. A., & Holmen, K.
1772 (2003). Mesoscale variations of tropospheric aerosols. *J. Atmos. Sci.*, 60,
1773 119–136. doi: 10.1175/1520-0469(2003)060<0119:MVOTA>2.0.CO;2
- 1774 Andrews, E., Ogren, J. A., Kinne, S., & Samset, B. (2017). Comparison of aod,
1775 aaod and column single scattering albedo from aeronet retrievals and in
1776 situ profiling measurements. *Atmos. Chem. Phys.*, 17(9), 6041–6072. Re-
1777 trieved from <https://www.atmos-chem-phys.net/17/6041/2017/> doi:
1778 10.5194/acp-17-6041-2017
- 1779 Andrews, T., Forster, P. M., Boucher, O., Bellouin, N., & Jones, A. (2010). Precip-
1780 itation, radiative forcing and global temperature change. *Geophys. Res. Lett.*,
1781 37. (L14701) doi: 10.1029/2010GL043991
- 1782 Atkinson, J. D., Murray, B. J., Woodhouse, M. T., Whale, T. F., Baustian, K. J.,
1783 Carslaw, K. S., . . . Malkin, T. L. (2013, 6). The importance of feldspar for ice
1784 nucleation by mineral dust in mixed-phase clouds. *Nature*, 498(7454), 355–8.
1785 doi: 10.1038/nature12278
- 1786 Barahona, D., Molod, A., Bacmeister, J., Nenes, A., Gettelman, A., Morrison,
1787 H., . . . Eichmann, A. (2014). Development of two-moment cloud micro-
1788 physics for liquid and ice within the NASA Goddard Earth Observing System
1789 Model (GEOS-5). *Geoscientific Model Development*, 7(4), 1733–1766. Re-
1790 trieved from <https://www.geosci-model-dev.net/7/1733/2014/> doi:
1791 10.5194/gmd-7-1733-2014
- 1792 Bellouin, N., Mann, G. W., Woodhouse, M. T., Johnson, C., Carslaw, K. S., &
1793 Dalvi, M. (2013). Impact of the modal aerosol scheme GLOMAP-mode on
1794 aerosol forcing in the Hadley Centre Global Environmental Model. *Atmo-
1795 spheric Chemistry and Physics*, 13(6), 3027–3044. Retrieved from [https://
1796 www.atmos-chem-phys.net/13/3027/2013/](https://www.atmos-chem-phys.net/13/3027/2013/) doi: 10.5194/acp-13-3027-2013
- 1797 Bellouin, N., Quaas, J., Morcrette, J.-J., & Boucher, O. (2013). Estimates of aerosol
1798 radiative forcing from the MACC re-analysis. *Atmos. Chem. Phys.*, 13, 2045–
1799 2062. doi: 10.5194/acp-13-2045-2013
- 1800 Bender, F., Charlson, R., Ekman, A., & Leahy, L. (2011). Quantification of
1801 monthly mean regional-scale albedo of marine stratiform clouds in satellite

- 1802 observations and GCMs. *J. Appl. Meteor. Climatol.*, *50*, 2139-2148. doi:
1803 10.1175/JAMC-D-11-049.1
- 1804 Benedetti, A., Morcrette, J.-J., Boucher, O., Dethof, A., Engelen, R. J., Fisher, M.,
1805 ... Suttie, M. (2009). Aerosol analysis and forecast in the European Centre
1806 for Medium-Range Weather Forecasts Integrated Forecast System: 2. data
1807 assimilation. *J. Geophys. Res. Atmos.*, *114*(D13). Retrieved from [https://](https://agupubs.onlinelibrary.wiley.com/doi/abs/10.1029/2008JD011115)
1808 agupubs.onlinelibrary.wiley.com/doi/abs/10.1029/2008JD011115 doi:
1809 10.1029/2008JD011115
- 1810 Beven, K., & Freer, J. (2001). Equifinality, data assimilation, and uncertainty es-
1811 timation in mechanistic modelling of complex environmental systems using
1812 the glue methodology. *Journal of Hydrology*, *249*(1), 11 - 29. Retrieved from
1813 <http://www.sciencedirect.com/science/article/pii/S0022169401004218>
1814 doi: [https://doi.org/10.1016/S0022-1694\(01\)00421-8](https://doi.org/10.1016/S0022-1694(01)00421-8)
- 1815 Bindoff, N., Stott, P., AchutaRao, K., Allen, M., Gillett, N., Gutzler, D., ... Zhang,
1816 X. (2013). Detection and attribution of climate change: from global to re-
1817 gional. In T. Stocker et al. (Eds.), *Climate change 2013: The physical sci-*
1818 *ence basis. contribution of working group i to the fifth assessment report of*
1819 *the intergovernmental panel on climate change* (pp. 867–952). Cambridge,
1820 United Kingdom and New York, NY, USA: Cambridge University Press. doi:
1821 10.1017/CBO9781107415324.022
- 1822 Bloch, M. R. (1965). A hypothesis for the change of ocean levels depending on the
1823 albedo of the polar ice caps. *Palaeogeogr. Palaeocl.*, *1*, 127–142.
- 1824 Blossey, P. N., Bretherton, C. S., Thornton, J. A., & Virts, K. S. (2018). Lo-
1825 cally enhanced aerosols over a shipping lane produce convective invigora-
1826 tion but weak overall indirect effects in cloud-resolving simulations. *Geo-*
1827 *physical Research Letters*, *45*(17), 9305-9313. Retrieved from [https://](https://agupubs.onlinelibrary.wiley.com/doi/abs/10.1029/2018GL078682)
1828 agupubs.onlinelibrary.wiley.com/doi/abs/10.1029/2018GL078682 doi:
1829 10.1029/2018GL078682
- 1830 Bogenschutz, P. A., Gettelman, A., Morrison, H., Larson, V. E., Craig, C., & Scha-
1831 nen, D. P. (2013). Higher-order turbulence closure and its impact on climate
1832 simulations in the Community Atmosphere Model. *Journal of Climate*, *26*(23),
1833 9655–9676. Retrieved from <https://doi.org/10.1175/JCLI-D-13-00075.1>
1834 doi: 10.1175/JCLI-D-13-00075.1
- 1835 Bollasina, M. A., Ming, Y., & Ramaswamy, V. (2011). Anthropogenic aerosols and
1836 the weakening of the South Asian summer monsoon. *Science*, *334*, 502–505.
1837 doi: 10.1126/science.1204994
- 1838 Bond, T. C., Doherty, S. J., Fahey, D. W., Forster, P. M., Berntsen, T., DeAngelo,
1839 B. J., ... Zender, C. S. (2013). Bounding the role of black carbon in the
1840 climate system: A scientific assessment. *J. Geophys. Res. Atmos.*, *118*(11),
1841 5380-5552. doi: 10.1002/jgrd.50171
- 1842 Booth, B., Harris, G., Jones, A., Wilcox, L., Hawcroft, M., & Carslaw, K. (2018).
1843 Comments on “rethinking the lower bound on aerosol radiative forcing”. *J.*
1844 *Climate*, *31*, 9407–9412. doi: 10.1175/JCLI-D-17-0369.1
- 1845 Boucher, O., & Haywood, J. (2001, Dec 01). On summing the components
1846 of radiative forcing of climate change. *Climate Dynamics*, *18*(3), 297–
1847 302. Retrieved from <https://doi.org/10.1007/s003820100185> doi:
1848 10.1007/s003820100185
- 1849 Boucher, O., & Lohmann, U. (1995). The sulfate-ccn-cloud albedo effect. *Tellus B*,
1850 *47*(3), 281-300. doi: 10.1034/j.1600-0889.47.issue3.1.x
- 1851 Boucher, O., & Quaas, J. (2013). Water vapour affects both rain and aerosol optical
1852 depth. *Nature Geosci.*, *6*, 4-5. doi: 10.1038/ngeo1692
- 1853 Boucher, O., Randall, D., Artaxo, P., Bretherton, C., Feingold, G., Forster, P., ...
1854 Zhang, X. (2013). Clouds and aerosols. In T. Stocker et al. (Eds.), *Climate*
1855 *change 2013: The physical science basis. contribution of working group i to the*
1856 *fifth assessment report of the intergovernmental panel on climate change* (pp.

- 1857 571–658). Cambridge, United Kingdom and New York, NY, USA: Cambridge
 1858 University Press. doi: 10.1017/CBO9781107415324.016
- 1859 Boucher, O., Schwartz, S. E., Ackerman, T. P., Anderson, T. L., Bergstrom, B.,
 1860 Bonnel, B., . . . Yang, F. (1998). Intercomparison of models representing di-
 1861 rect shortwave radiative forcing by sulfate aerosols. *J. Geophys. Res.*, *103*,
 1862 16979–16998. doi: 10.1029/98JD00997
- 1863 Brenguier, J.-L., Pawlowska, H., & Schüller, L. (2003). Cloud microphysical and
 1864 radiative properties for parameterization and satellite monitoring of the in-
 1865 direct effect of aerosol on climate. *J. Geophys. Res. Atmos.*, *108*(D15). doi:
 1866 10.1029/2002JD002682
- 1867 Brenguier, J.-L., Pawlowska, H., Schüller, L., Preusker, R., Fischer, J., & Fouquart,
 1868 Y. (2000). Radiative properties of boundary layer clouds: Droplet effective
 1869 radius versus number concentration. *J. Atmos. Sci.*, *57*, 803–821.
- 1870 Brennan, J., Kaufman, Y., Koren, I., & Rong Rong, L. (2005, 1). Aerosol-cloud
 1871 interaction-misclassification of MODIS clouds in heavy aerosol. *IEEE T.*
 1872 *Geosci. Remote*, *43*(4), 911–915. doi: 10.1109/TGRS.2005.844662
- 1873 Bretherton, C. S., Blossey, P. N., & Uchida, J. (2007). Cloud droplet sedimenta-
 1874 tion, entrainment efficiency, and subtropical stratocumulus albedo. *Geophys.*
 1875 *Res. Lett.*, *34*(3). doi: 10.1029/2006GL027648
- 1876 Campmany, E., Grainger, R. G., & Dean, S. M. (2009). Automatic detection of ship
 1877 tracks in atsr-2 satellite imagery. *Atmos. Chem. Phys.*, *8*, 1899–1905. doi: 10
 1878 .5194/acp-9-1899-2009
- 1879 Carslaw, K. S., Gordon, H., Hamilton, D. S., Johnson, J. S., Regayre, L. A., Yosh-
 1880 ioka, M., & Pringle, K. J. (2017, Mar 01). Aerosols in the pre-industrial atmo-
 1881 sphere. *Current Climate Change Reports*, *3*(1), 1–15. Retrieved from [https://](https://doi.org/10.1007/s40641-017-0061-2)
 1882 doi.org/10.1007/s40641-017-0061-2 doi: 10.1007/s40641-017-0061-2
- 1883 Carslaw, K. S., Lee, L. A., Reddington, C. L., Pringle, K. J., Rap, A., Forster,
 1884 P. M., . . . Pierce, J. R. (2013). Large contribution of natural aerosols to
 1885 uncertainty in indirect forcing. *Nature*, *503*, 67–71. doi: 10.1038/nature12674
- 1886 Chand, D., Wood, R., Anderson, T. L., Satheesh, S. K., & Charlson, R. J. (2009).
 1887 Satellite-derived direct radiative effect of aerosols dependent on cloud cover.
 1888 *Nature Geoscience*, *2*, 181–184. doi: 10.1038/ngeo437
- 1889 Chand, D., Wood, R., Ghan, S. J., Wang, M., Ovchinnikov, M., Rasch, P. J., . . .
 1890 Moore, T. (2012, 9). Aerosol optical depth increase in partly cloudy condi-
 1891 tions. *J. Geophys. Res.*, *117*(D17), 17207. doi: 10.1029/2012JD017894
- 1892 Charlson, R. J., Schwartz, S. E., Hales, J. M., Cess, R. D., Coakley, J. A., Hansen,
 1893 J. E., & Hofmann, D. J. (1992). Climate forcing by anthropogenic aerosols.
 1894 *Science*, *255*(5043), 423–430. Retrieved from [https://science.sciencemag](https://science.sciencemag.org/content/255/5043/423)
 1895 [.org/content/255/5043/423](https://science.sciencemag.org/content/255/5043/423) doi: 10.1126/science.255.5043.423
- 1896 Chen, Y.-C., Christensen, M. W., Stephens, G. L., & Seinfeld, J. H. (2014, 1).
 1897 Satellite-based estimate of global aerosol-cloud radiative forcing by marine
 1898 warm clouds. *Nat. Geosci.* doi: 10.1038/NGEO2214
- 1899 Cherian, R., Quaas, J., Salzmann, M., & Wild, M. (2014). Pollution trends over eu-
 1900 rope constrain global aerosol forcing as simulated by climate models. *Geophys.*
 1901 *Res. Lett.*, *41*, 2176–2181. doi: 10.1002/2013GL058715
- 1902 Choi, Y.-S., Lindzen, R. S., Ho, C.-H., & Kim, J. (2010, 1). Space observations
 1903 of cold-cloud phase change. *Proc. Nat. Acad. Sci. USA*, *107*(25), 11211–11216.
 1904 doi: 10.1073/pnas.1006241107
- 1905 Christensen, M. W., Chen, Y.-C., & Stephens, G. L. (2016). Aerosol indirect effect
 1906 dictated by liquid clouds. *J. Geophys. Res. Atmos.*, *121*(24), 14,636–14,650.
 1907 doi: 10.1002/2016JD025245
- 1908 Christensen, M. W., Neubauer, D., Poulsen, C. A., Thomas, G. E., McGarragh,
 1909 G. R., Povey, A. C., . . . Grainger, R. G. (2017, 1). Unveiling aerosol-cloud
 1910 interactions - part 1: Cloud contamination in satellite products enhances the
 1911 aerosol indirect forcing estimate. *Atmos. Chem. Phys.*, *17*(21), 13151–13164.

- 1912 doi: 10.5194/acp-17-13151-2017
- 1913 Christensen, M. W., & Stephens, G. L. (2011). Microphysical and macrophysical
1914 responses of marine stratocumulus polluted by underlying ships: Evidence of
1915 cloud deepening. *J. Geophys. Res.*, *116*(D3).
- 1916 Christensen, M. W., Suzuki, K., Zambri, B., & Stephens, G. L. (2014). Ship track
1917 observations of a reduced shortwave aerosol indirect effect in mixed-phase
1918 clouds. *Geophys. Res. Lett.*, *41*(19), 6970-6977. doi: 10.1002/2014GL061320
- 1919 Chung, E.-S., & Soden, B. J. (2017). Hemispheric climate shifts driven by anthro-
1920 pogenic aerosol-cloud interactions. *Nature Geosci.*, *10*, 566–571. doi: 10.1038/
1921 ngeo2988
- 1922 Chýlek, P., & Coakley, J. A. (1974). Aerosols and climate. *Science*, *183*(4120), 75–
1923 77. Retrieved from <https://science.sciencemag.org/content/183/4120/75>
1924 doi: 10.1126/science.183.4120.75
- 1925 Chylek, P., Dubey, M. K., Lohmann, U., Ramanathan, V., Kaufman, Y. J., Lesins,
1926 G., ... Olsen, S. (2006, 1). Aerosol indirect effect over the indian ocean.
1927 *Geophys. Res. Lett.*, *33*(6), L06806. doi: 10.1029/2005GL025397
- 1928 Conover, J. H. (1966). Anomalous cloud lines. *J. Atmos. Sci.*, *23*, 778–785.
- 1929 Coopman, Q., Riedi, J., Finch, D. P., & Garrett, T. J. (2018). Evidence for changes
1930 in arctic cloud phase due to long-range pollution transport. *Geophys. Res.*
1931 *Lett.*, *45*(19), 10,709-10,718. Retrieved from [https://agupubs.onlinelibrary](https://agupubs.onlinelibrary.wiley.com/doi/abs/10.1029/2018GL079873)
1932 [.wiley.com/doi/abs/10.1029/2018GL079873](https://agupubs.onlinelibrary.wiley.com/doi/abs/10.1029/2018GL079873) doi: 10.1029/2018GL079873
- 1933 Costantino, L. (2012). *Analysis of aerosol-cloud interaction from space* (Unpublished
1934 doctoral dissertation). Université de Versailles et Saint-Quentin-en-Yvelines.
- 1935 Cziczo, D. J., Froyd, K. D., Gallavardin, S. J., Moehler, O., Benz, S., Saathoff,
1936 H., & Murphy, D. M. (2009, 1). Deactivation of ice nuclei due to atmo-
1937 spherically relevant surface coatings. *Environ. Res. Lett.*, *4*(4), 044013. doi:
1938 10.1088/1748-9326/4/4/044013
- 1939 de Graaf, M., Bellouin, N., Tilstra, L. G., Haywood, J., & Stammes, P. (2014).
1940 Aerosol direct radiative effect of smoke over clouds over the southeast at-
1941 lantic ocean from 2006 to 2009. *Geophys. Res. Lett.*, *41*(21), 7723-7730.
1942 Retrieved from [https://agupubs.onlinelibrary.wiley.com/doi/abs/](https://agupubs.onlinelibrary.wiley.com/doi/abs/10.1002/2014GL061103)
1943 [10.1002/2014GL061103](https://agupubs.onlinelibrary.wiley.com/doi/abs/10.1002/2014GL061103) doi: 10.1002/2014GL061103
- 1944 DeMott, P. J., Rogers, D. C., & Kreidenweis, S. M. (1997). The susceptibility of
1945 ice formation in upper tropospheric clouds to insoluble aerosol components. *J.*
1946 *Geophys. Res.*, *102*(D16), 19575–19584. doi: 10.1029/97JD01138
- 1947 Dey, S., Di, G. L., Zhao, G., Jones, A. L., & McFarquhar, G. M. (2011). Satellite-
1948 observed relationships between aerosol and trade-wind cumulus cloud
1949 properties over the indian ocean. *Geophys. Res. Lett.*, *38*, 01804. doi:
1950 10.1029/2010GL045588
- 1951 Ding, X., Zheng, M., Yu, L., Zhang, X., Weber, R. J., Yan, B., ... Wang, X.
1952 (2008). Spatial and seasonal trends in biogenic secondary organic aerosol
1953 tracers and water-soluble organic carbon in the southeastern united states.
1954 *Environmental Science & Technology*, *42*(14), 5171-5176. Retrieved
1955 from <https://doi.org/10.1021/es7032636> (PMID: 18754365) doi:
1956 10.1021/es7032636
- 1957 Eck, T., Holben, B. N., Reid, J. S., Dubovik, O., Smirnov, A., O'Neill, N. T., ...
1958 Kinne, S. (1999). Wavelength dependence of the optical depth of biomass
1959 burning, urban, and desert dust aerosols. *J. Geophys. Res. Atmos.*, *104*(D24),
1960 31333-31349. Retrieved from [https://agupubs.onlinelibrary.wiley.com/](https://agupubs.onlinelibrary.wiley.com/doi/abs/10.1029/1999JD900923)
1961 [doi/abs/10.1029/1999JD900923](https://agupubs.onlinelibrary.wiley.com/doi/abs/10.1029/1999JD900923) doi: 10.1029/1999JD900923
- 1962 Evan, A. T., Flamant, C., Fiedler, S., & Doherty, O. (2014). An analysis of aeolian
1963 dust in climate models. *Geophys. Res. Lett.* doi: 10.1002/GL060545
- 1964 Eyring, V., Bony, S., Meehl, G. A., Senior, C. A., Stevens, B., Stouffer, R. J., &
1965 Taylor, K. E. (2016). Overview of the Coupled Model Intercomparison Project
1966 Phase 6 (CMIP6) experimental design and organization. *Geosci. Model Dev.*,

- 1967 9(5), 1937–1958. doi: 10.5194/gmd-9-1937-2016
- 1968 Fan, J., Leung, L. R., Rosenfeld, D., Chen, Q., Li, Z., Zhang, J., & Yan, H. (2013).
1969 Microphysical effects determine macrophysical response for aerosol impacts
1970 on deep convective clouds. *Proc. Nat. Acad. Sci. USA*, 110(48), E4581–
1971 E4590. Retrieved from <https://www.pnas.org/content/110/48/E4581> doi:
1972 10.1073/pnas.1316830110
- 1973 Feingold, G., Balsells, J., Glassmeier, F., Yamaguchi, T., Kazil, J., & McComiskey,
1974 A. (2017). Analysis of albedo versus cloud fraction relationships in liq-
1975 uid water clouds using heuristic models and large eddy simulation. *J.*
1976 *Geophys. Res. Atmos.*, 122(13), 7086–7102. Retrieved from [https://](https://agupubs.onlinelibrary.wiley.com/doi/abs/10.1002/2017JD026467)
1977 agupubs.onlinelibrary.wiley.com/doi/abs/10.1002/2017JD026467 doi:
1978 10.1002/2017JD026467
- 1979 Feingold, G., Eberhard, W. L., Veron, D. E., & Previdi, M. (2003). First measure-
1980 ments of the Twomey indirect effect using ground-based remote sensors. *Geo-*
1981 *phys. Res. Lett.*, 30, 1287. doi: 10.1029/2002GL016633
- 1982 Feingold, G., Jiang, H., & Harrington, J. Y. (2005). On smoke suppression of clouds
1983 in Amazonia. *Geophysical Research Letters*, 32(2). Retrieved from [https://](https://agupubs.onlinelibrary.wiley.com/doi/abs/10.1029/2004GL021369)
1984 agupubs.onlinelibrary.wiley.com/doi/abs/10.1029/2004GL021369 doi:
1985 10.1029/2004GL021369
- 1986 Feingold, G., Koren, I., Yamaguchi, T., & Kazil, J. (2015). On the reversibility of
1987 transitions between closed and open cellular convection. *Atmos. Chem. Phys.*,
1988 15(13), 7351–7367. Retrieved from [https://www.atmos-chem-phys.net/15/](https://www.atmos-chem-phys.net/15/7351/2015/)
1989 [7351/2015/](https://www.atmos-chem-phys.net/15/7351/2015/) doi: 10.5194/acp-15-7351-2015
- 1990 Feingold, G., Kreidenweis, S. M., Stevens, B., & Cotton, W. R. (1996). Numer-
1991 ical simulations of stratocumulus processing of cloud condensation nuclei
1992 through collision-coalescence. *Journal of Geophysical Research: Atmospheres*,
1993 101(D16), 21391–21402. doi: 10.1029/96JD01552
- 1994 Fiedler, S., Kinne, S., Huang, W. T. K., Räisänen, P., O’Donnell, D., Bellouin,
1995 N., ... Lohmann, U. (2019). Anthropogenic aerosol forcing – insights
1996 from multiple estimates from aerosol-climate models with reduced com-
1997 plexity. *Atmospheric Chemistry and Physics*, 19(10), 6821–6841. Re-
1998 trieved from <https://www.atmos-chem-phys.net/19/6821/2019/> doi:
1999 10.5194/acp-19-6821-2019
- 2000 Fiedler, S., Knippertz, P., Woodward, S., Martin, G. M., Bellouin, N., Ross, A. N.,
2001 ... Tegen, I. (2016). A process-based evaluation of dust-emitting winds in
2002 the CMIP5 simulation of HadGEM2-ES. *Clim. Dyn.*, 46(3), 1107–1130. doi:
2003 10.1007/s00382-015-2635-9
- 2004 Field, P. R., & Heymsfield, A. J. (2015). Importance of snow to global precipita-
2005 tion. *Geophys. Res. Lett.*, 42(21), 9512–9520. Retrieved from [https://agupubs](https://agupubs.onlinelibrary.wiley.com/doi/abs/10.1002/2015GL065497)
2006 [.onlinelibrary.wiley.com/doi/abs/10.1002/2015GL065497](https://agupubs.onlinelibrary.wiley.com/doi/abs/10.1002/2015GL065497) doi: 10.1002/
2007 2015GL065497
- 2008 Flanner, M. G., Zender, C. S., Randerson, J. T., & Rasch, P. J. (2007). Present-
2009 day climate forcing and response from black carbon in snow. *J. Geophys. Res.*,
2010 112. doi: 10.1029/2006JD008003
- 2011 Forster, P. (2016). Inference of climate sensitivity from analysis of Earth’s energy
2012 budget. *Annu. Rev. Earth Planet. Sci.*, 85–106. doi: 10.1146/annurev-earth
2013 -060614-105156
- 2014 Forster, P., Ramaswamy, V., Artaxo, P., Berntsen, T., Betts, R., Fahey, D., ... Dor-
2015 land, R. V. (2007). Clouds and aerosols. In S. Solomon et al. (Eds.), *Climate*
2016 *change 2007: The physical science basis. contribution of working group i to the*
2017 *fourth assessment report of the intergovernmental panel on climate change* (pp.
2018 130–234). Cambridge, United Kingdom and New York, NY, USA: Cambridge
2019 University Press.
- 2020 Garrett, T. J., Russell, L. M., Ramaswamy, V., Maria, S. F., & Huebert, B. J.
2021 (2003). Microphysical and radiative evolution of aerosol plumes over the trop-

- ical north atlantic ocean. *J. Geophys. Res. Atmos.*, *108*(D1), AAC 11-1-AAC 11-16. doi: 10.1029/2002JD002228
- Garrett, T. J., Zhao, C., Dong, X., Mace, G. G., & Hobbs, P. V. (2004). Effects of varying aerosol regimes on low-level arctic stratus. *Geophysical Research Letters*, *31*(17). doi: 10.1029/2004GL019928
- Gasparini, B., & Lohmann, U. (2016, 5). Why cirrus cloud seeding cannot substantially cool the planet. *J. Geophys. Res.*, *121*, 4877–4893. doi: 10.1002/2015JD024666
- Gassó, S. (2008). Satellite observations of the impact of weak volcanic activity on marine clouds. *J. Geophys. Res. Atmos.*, *113*(D14).
- Gottelman, A. (2015, 1). Putting the clouds back in aerosol-cloud interactions. *Atmos. Chem. Phys.*, *15*(21), 12397–12411. doi: 10.5194/acp-15-12397-2015
- Gottelman, A., Liu, X., Barahona, D., Lohmann, U., & Chen, C. (2012). Climate impacts of ice nucleation. *J. Geophys. Res.*, *117*. doi: 10.1029/2012JD017950
- Gottelman, A., & Morrison, H. (2015). Advanced two-moment bulk microphysics for global models. part I: Off-line tests and comparison with other schemes. *Journal of Climate*, *28*(3), 1268–1287. Retrieved from <https://doi.org/10.1175/JCLI-D-14-00102.1> doi: 10.1175/JCLI-D-14-00102.1
- Ghan, S., Wang, M., Zhang, S., Ferrachat, S., Gottelman, A., Griesfeller, J., ... Zhang, K. (2016, 1). Challenges in constraining anthropogenic aerosol effects on cloud radiative forcing using present-day spatiotemporal variability. *P. Natl. Acad. Sci. USA*, 201514036. doi: 10.1073/pnas.1514036113
- Ghan, S. J., & Schwartz, S. E. (2007). Aerosol properties and processes: A path from field and laboratory measurements to global climate models. *Bull. Amer. Meteorol. Soc.*, *88*, 1059–1083. doi: 10.1175/BAMS-88-7-1059
- Ginoux, P., Garbuzov, D., & Hsu, N. C. (2010). Identification of anthropogenic and natural dust sources using Moderate Resolution Imaging Spectroradiometer (MODIS) Deep Blue level 2 data. *J. Geophys. Res. Atmos.*, *115*(D5). doi: 10.1029/2009JD012398
- Ginoux, P., Prospero, J. M., Gill, T. E., Hsu, N. C., & Zhao, M. (2012). Global-scale attribution of anthropogenic and natural dust sources and their emission rates based on MODIS Deep Blue aerosol products. *Rev. Geophys.*, *50*(3). doi: 10.1029/2012RG000388
- Girard, E., Blanchet, J.-P., , Dubois, & Y. (2004). Effects of arctic sulphuric acid aerosols on wintertime low-level atmospheric ice crystals, humidity and temperature at alert, nunavut. *Atmos. Res.*, *73*, 131–148.
- Golaz, J., Horowitz, L. W., , & Levy, H. (2013). Cloud tuning in a coupled climate model: Impact on 20th century warming. *Geophys. Res. Lett.*, *40*, 2246–2251. doi: 10.1002/grl.50232
- Gonzi, S., Dubovik, O., Baumgartner, D., & Putz, E. (2007). Clear-sky aerosol radiative forcing effects based on multi-site AERONET observations over europe. *Meteorology and Atmospheric Physics*, *96*, 277–291. doi: 10.1007/s00703-006-0212-9
- Goren, T., & Rosenfeld, D. (2012). Satellite observations of ship emission induced transitions from broken to closed cell marine stratocumulus over large areas. *J. Geophys. Res. Atmos.*, *117*(D17). doi: 10.1029/2012JD017981
- Grandey, B. S., Stier, P., & Wagner, T. M. (2013, 1). Investigating relationships between aerosol optical depth and cloud fraction using satellite, aerosol reanalysis and general circulation model data. *Atmos. Chem. Phys.*, *13*(6), 3177–3184. doi: 10.5194/acp-13-3177-2013
- Grassl, H. (1975). Albedo reduction and radiative heating of clouds by absorbing aerosol particles. *Beiträge zur Physik der Atmosphäre*, *48*, 199–210.
- Gregory, J. M., Andrews, T., Good, P., Mauritsen, T., & Forster, P. M. (2016, Dec 01). Small global-mean cooling due to volcanic radiative forcing. *Clim. Dyn.*, *47*(12), 3979–3991. Retrieved from <https://doi.org/10.1007/>

- s00382-016-3055-1 doi: 10.1007/s00382-016-3055-1
- 2077 Grosvenor, D. P., Sourdeval, O., Zuidema, P., Ackerman, A., Alexandrov, M. D.,
2078 Bennartz, R., ... Quaas, J. (2018). Remote sensing of droplet number con-
2079 centration in warm clouds: A review of the current state of knowledge and
2080 perspectives. *Rev. Geophys.*, *56*, 409–453. doi: 10.1029/2017RG000593
- 2081 Gryspeerdt, E., Goren, T., Sourdeval, O., Quaas, J., Mülmenstädt, J., Dipu, S.,
2082 ... Christensen, M. (2019). Constraining the aerosol influence on cloud
2083 liquid water path. *Atmospheric Chemistry and Physics*, *19*(8), 5331–5347.
2084 Retrieved from <https://www.atmos-chem-phys.net/19/5331/2019/> doi:
2085 10.5194/acp-19-5331-2019
- 2086 Gryspeerdt, E., Mülmenstädt, J., Gettelman, A., Malavelle, F. F., Morrison, H.,
2087 Neubauer, D., ... Zhang, K. (2019). Surprising similarities in model and
2088 observational aerosol radiative forcing estimates. *Atmospheric Chemistry and*
2089 *Physics Discussions*, *2019*, 1–18. Retrieved from [https://www.atmos-chem-](https://www.atmos-chem-phys-discuss.net/acp-2019-533/)
2090 [phys-discuss.net/acp-2019-533/](https://www.atmos-chem-phys-discuss.net/acp-2019-533/) doi: 10.5194/acp-2019-533
- 2091 Gryspeerdt, E., Quaas, J., & Bellouin, N. (2016, 1). Constraining the aerosol in-
2092 fluence on cloud fraction. *J. Geophys. Res.*, *121*(7), 3566–3583. doi: 10.1002/
2093 2015JD023744
- 2094 Gryspeerdt, E., Quaas, J., Ferrachat, S., Gettelman, A., Ghan, S., Lohmann, U.,
2095 ... Zhang, K. (2017, 1). Constraining the instantaneous aerosol influence
2096 on cloud albedo. *Proc. Nat. Acad. Sci. USA*, *114*(19), 4899–4904. doi:
2097 10.1073/pnas.1617765114
- 2098 Gryspeerdt, E., Sourdeval, O., Quaas, J., Delanoë, J., Krämer, M., & Kühne, P.
2099 (2018, 1). Ice crystal number concentration estimates from lidar-radar satellite
2100 remote sensing - part 2: Controls on the ice crystal number concentration.
2101 *Atmos. Chem. Phys.*, *18*(19), 14351–14370. doi: 10.5194/acp-18-14351-2018
- 2102 Gryspeerdt, E., & Stier, P. (2012, 11). Regime-based analysis of aerosol-cloud inter-
2103 actions. *Geophys. Res. Lett.*, *39*, 21802. doi: 10.1029/2012GL053221
- 2104 Gryspeerdt, E., Stier, P., & Grandey, B. S. (2014, 1). Cloud fraction mediates the
2105 aerosol optical depth-cloud top height relationship. *Geophys. Res. Lett.*, *41*,
2106 3622–3627. doi: 10.1002/2014GL059524
- 2107 Gryspeerdt, E., Stier, P., & Partridge, D. G. (2014a, 1). Links between satellite-
2108 retrieved aerosol and precipitation. *Atmos. Chem. Phys.*, *14*(18), 9677–9694.
2109 doi: 10.5194/acp-14-9677-2014
- 2110 Gryspeerdt, E., Stier, P., & Partridge, D. G. (2014b, 1). Satellite observations of
2111 cloud regime development: the role of aerosol processes. *Atmos. Chem. Phys.*,
2112 *14*(3), 1141–1158. doi: 10.5194/acp-14-1141-2014
- 2113 Gryspeerdt, E., Stier, P., White, B. A., & Kipling, Z. (2015). Wet scavenging lim-
2114 its the detection of aerosol effects on precipitation. *Atmos. Chem. Phys.*, *15*,
2115 7557–7570. doi: 10.5194/acp-15-7557-2015
- 2116 Halthore, R. N., Crisp, D., Schwartz, S. E., Anderson, G. P., Berk, A., Bonnel, B.,
2117 ... Wiscombe, W. (2005). Intercomparison of shortwave radiative trans-
2118 fer codes and measurements. *J. Geophys. Res. Atmos.*, *110*(D11). doi:
2119 10.1029/2004JD005293
- 2120 Hamilton, D. S., Hantson, S., Scott, C. E., Kaplan, J. O., Pringle, K. J., Nieradzik,
2121 L. P., ... Carslaw, K. S. (2018). Reassessment of pre-industrial fire emissions
2122 strongly affects anthropogenic aerosol forcing. *Nature Comm.*, *9*(3182). doi:
2123 10.1038/s41467-018-05592-9
- 2124 Han, Q., Rossow, W. B., Zeng, J., & Welch, R. (2002, 1). Three different behav-
2125 iors of liquid water path of water clouds in aerosol-cloud interactions. *J. At-*
2126 *mos. Sci.*, *59*(3), 726–735. doi: 10.1175/1520-0469(2002)059<0726:TDBOLW>2
2127 .0.CO;2
- 2128 Hansen, J., Sato, M., & Ruedy, R. (1997). Radiative forcing and climate response. *J.*
2129 *Geophys. Res.*, *102*(D6), 6831–6864. doi: 10.1029/96JD03436
- 2130 Hansen, J., Sato, M., Ruedy, R., Nazarenko, L., Lacis, A., Schmidt, G. A., ...
- 2131

- 2132 Zhang, S. (2005). Efficacy of climate forcings. *J. Geophys. Res.*, *110*. doi:
2133 10.1029/2005JD005776
- 2134 Hansen, J. E., & Travis, L. D. (1974). Light scattering in planetary atmospheres.
2135 *Space Sci. Rev.*, *16*, 527–610. doi: 10.1007/BF00168069
- 2136 Hartmann, D., A.M.G. Klein T., Rusticucci, M., Alexander, L., Brönnimann, S.,
2137 Charabi, Y., . . . Zhai, P. (2013). Observations: Atmosphere and surface.
2138 In T. Stocker et al. (Eds.), *Climate change 2013: The physical science basis.*
2139 *contribution of working group i to the fifth assessment report of the intergov-*
2140 *ernmental panel on climate change.* Cambridge, United Kingdom and New
2141 York, NY, USA: Cambridge University Press, Cambridge, United Kingdom
2142 and New York, NY, USA.
- 2143 Haywood, J. (2015). Atmospheric aerosols and their role in climate change. In
2144 T. Letcher (Ed.), *Climate change, observed impacts on planet earth.* Cam-
2145 bridge, United Kingdom and New York, NY, USA: Elsevier.
- 2146 Haywood, J., Francis, P., Osborne, S., Glew, M., Loeb, N., Highwood, E., . . .
2147 Hirst, E. (2003). Radiative properties and direct radiative effect of sa-
2148 haran dust measured by the c-130 aircraft during shade: 1. solar spec-
2149 trum. *J. Geophys. Res. Atmos.*, *108*(D18). Retrieved from [https://](https://agupubs.onlinelibrary.wiley.com/doi/abs/10.1029/2002JD002687)
2150 agupubs.onlinelibrary.wiley.com/doi/abs/10.1029/2002JD002687 doi:
2151 10.1029/2002JD002687
- 2152 Haywood, J. M., Ramaswamy, V., & Donner, L. J. (1997, 1). A limited-area-model
2153 case study of the effects of sub-grid scale variations in relative humidity and
2154 cloud upon the direct radiative forcing of sulfate aerosol. *Geophys. Res. Lett.*,
2155 *24*(2), 143–146. doi: 10.1029/96GL03812
- 2156 Haywood, J. M., Ramaswamy, V., & Soden, B. J. (1999). Tropospheric aerosol
2157 climate forcing in clear-sky satellite observations over the oceans. *Science*,
2158 *283*(5406), 1299–1303. Retrieved from [http://science.sciencemag.org/](http://science.sciencemag.org/content/283/5406/1299)
2159 [content/283/5406/1299](http://science.sciencemag.org/content/283/5406/1299) doi: 10.1126/science.283.5406.1299
- 2160 Haywood, J. M., & Shine, K. P. (1995). The effect of anthropogenic sulfate and
2161 soot aerosol on the clear sky planetary radiation budget. *Geophys. Res. Lett.*,
2162 *22*(5), 603–606. doi: 10.1029/95GL00075
- 2163 Heyn, I., Block, K., Mülmenstädt, J., Gryspeerd, E., Kühne, P., Salzmann, M., &
2164 Quaas, J. (2017, 1). Assessment of simulated aerosol effective radiative forc-
2165 ings in the terrestrial spectrum. *Geophys. Res. Lett.*, *44*(2), 1001–1007. doi:
2166 10.1002/2016GL071975
- 2167 Hill, A. A., Feingold, G., & Jiang, H. (2009). The influence of entrainment and mix-
2168 ing assumption on aerosol-cloud interactions in marine stratocumulus. *J. At-*
2169 *mos. Sci.*, *66*(5), 1450–1464. doi: 10.1175/2008JAS2909.1
- 2170 Hobbs, P. V., Radke, L. F., & Shumway, S. E. (1970). Cloud condensation nuclei
2171 from industrial sources and their apparent influence on precipitation in wash-
2172 ington state. *J. Atmos. Sci.*, *27*, 81–89. doi: 10.1175/1520-0469(1970)027<0091:
2173 CCNFIS>2.0.CO;2
- 2174 Hodnebrog, Ø., Myhre, G., & Samset, B. (2014). How shorter black carbon lifetime
2175 alters its climate effect. *Nature Comm.*, *5*(5065). doi: [https://doi.org/10.1038/](https://doi.org/10.1038/ncomms6065)
2176 [ncomms6065](https://doi.org/10.1038/ncomms6065)
- 2177 Hoesly, R. M., Smith, S. J., Feng, L., Klimont, Z., Janssens-Maenhout, G., Pitkanen,
2178 T., . . . Zhang, Q. (2018). Historical (1750–2014) anthropogenic emissions
2179 of reactive gases and aerosols from the community emissions data system
2180 (ceds). *Geosci. Model Devel.*, *11*(1), 369–408. Retrieved from [https://](https://www.geosci-model-dev.net/11/369/2018/)
2181 www.geosci-model-dev.net/11/369/2018/ doi: 10.5194/gmd-11-369-2018
- 2182 Holben, B., Eck, T., Slutsker, I., Tanré, D., Buis, J., Setzer, A., . . . Smirnov, A.
2183 (1998). Aeronet – a federated instrument network and data archive for aerosol
2184 characterization. *Remote Sens. Environ.*, *66*(1), 1 - 16. Retrieved from
2185 <http://www.sciencedirect.com/science/article/pii/S0034425798000315>
2186 doi: [https://doi.org/10.1016/S0034-4257\(98\)00031-5](https://doi.org/10.1016/S0034-4257(98)00031-5)

- 2187 Hoose, C., Lohmann, U., Stier, P., Verheggen, B., & Weingartner, E. (2008). Aerosol
2188 processing in mixed-phase clouds in ECHAM5-HAM: Model description
2189 and comparison to observations. *J. Geophys. Res. Atmos.*, *113*(D7). doi:
2190 10.1029/2007JD009251
- 2191 Hoose, C., & Möhler, O. (2012, 10). Heterogeneous ice nucleation on atmospheric
2192 aerosols: a review of results from laboratory experiments. *Atmos. Chem.*
2193 *Phys.*, *12*, 9817–9854. doi: 10.5194/acp-12-9817-2012
- 2194 Hu, Y., Rodier, S., Xu, K.-m., Sun, W., Huang, J., Lin, B., ... Josset, D. (2010).
2195 Occurrence, liquid water content, and fraction of supercooled water clouds
2196 from combined caliop/iir/modis measurements. *J. Geophys. Res. Atmos.*,
2197 *115*(D4). Retrieved from [https://agupubs.onlinelibrary.wiley.com/doi/](https://agupubs.onlinelibrary.wiley.com/doi/abs/10.1029/2009JD012384)
2198 [abs/10.1029/2009JD012384](https://agupubs.onlinelibrary.wiley.com/doi/abs/10.1029/2009JD012384) doi: 10.1029/2009JD012384
- 2199 Huang, J. P., Liu, J. J., Chen, B., & Nasiri, S. L. (2015). Detection of anthropogenic
2200 dust using CALIPSO lidar measurements. *Atmos. Chem. Phys.*, *15*(20),
2201 11653–11665. doi: 10.5194/acp-15-11653-2015
- 2202 Jacobson, M. Z., & Seinfeld, J. H. (2004). Evolution of nanoparticle size and mix-
2203 ing state near the point of emission. *Atmos. Environ.*, *38*, 1839–1850. doi: 10
2204 .1016/j.atmosenv.2004.01.014
- 2205 Jensen, E. J., Diskin, G., Lawson, R. P., Lance, S., Bui, T. P., Hlavka, D., ... Gao,
2206 R. (2013, 1). Ice nucleation and dehydration in the tropical tropopause layer.
2207 *Proc. Nat. Acad. Sci. USA*, *110*(6), 2041–2046. doi: 10.1073/pnas.1217104110
- 2208 Jensen, E. J., Ueyama, R., Pfister, L., Bui, T. V., Lawson, R. P., Woods, S., ... Av-
2209 ery, M. A. (2016, 1). On the susceptibility of cold tropical cirrus to ice nuclei
2210 abundance. *J. Atmos. Sci.*, *73*(6), 2445–2464. doi: 10.1175/JAS-D-15-0274.1
- 2211 Jiao, C., Flanner, M. G., Balkanski, Y., Bauer, S. E., Bellouin, N., Berntsen,
2212 T. K., ... Zhang, K. (2014). An AeroCom assessment of black carbon
2213 in Arctic snow and sea ice. *Atmos. Chem. Phys.*, *14*, 2399–2417. doi:
2214 10.5194/acp-14-2399-2014
- 2215 Jing, X., & Suzuki, K. (2018, 1). The impact of process-based warm rain con-
2216 straints on the aerosol indirect effect. *Geophys. Res. Lett.* doi: 10.1029/
2217 2018GL079956
- 2218 Johnson, B. T., Shine, K. P., & Forster, P. M. (2004). The semi-direct aerosol effect:
2219 Impact of absorbing aerosols on marine stratocumulus. *Quart. J. Roy. Meteorol.*
2220 *Soc.*, *130*(599), 1407–1422. Retrieved from [https://rmets.onlinelibrary](https://rmets.onlinelibrary.wiley.com/doi/abs/10.1256/qj.03.61)
2221 [.wiley.com/doi/abs/10.1256/qj.03.61](https://rmets.onlinelibrary.wiley.com/doi/abs/10.1256/qj.03.61) doi: 10.1256/qj.03.61
- 2222 Johnson, J. S., Regayre, L. A., Yoshioka, M., Pringle, K. J., Lee, L. A., Sexton,
2223 D. M. H., ... Carslaw, K. S. (2018). The importance of comprehensive pa-
2224 rameter sampling and multiple observations for robust constraint of aerosol
2225 radiative forcing. *Atmospheric Chemistry and Physics*, *18*(17), 13031–13053.
2226 Retrieved from <https://www.atmos-chem-phys.net/18/13031/2018/> doi:
2227 10.5194/acp-18-13031-2018
- 2228 Jones, G. S., Stott, P. A., & Mitchell, J. F. B. (2016). Uncertainties in the attri-
2229 bution of greenhouse gas warming and implications for climate prediction. *J.*
2230 *Geophys. Res. Atmos.*, *121*, 6969–6992. doi: 10.1002/2015JD024337
- 2231 Kacenelenbogen, M. S., Vaughan, M. A., Redemann, J., Young, S. A., Liu, Z., Hu,
2232 Y., ... Powell, K. A. (2019). Estimations of global shortwave direct aerosol
2233 radiative effects above opaque water clouds using a combination of A-Train
2234 satellite sensors. *Atmospheric Chemistry and Physics*, *19*(7), 4933–4962.
2235 Retrieved from <https://www.atmos-chem-phys.net/19/4933/2019/> doi:
2236 10.5194/acp-19-4933-2019
- 2237 Kanitz, T., Seifert, P., Ansmann, A., Engelmann, R., Althausen, D., Casiccia, C., &
2238 Rohwer, E. G. (2011, 1). Contrasting the impact of aerosols at northern and
2239 southern midlatitudes on heterogeneous ice formation. *Geophys. Res. Lett.*,
2240 *38*(17). doi: 10.1029/2011GL048532
- 2241 Kanji, Z. A., Ladino, L. A., Wex, H., Boose, Y., Burkert-Kohn, M., Cziczo, D. J., &

- 2242 Krämer, M. (2017, 1). Overview of ice nucleating particles. *Met. Mono.*, *58*,
 2243 1.1–1.33. doi: 10.1175/AMSMONOGRAPHS-D-16-0006.1
- 2244 Kärcher, B., & Lohmann, U. (2003). A parameterization of cirrus cloud forma-
 2245 tion: Heterogeneous freezing. *J. Geophys. Res.*, *108*(D14), 4402. doi: 10.1029/
 2246 2002JD003220
- 2247 Kasoar, M., Shawki, D., & Voulgarikis, A. (2018). Similar spatial patterns of
 2248 global climate response to aerosols from different regions. *npj Climate and
 2249 Atmospheric Science*, *1*(12). Retrieved from [https://doi.org/10.1038/
 2250 s41612-018-0022-z](https://doi.org/10.1038/s41612-018-0022-z) doi: 10.1038/s41612-018-0022-z
- 2251 Kaufman, Y. J., & Koren, I. (2006, 8). Smoke and pollution aerosol effect on cloud
 2252 cover. *Science*, *313*(5787), 655–8. doi: 10.1126/science.1126232
- 2253 Kaufman, Y. J., Koren, I., Remer, L. A., Rosenfeld, D., & Rudich, Y. (2005).
 2254 The effect of smoke, dust, and pollution aerosol on shallow cloud develop-
 2255 ment over the atlantic ocean. *Proc. Nat. Acad. Sci. USA*, *102*, 11207. doi:
 2256 10.1073/pnas.0505191102
- 2257 Kay, J. E., & Wood, R. (2008, 5). Timescale analysis of aerosol sensitivity during
 2258 homogeneous freezing and implications for upper tropospheric water vapor
 2259 budgets. *Geophys. Res. Lett.*, *35*, L10809. doi: 10.1029/2007GL032628
- 2260 Keil, A., & Haywood, J. M. (2003). Solar radiative forcing by biomass burn-
 2261 ing aerosol particles during safari 2000: A case study based on measured
 2262 aerosol and cloud properties. *J. Geophys. Res. Atmos.*, *108*(D13). Retrieved
 2263 from [https://agupubs.onlinelibrary.wiley.com/doi/abs/10.1029/
 2264 2002JD002315](https://agupubs.onlinelibrary.wiley.com/doi/abs/10.1029/2002JD002315) doi: 10.1029/2002JD002315
- 2265 Khain, A. P., Rosenfeld, D., & Pokrovsky, A. (2001). Simulating convective clouds
 2266 with sustained supercooled liquid water down to -37.5°C using a spectral mi-
 2267 crophysics model. *Geophysical Research Letters*, *28*(20), 3887–3890. Retrieved
 2268 from [https://agupubs.onlinelibrary.wiley.com/doi/abs/10.1029/
 2269 2000GL012662](https://agupubs.onlinelibrary.wiley.com/doi/abs/10.1029/2000GL012662) doi: 10.1029/2000GL012662
- 2270 Khairoutdinov, M., & Kogan, Y. (2000, 1). A new cloud physics parameterization
 2271 in a large-eddy simulation model of marine stratocumulus. *Mon. Wea. Rev.*,
 2272 *128*(1), 229–243. doi: 10.1175/1520-0493(2000)128<0229:ANCPPI>2.0.CO;2
- 2273 Kim, B.-G., Miller, M. A., Schwartz, S. E., Liu, Y., & Min, Q. (2008). The role of
 2274 adiabaticity in the aerosol first indirect effect. *Journal of Geophysical Research:
 2275 Atmospheres*, *113*(D5). doi: 10.1029/2007JD008961
- 2276 Kim, B.-G., Schwartz, S. E., Miller, M. A., & Min, Q. (2003). Effective radius of
 2277 cloud droplets by ground-based remote sensing: Relationship to aerosol. *J.
 2278 Geophys. Res. Atmos.*, *108*(D23). doi: 10.1029/2003JD003721
- 2279 King, M. D., Kaufman, Y. J., Tané, D., & Nakajima, T. (1999). Remote sensing
 2280 of tropospheric aerosols from space: Past, present, and future. *Bull. Amer.
 2281 Meteorol. Soc.*, *80*(11), 2229–2260. doi: 10.1175/1520-0477(1999)080<2229:
 2282 RSOTAF>2.0.CO;2
- 2283 Kinne, S. (2019). Aerosol radiative effects with MACv2. *Atmospheric Chemistry and
 2284 Physics*, *19*(16), 10919–10959. Retrieved from [https://www.atmos-chem-phys
 2285 .net/19/10919/2019/](https://www.atmos-chem-phys.net/19/10919/2019/) doi: 10.5194/acp-19-10919-2019
- 2286 Kinne, S., O’Donnell, D., Stier, P., Kloster, S., Zhang, K., Schmidt, H., ... Stevens,
 2287 B. (2013). MAC-v1: A new global aerosol climatology for climate studies. *J.
 2288 Adv. Model. Earth Syst.*, *5*(4), 704–740. doi: 10.1002/jame.20035
- 2289 Kinne, S., Schulz, M., Textor, C., Guibert, S., Balkanski, Y., Bauer, S. E., ... Tie,
 2290 X. (2006). An aerocom initial assessment optical properties in aerosol com-
 2291 ponent modules of global models. *Atmos. Chem. Phys.*, *6*, 1815–1834. doi:
 2292 10.5194/acp-6-1815-2006
- 2293 Kipling, Z., Stier, P., Schwarz, J. P., Perring, A. E., Spackman, J. R., Mann,
 2294 G. W., ... Telford, P. J. (2013). Constraints on aerosol processes in cli-
 2295 mate models from vertically-resolved aircraft observations of black car-
 2296 bon. *Atmos. Chem. Phys.*, *13*(12), 5969–5986. Retrieved from <https://>

- 2297 www.atmos-chem-phys.net/13/5969/2013/ doi: 10.5194/acp-13-5969-2013
- 2298 Kirkby, J., Duplissy, J., Sengupta, K., Frege, C., Gordon, H., Williamson, C., ...
- 2299 Curtius, J. (2016). Ion-induced nucleation of pure biogenic particles. *Nature*,
- 2300 *533*, 521–526. doi: 10.1038/nature17953
- 2301 Kittaka, C., Winker, D. M., Vaughan, M. A., Omar, A., & Remer, L. A. (2011).
- 2302 Intercomparison of column aerosol optical depths from calipso and modis-
- 2303 aqua. *Atmos. Meas. Tech.*, *4*(2), 131–141. Retrieved from [https://](https://www.atmos-meas-tech.net/4/131/2011/)
- 2304 www.atmos-meas-tech.net/4/131/2011/ doi: 10.5194/amt-4-131-2011
- 2305 Klein, S. A., & Hall, A. (2015, Dec 01). Emergent constraints for cloud feedbacks.
- 2306 *Current Climate Change Reports*, *1*(4), 276–287. doi: 10.1007/s40641-015-0027
- 2307 -1
- 2308 Knutti, R., Rugenstein, M. A. A., & Hegerl, G. C. (2017). Beyond equilibrium cli-
- 2309 mate sensitivity. *Nature Geoscience*, *10*, 727–736. doi: 10.1038/ngeo3017
- 2310 Knutti, R., Stocker, T. F., Joos, F., & Plattner, G.-K. (2002). Constraints on ra-
- 2311 diative forcing and future climate change from observations and climate model
- 2312 ensembles. *Nature*, *416*, 719–723. doi: 10.1038/416719a
- 2313 Koch, D., & Del Genio, A. D. (2010). Black carbon absorption effects on cloud
- 2314 cover: Review and synthesis. *Atmos. Chem. Phys.*, *10*, 7685–7696. doi: 10
- 2315 .5194/acp-10-7685-2010
- 2316 Koffi, B., Schulz, M., Bréon, F.-M., Dentener, F., Steensen, B. M., Griesfeller, J.,
- 2317 ... Zhang, K. (2016). Evaluation of the aerosol vertical distribution in global
- 2318 aerosol models through comparison against CALIOP measurements: AeroCom
- 2319 phase II results. *J. Geophys. Res. Atmos.*, *121*(12), 7254–7283. Retrieved
- 2320 from [https://agupubs.onlinelibrary.wiley.com/doi/abs/10.1002/](https://agupubs.onlinelibrary.wiley.com/doi/abs/10.1002/2015JD024639)
- 2321 [2015JD024639](https://agupubs.onlinelibrary.wiley.com/doi/abs/10.1002/2015JD024639) doi: 10.1002/2015JD024639
- 2322 Köhler, H. (1936). The nucleus in and the growth of hygroscopic droplets. *Trans.*
- 2323 *Farad. Soc.*, *32*, 1152–1161.
- 2324 Köhler, H. (1936). The nucleus in and the growth of hygroscopic droplets. *Trans.*
- 2325 *Faraday Soc.*, *32*, 1152–1161. doi: 10.1039/TF9363201152
- 2326 Kok, J. F., Ward, D. S., Mahowald, N. M., & Evan, A. T. (2018). Global and re-
- 2327 gional importance of the direct dust-climate feedback. *Nature Comm.*, *9*(1),
- 2328 241.
- 2329 Koren, I., Feingold, G., & Remer, L. A. (2010). The invigoration of deep con-
- 2330 vective clouds over the atlantic: aerosol effect, meteorology or retrieval arti-
- 2331 fact? *Atmos. Chem. Phys.*, *10*(18), 8855–8872. Retrieved from [https://](https://www.atmos-chem-phys.net/10/8855/2010/)
- 2332 www.atmos-chem-phys.net/10/8855/2010/ doi: 10.5194/acp-10-8855-2010
- 2333 Koren, I., Kaufman, Y. J., Remer, L. A., & Martins, J. V. (2004). Measurement
- 2334 of the effect of amazon smoke on inhibition of cloud formation. *Science*,
- 2335 *303*(5662), 1342–1345. Retrieved from [http://science.sciencemag.org/](http://science.sciencemag.org/content/303/5662/1342)
- 2336 [content/303/5662/1342](http://science.sciencemag.org/content/303/5662/1342) doi: 10.1126/science.1089424
- 2337 Koren, I., Kaufman, Y. J., Rosenfeld, D., Remer, L. A., & Rudich, Y. (2005).
- 2338 Aerosol invigoration and restructuring of atlantic convective clouds. *Geophys.*
- 2339 *Res. Lett.*, *32*, 14828. doi: 10.1029/2005GL023187
- 2340 Koren, I., Remer, L. A., Altaratz, O., Martins, J. V., & Davidi, A. (2010, 1).
- 2341 Aerosol-induced changes of convective cloud anvils produce strong cli-
- 2342 mate warming. *Atmos. Chem. Phys.*, *10*(10), 5001–5010. doi: 10.5194/
- 2343 acp-10-5001-2010
- 2344 Krämer, M., Rolf, C., Luebke, A., Afchine, A., Spelten, N., Costa, A., ... Avallone,
- 2345 L. (2016, 1). A microphysics guide to cirrus clouds - part 1: Cirrus types.
- 2346 *Atmos. Chem. Phys.*, *16*(5), 3463–3483. doi: 10.5194/acp-16-3463-2016
- 2347 Kravitz, B., Robock, A., Tilmes, S., Boucher, O., English, J., Irvine, P., ... Watan-
- 2348 abe, S. (2015). The Geoengineering Model Intercomparison Project Phase 6
- 2349 (GeoMIP6): Simulation design and preliminary results. *Geosci. Model Devel.*,
- 2350 *8*, 3379–3392.
- 2351 Kretzschmar, J., Salzmann, M., Mülmenstädt, J., Boucher, O., & Quaas, J. (2017).

- 2352 Comment on “rethinking the lower bound on aerosol radiative forcing”. *J. Cli-*
 2353 *mate*, *30*, 6579–6584. doi: 10.1175/JCLI-D-16-0668.1
- 2354 Kristiansen, N. I., Stohl, A., & Wotawa, G. (2012). Atmospheric removal
 2355 times of the aerosol-bound radionuclides ^{137}Cs and ^{131}I measured after
 2356 the Fukushima Dai-ichi nuclear accident – a constraint for air quality
 2357 and climate models. *Atmos. Chem. Phys.*, *12*(22), 10759–10769. Re-
 2358 trieved from <https://www.atmos-chem-phys.net/12/10759/2012/> doi:
 2359 10.5194/acp-12-10759-2012
- 2360 Kuebbeler, M., Lohmann, U., Hendricks, J., & Kärcher, B. (2014). Dust ice nuclei
 2361 effects on cirrus clouds. *Atmos. Chem. Phys.*, *14*, 3027–3046. doi: 10.5194/acp-
 2362 -14-3027-2014
- 2363 Kulmala, M., Asmi, A., Lappalainen, H. K., Baltensperger, U., Brenguier, J.-
 2364 L., Facchini, M. C., ... Pandis, S. N. (2011). General overview: Euro-
 2365 pean integrated project on aerosol cloud climate and air quality interac-
 2366 tions (eucaari); integrating aerosol research from nano to global scales. *At-*
 2367 *mospheric Chemistry and Physics*, *11*(24), 13061–13143. Retrieved from
 2368 <https://www.atmos-chem-phys.net/11/13061/2011/> doi: 10.5194/
 2369 acp-11-13061-2011
- 2370 Lamarque, J.-F., Bond, T. C., Eyring, V., Granier, C., Heil, A., Klimont, Z., ...
 2371 van Vuuren, D. P. (2010). Historical (1850–2000) gridded anthropogenic
 2372 and biomass burning emissions of reactive gases and aerosols: method-
 2373 ology and application. *Atmos. Chem. Phys.*, *10*(15), 7017–7039. Re-
 2374 trieved from <https://www.atmos-chem-phys.net/10/7017/2010/> doi:
 2375 10.5194/acp-10-7017-2010
- 2376 Leahy, L. V., Anderson, T. L., Eck, T. F., & Bergstrom, R. W. (2007). A syn-
 2377 thesis of single scattering albedo of biomass burning aerosol over southern
 2378 africa during SAFARI 2000. *Geophysical Research Letters*, *34*(12). doi:
 2379 10.1029/2007GL029697
- 2380 Lebsock, M., Stephens, G., & Kummerow, C. (2008). Multisensor satellite observa-
 2381 tions of aerosol effects on warm clouds. *J. Geophys. Res.*, *113*, D15205. doi: 10
 2382 .1029/2008JD009876
- 2383 Lee, L. A., Carslaw, K. S., Pringle, K. J., Mann, G. W., & Spracklen, D. V.
 2384 (2011). Emulation of a complex global aerosol model to quantify sensitivity
 2385 to uncertain parameters. *Atmos. Chem. Phys.*, *11*(23), 12253–12273. Re-
 2386 trieved from <https://www.atmos-chem-phys.net/11/12253/2011/> doi:
 2387 10.5194/acp-11-12253-2011
- 2388 Lee, Y. H., Adams, P. J., & Shindell, D. T. (2015). Evaluation of the global
 2389 aerosol microphysical ModelE2-TOMAS model against satellite and ground-
 2390 based observations. *Geoscientific Model Development*, *8*(3), 631–667. Re-
 2391 trieved from <https://www.geosci-model-dev.net/8/631/2015/> doi:
 2392 10.5194/gmd-8-631-2015
- 2393 Levy, R. C., Mattoo, S., Munchak, L. A., Remer, L. A., Sayer, A. M., Patadia,
 2394 F., & Hsu, N. C. (2013). The collection 6 modis aerosol products over
 2395 land and ocean. *Atmospheric Measurement Techniques*, *6*(11), 2989–3034.
 2396 Retrieved from <https://www.atmos-meas-tech.net/6/2989/2013/> doi:
 2397 10.5194/amt-6-2989-2013
- 2398 Li, J., Jian, B., Huang, J., Hu, Y., Zhao, C., Kawamoto, K., ... Wu, M. (2018).
 2399 Long-term variation of cloud droplet number concentrations from space-based
 2400 lidar [Journal Article]. *Remote Sensing of Environment*, *213*, 144–161.
- 2401 Liu, X., Easter, R. C., Ghan, S. J., Zaveri, R., Rasch, P., Shi, X., ... Mitchell,
 2402 D. (2012). Toward a minimal representation of aerosols in climate mod-
 2403 els: description and evaluation in the Community Atmosphere Model CAM5.
 2404 *Geoscientific Model Development*, *5*(3), 709–739. Retrieved from [https://](https://www.geosci-model-dev.net/5/709/2012/)
 2405 www.geosci-model-dev.net/5/709/2012/ doi: 10.5194/gmd-5-709-2012
- 2406 Loeb, N., Manalo-Smith, N., Su, W., Shankar, M., & Thomas, S. (2016). CERES

- 2407 top-of-atmosphere earth radiation budget climate data record: Accounting
 2408 for in-orbit changes in instrument calibration. *Remote Sens.*, 8, 182. doi:
 2409 10.3390/rs8030182
- 2410 Loeb, N. G., & Schuster, G. L. (2008, 7). An observational study of the relationship
 2411 between cloud, aerosol and meteorology in broken low-level cloud conditions.
 2412 *J. Geophys. Res.*, 113, 14214. doi: 10.1029/2007JD009763
- 2413 Lohmann, U. (2002). A glaciation indirect aerosol effect caused by soot aerosols.
 2414 *Geophys. Res. Lett.*, 29(4). doi: 10.1029/2001GL014357
- 2415 Lohmann, U. (2008). Global anthropogenic aerosol effects on convective clouds in
 2416 ecam5-ham. *Atmos. Chem. Phys.*, 8(7), 2115–2131. Retrieved from [https://](https://www.atmos-chem-phys.net/8/2115/2008/)
 2417 www.atmos-chem-phys.net/8/2115/2008/ doi: 10.5194/acp-8-2115-2008
- 2418 Lohmann, U. (2017). Anthropogenic aerosol influences on mixed-phased clouds.
 2419 *Curr. Clim. Change Rep.*, 3, 32-44. doi: 10.1007/s40641-017-0059-9
- 2420 Lohmann, U., & Feichter, J. (2001). Can the direct and semi-direct aerosol effect
 2421 compete with the indirect effect on a global scale? *Geophys. Res. Lett.*, 28(1),
 2422 159-161. doi: 10.1029/2000GL012051
- 2423 Lohmann, U., & Kärcher, B. (2002, 1). First interactive simulations of cirrus clouds
 2424 formed by homogeneous freezing in the ECHAM general circulation model. *J.*
 2425 *Geophys. Res.*, 107(D10). doi: 10.1029/2001JD000767
- 2426 Lohmann, U., & Lesins, G. (2002). Stronger constraints on the anthropogenic in-
 2427 direct aerosol effect. *Science*, 298(5595), 1012–1015. doi: 10.1126/science
 2428 .1075405
- 2429 Lowenthal, D. H., Borys, R. D., Choulaton, T. W., Bower, K. N., Flynn, M. J.,
 2430 & Gallagher, M. W. (2004). Parameterization of the cloud droplet-
 2431 sulfate relationship. *Atmos. Environ.*, 38(2), 287 - 292. Retrieved from
 2432 <http://www.sciencedirect.com/science/article/pii/S1352231003008082>
 2433 doi: <https://doi.org/10.1016/j.atmosenv.2003.09.046>
- 2434 Lu, M.-L., Sorooshian, A., Jonsson, H. H., Feingold, G., Flagan, R. C., & Seinfeld,
 2435 J. H. (2009). Marine stratocumulus aerosol-cloud relationships in the MASE-II
 2436 experiment: Precipitation susceptibility in eastern Pacific marine stratocumu-
 2437 lus. *J. Geophys. Res.*, 114, D24203. doi: 10.1029/2009JD012774
- 2438 Ma, P.-L., Rasch, P. J., Chepfer, H., Winker, D. M., & Ghan, S. J. (2018). Obser-
 2439 vational constraint on cloud susceptibility weakened by aerosol retrieval limita-
 2440 tions [Journal Article]. *Nature Comm.*, 9(1), 2640. Retrieved from [https://](https://doi.org/10.1038/s41467-018-05028-4)
 2441 doi.org/10.1038/s41467-018-05028-4 doi: 10.1038/s41467-018-05028-4
- 2442 Mace, G. G., & Abernathy, A. C. (2016, 1). Observational evidence for aerosol invig-
 2443 oration in shallow cumulus downstream of mount kilauea. *Geophys. Res. Lett.*,
 2444 43(6), 2981–2988. doi: 10.1002/2016GL067830
- 2445 Mahowald, N. M. (2007). Anthropocene changes in desert area: Sensitiv-
 2446 ity to climate model predictions. *Geophys. Res. Lett.*, 34(18). doi:
 2447 10.1029/2007GL030472
- 2448 Mahowald, N. M., & Luo, C. (2003). A less dusty future? *Geophys. Res. Lett.*,
 2449 30(17). doi: 10.1029/2003GL017880
- 2450 Mahrt, F., Marcolli, C., David, R. O., Grönquist, P., Barthazy Meier, E. J.,
 2451 Lohmann, U., & Kanji, Z. A. (2018, 1). Ice nucleation abilities of soot par-
 2452 ticles determined with the horizontal ice nucleation chamber. *Atmos. Chem.*
 2453 *Phys.*, 18(18), 13363–13392. doi: 10.5194/acp-18-13363-2018
- 2454 Malavelle, F. F., Haywood, J. M., Jones, A., Gettelman, A., Clarisse, L., Bauduin,
 2455 S., ... Thordarson, T. (2017, 1). Strong constraints on aerosol-cloud in-
 2456 teractions from volcanic eruptions. *Nature*, 546(7659), 485–491. doi:
 2457 10.1038/nature22974
- 2458 Marlon, J. R., Kelly, R., Daniau, A.-L., Vanni re, B., Power, M. J., Bartlein, P., ...
 2459 Zhihai, T. (2016). Reconstructions of biomass burning from sediment-charcoal
 2460 records to improve data–model comparisons. *Biogeosciences*, 13(11), 3225–
 2461 3244. Retrieved from <https://www.biogeosciences.net/13/3225/2016/>

- doi: 10.5194/bg-13-3225-2016
- 2462
2463 Martin, G. M., Johnson, D. W., & Spice, A. (1994). The measurement and parame-
2464 terization of effective radius of droplets in warm stratocumulus clouds. *Journal*
2465 *of the Atmospheric Sciences*, *51*(13), 1823-1842. doi: 10.1175/1520-0469(1994)
2466 051(1823:TMAPOE)2.0.CO;2
- 2467 Mauger, G. S., & Norris, J. R. (2007, 8). Meteorological bias in satellite estimates
2468 of aerosol-cloud relationships. *Geophys. Res. Lett.*, *34*, L16824. doi: 10.1029/
2469 2007GL029952
- 2470 McComiskey, A., & Feingold, G. (2012). The scale problem in quantifying aerosol in-
2471 direct effects. *Atmos. Chem. Phys.*, *12*, 1031-1049. doi: 10.5194/acp-12-1031
2472 -2012
- 2473 McComiskey, A., Feingold, G., Frisch, A. S., Turner, D. D., Miller, M. A., Chiu,
2474 J. C., ... Ogren, J. A. (2009). An assessment of aerosol-cloud interactions
2475 in marine stratus clouds based on surface remote sensing. *J. Geophys. Res.*
2476 *Atmos.*, *114*(D9). doi: 10.1029/2008JD011006
- 2477 McCormick, R. A., & Ludwig, J. H. (1967). Climate modification by at-
2478 mospheric aerosols. *Science*, *156*(3780), 1358-1359. Retrieved from
2479 <https://science.sciencemag.org/content/156/3780/1358> doi:
2480 10.1126/science.156.3780.1358
- 2481 McCoy, D. T., Bender, F. A. M., Grosvenor, D. P., Mohrmann, J. K., Hartmann,
2482 D. L., Wood, R., & Field, P. R. (2018). Predicting decadal trends in cloud
2483 droplet number concentration using reanalysis and satellite data [Journal
2484 Article]. *Atmos. Chem. Phys.*, *18*(3), 2035-2047. Retrieved from [https://](https://www.atmos-chem-phys.net/18/2035/2018/)
2485 www.atmos-chem-phys.net/18/2035/2018/ doi: 10.5194/acp-18-2035-2018
- 2486 McCoy, D. T., Bender, F. A.-M., Mohrmann, J. K. C., Hartmann, D. L., Wood, R.,
2487 & Grosvenor, D. P. (2017, 2). The global aerosol-cloud first indirect effect
2488 estimated using MODIS, MERRA, and AeroCom. *J. Geophys. Res.*, *122*,
2489 1779-1796. doi: 10.1002/2016JD026141
- 2490 McCoy, D. T., Field, P. R., Schmidt, A., Grosvenor, D. P., Bender, F. A.-M., Ship-
2491 way, B. J., ... Elsaesser, G. S. (2018, 1). Aerosol midlatitude cyclone indirect
2492 effects in observations and high-resolution simulations. *Atmos. Chem. Phys.*,
2493 *18*(8), 5821-5846. doi: 10.5194/acp-18-5821-2018
- 2494 McCoy, D. T., & Hartmann, D. L. (2015). Observations of a substantial cloud-
2495 aerosol indirect effect during the 2014-2015 Bárðarbunga-veidivötn fis-
2496 sure eruption in Iceland. *Geophys. Res. Lett.*, *42*(23), 10,409-10,414. doi:
2497 10.1002/2015GL067070
- 2498 McFiggans, G., Artaxo, P., Baltensperger, U., Coe, H., Facchini, M. C., Feingold,
2499 G., ... Weingartner, E. (2006). The effect of physical and chemical aerosol
2500 properties on warm cloud droplet activation. *Atmos. Chem. Phys.*, *6*, 2593-
2501 2649. doi: 10.5194/acp-6-2593-2006
- 2502 Michibata, T., Suzuki, K., Sato, Y., & Takemura, T. (2016, 12). The source
2503 of discrepancies in aerosol-cloud-precipitation interactions between GCM
2504 and a-train retrievals. *Atmos. Chem. Phys.*, *16*, 15413-15424. doi:
2505 10.5194/acp-16-15413-2016
- 2506 Mitchell, D. L., Garnier, A., Pelon, J., & Erfani, E. (2018, 1). CALIPSO (IIR-
2507 CALIOP) retrievals of cirrus cloud ice-particle concentrations. *Atmos. Chem.*
2508 *Phys.*, *18*(23), 17325-17354. doi: 10.5194/acp-18-17325-2018
- 2509 Mitchell, J. M. J. (1971). The effect of atmospheric aerosols on climate with special
2510 reference to temperature near the earth's surface. *J. Applied Meteorology*, *10*,
2511 703-714.
- 2512 Morgan, M. G., Adams, P. J., & Keith, D. W. (2006). Elicitation of expert judg-
2513 ments of aerosol forcing. *Climatic Change*, *75*, 195. doi: 10.1007/s10584-005
2514 -9025-y
- 2515 Mülmenstädt, J., & Feingold, G. (2018, Mar 01). The radiative forcing of aerosol-
2516 cloud interactions in liquid clouds: Wrestling and embracing uncertainty. *Cur-*

- 2517 *rent Climate Change Reports*, 4(1), 23–40. Retrieved from [https://doi.org/](https://doi.org/10.1007/s40641-018-0089-y)
 2518 10.1007/s40641-018-0089-y doi: 10.1007/s40641-018-0089-y
- 2519 Müllenstädt, J., Gryspeerdt, E., Salzmänn, M., Ma, P.-L., Dipu, S., & Quaas, J.
 2520 (2019, 1). Separating radiative forcing by aerosol-cloud interactions and fast
 2521 cloud adjustments in the ECHAM-HAMMOZ aerosol-climate model using the
 2522 method of partial radiative perturbations. *Atmos. Chem. Phys. Discuss.*, 1–20.
 2523 doi: 10.5194/acp-2018-1304
- 2524 Murphy, D. M., Solomon, S., Portmann, R. W., Rosenlof, K. H., Forster, P. M., &
 2525 Wong, T. (2009). An observationally based energy balance for the Earth since
 2526 1950. *J. Geophys. Res. Atmos.*, 114(D17). doi: 10.1029/2009JD012105
- 2527 Myhre, G., Aas, W., Cherian, R., Collins, W., Faluvegi, G., Flanner, M., . . . Tsyro,
 2528 S. (2017). Multi-model simulations of aerosol and ozone radiative forcing
 2529 due to anthropogenic emission changes during the period 1990–2015. *Atmos.*
 2530 *Chem. Phys.*, 17, 2709–2720. doi: 10.5194/acp-17-2709-2017
- 2531 Myhre, G., Boucher, O., Bréon, F.-M., Forster, P., & Shindell, D. (2015). Declin-
 2532 ing uncertainty in transient climate response as CO₂ forcing dominates future
 2533 climate change. *Nature Geosci.*, 8, 181–185. doi: 10.1038/ngeo2371
- 2534 Myhre, G., Kramer, R. J., Smith, C. J., Hodnebrog, Ø., Forster, P., Soden, B. J., . . .
 2535 Watson-Parris, D. (2018). Quantifying the importance of rapid adjustments
 2536 for global precipitation changes. *Geophys. Res. Lett.*, 45(20), 11,399–11,405.
 2537 Retrieved from [https://agupubs.onlinelibrary.wiley.com/doi/abs/](https://agupubs.onlinelibrary.wiley.com/doi/abs/10.1029/2018GL079474)
 2538 10.1029/2018GL079474 doi: 10.1029/2018GL079474
- 2539 Myhre, G., Samset, B. H., Schulz, M., Balkanski, Y., Bauer, S., Berntsen, T. K.,
 2540 . . . Zhou, C. (2013). Radiative forcing of the direct aerosol effect from
 2541 aerocom phase ii simulations. *Atmos. Chem. Phys.*, 13, 1853–1877. doi:
 2542 10.5194/acp-13-1853-2013
- 2543 Myhre, G., Shindell, D., Bréon, F.-M., Collins, W., Fuglestedt, J., Huang, J., . . .
 2544 Zhang, H. (2013). Anthropogenic and natural radiative forcing. In T. Stocker
 2545 et al. (Eds.), *Climate change 2013: The physical science basis. contribution of*
 2546 *working group i to the fifth assessment report of the intergovernmental panel*
 2547 *on climate change* (pp. 659–740). Cambridge, United Kingdom and New York,
 2548 NY, USA: Cambridge University Press. doi: 10.1017/CBO9781107415324.018
- 2549 Nakajima, T., Higurashi, A., Kawamoto, K., & Penner, J. E. (2001). A possible cor-
 2550 relation between satellite-derived cloud and aerosol microphysical parameters.
 2551 *Geophys. Res. Lett.*, 28, 1171. doi: 10.1029/2000GL012186
- 2552 Nakajima, T., & Schulz, M. (2009). What do we know about large-scale changes
 2553 of aerosols, clouds, and the radiation budget? *Clouds in the Perturbed Cli-*
 2554 *mate System. Proceedings Ernst Strüngmann Forum.* doi: 10.7551/mitpress/
 2555 9780262012874.003.0017
- 2556 Nam, C., Bony, S., Dufresne, J.-L., & Chepfer, H. (2012). The "too few, too bright"
 2557 tropical low-cloud problem in CMIP5 models. *Geophys. Res. Lett.*, 39, L21801.
 2558 doi: 10.1029/2012GL053421
- 2559 Nemesure, S., Wagener, R., & Schwartz, S. E. (1995). Direct shortwave forc-
 2560 ing of climate by the anthropogenic sulfate aerosol: Sensitivity to parti-
 2561 cle size, composition, and relative humidity. *Journal of Geophysical Re-*
 2562 *search: Atmospheres*, 100(D12), 26105–26116. Retrieved from [https://](https://agupubs.onlinelibrary.wiley.com/doi/abs/10.1029/95JD02897)
 2563 agupubs.onlinelibrary.wiley.com/doi/abs/10.1029/95JD02897 doi:
 2564 10.1029/95JD02897
- 2565 Neubauer, D., Christensen, M. W., Poulsen, C. A., & Lohmann, U. (2017,
 2566 1). Unveiling aerosol-cloud interactions - part 2: Minimising the effects
 2567 of aerosol swelling and wet scavenging in ECHAM6-HAM2 for compari-
 2568 son to satellite data. *Atmos. Chem. Phys.*, 17(21), 13165–13185. doi:
 2569 10.5194/acp-17-13165-2017
- 2570 Neubauer, D., Lohmann, U., Hoose, C., & Frontoso, M. G. (2014). Im-
 2571 pact of the representation of marine stratocumulus clouds on the anthro-

- 2572 pogenic aerosol effect. *Atmos. Chem. Phys.*, *14*(21), 11997–12022. Re-
 2573 trieved from <https://www.atmos-chem-phys.net/14/11997/2014/> doi:
 2574 10.5194/acp-14-11997-2014
- 2575 Norgren, M. S., de Boer, G., & Shupe, M. D. (2018). Observed aerosol suppres-
 2576 sion of cloud ice in low-level arctic mixed-phase clouds. *Atmos. Chem. Phys.*,
 2577 *18*(18), 13345–13361. Retrieved from [https://www.atmos-chem-phys.net/](https://www.atmos-chem-phys.net/18/13345/2018/)
 2578 [18/13345/2018/](https://www.atmos-chem-phys.net/18/13345/2018/) doi: 10.5194/acp-18-13345-2018
- 2579 Oikawa, E., Nakajima, T., & Winker, D. (2018). An evaluation of the short-
 2580 wave direct aerosol radiative forcing using CALIOP and MODIS observa-
 2581 tions. *J. Geophys. Res. Atmos.*, *123*(2), 1211–1233. Retrieved from [https://](https://agupubs.onlinelibrary.wiley.com/doi/abs/10.1002/2017JD027247)
 2582 agupubs.onlinelibrary.wiley.com/doi/abs/10.1002/2017JD027247 doi:
 2583 10.1002/2017JD027247
- 2584 Oreopoulos, L., Cho, N., Lee, D., & Kato, S. (2016). Radiative effects of global
 2585 modis cloud regimes. *J. Geophys. Res. Atmos.*, *121*(5), 2299–2317. doi: 10
 2586 .1002/2015JD024502
- 2587 Oreopoulos, L., & Platnick, S. (2008). Radiative susceptibility of cloudy
 2588 atmospheres to droplet number perturbations: 2. global analysis from
 2589 modis. *Journal of Geophysical Research: Atmospheres*, *113*(D14). doi:
 2590 10.1029/2007JD009655
- 2591 Painemal, D., & Zuidema, P. (2013). The first aerosol indirect effect quantified
 2592 through airborne remote sensing during vocals-rx. *Atmospheric Chemistry*
 2593 *and Physics*, *13*(2), 917–931. Retrieved from [https://www.atmos-chem-phys](https://www.atmos-chem-phys.net/13/917/2013/)
 2594 [.net/13/917/2013/](https://www.atmos-chem-phys.net/13/917/2013/) doi: 10.5194/acp-13-917-2013
- 2595 Peers, F., Waquet, F., Cornet, C., Dubuisson, P., Ducos, F., Goloub, P., ...
 2596 Thieuleux, F. (2015). Absorption of aerosols above clouds from polder/parasol
 2597 measurements and estimation of their direct radiative effect. *Atmos. Chem.*
 2598 *Phys.*, *15*(8), 4179–4196. Retrieved from [https://www.atmos-chem-phys](https://www.atmos-chem-phys.net/15/4179/2015/)
 2599 [.net/15/4179/2015/](https://www.atmos-chem-phys.net/15/4179/2015/) doi: 10.5194/acp-15-4179-2015
- 2600 Penner, J. (2019). Soot, sulfate, dust and the climate – three ways through the fog.
 2601 *Nature*, *570*, 158–159. doi: 10.1038/d41586-019-01791-6
- 2602 Penner, J., Andreae, M., Annegarn, H., Barrie, L., Feichter, J., Hegg, D., ... Pitari,
 2603 G. (2001). Aerosols, their direct and indirect effects. In J. Houghton et
 2604 al. (Eds.), *Climate change 2001: Working group i: The scientific basis* (pp.
 2605 289–348). Cambridge, United Kingdom and New York, NY, USA: Cambridge
 2606 University Press.
- 2607 Penner, J. E., Chen, Y., Wang, M., & Liu, X. (2009). Possible influence of anthro-
 2608 pogenic aerosols on cirrus clouds and anthropogenic forcing. *Atmos. Chem.*
 2609 *Phys.*, *9*(3), 879–896. Retrieved from [https://www.atmos-chem-phys.net/9/](https://www.atmos-chem-phys.net/9/879/2009/)
 2610 [879/2009/](https://www.atmos-chem-phys.net/9/879/2009/) doi: 10.5194/acp-9-879-2009
- 2611 Penner, J. E., Xu, L., & Wang, M. (2011, 8). Satellite methods underestimate indi-
 2612 rect climate forcing by aerosols. *P. Natl. Acad. Sci. USA*, *108*, 13404. doi: 10
 2613 .1073/pnas.1018526108
- 2614 Penner, J. E., Zhang, S. Y., & Chuang, C. C. (2003). Soot and smoke aerosol
 2615 may not warm climate. *J. Geophys. Res. Atmos.*, *108*(D21). doi: 10.1029/
 2616 2003JD003409
- 2617 Penner, J. E., Zhou, C., Garnier, A., & Mitchell, D. L. (2018). Anthropogenic
 2618 aerosol indirect effects in cirrus clouds. *Journal of Geophysical Research:*
 2619 *Atmospheres*, *123*(20), 11,652–11,677. doi: 10.1029/2018JD029204
- 2620 Petersik, P., Salzmann, M., Kretschmar, J., Cherian, R., Mewes, D., & Quaas, J.
 2621 (2018). Subgrid-scale variability of clear-sky relative humidity and forcing by
 2622 aerosol-radiation interactions in an atmosphere model. *Atmos. Chem. Phys.*,
 2623 *18*, 8589–8599. doi: 10.5194/acp-18-8589-2018
- 2624 Pincus, R., & Baker, M. (1994). Effects of precipitation on the albedo susceptibility
 2625 of clouds in the marine boundary layer. *Nature*, *372*, 250.
- 2626 Pincus, R., & Mauritsen, T. (2017). Committed warming inferred from observations.

- 2627 *Nature Climate Change*, *7*, 652–655.
- 2628 Platnick, S., Meyer, K. G., King, M. D., Wind, G., Amarasinghe, N., Marchant, B.,
2629 ... Riedi, J. (2017). The MODIS cloud optical and microphysical products:
2630 Collection 6 updates and examples from Terra and Aqua. *IEEE Transact.*
2631 *Geosci. Remote Sens.*, *55*(1), 502–525. doi: 10.1109/TGRS.2016.2610522
- 2632 Platnick, S., & Twomey, S. (1994). Determining the susceptibility of cloud
2633 albedo to changes in droplet concentration with the advanced very high res-
2634 olution radiometer. *Journal of Applied Meteorology*, *33*(3), 334–347. doi:
2635 10.1175/1520-0450(1994)033<0334:DTSOCA>2.0.CO;2
- 2636 Possner, A., Wang, H., Wood, R., Caldeira, K., & Ackerman, T. P. (2018). The
2637 efficacy of aerosol–cloud radiative perturbations from near-surface emissions
2638 in deep open-cell stratocumuli. *Atmospheric Chemistry and Physics*, *18*(23),
2639 17475–17488. Retrieved from [https://www.atmos-chem-phys.net/18/17475/](https://www.atmos-chem-phys.net/18/17475/2018/)
2640 2018/ doi: 10.5194/acp-18-17475-2018
- 2641 Quaas, J., Boucher, O., Bellouin, N., & Kinne, S. (2008). Satellite-based estimate
2642 of the direct and indirect aerosol climate forcing. *J. Geophys. Res.*, *113*, 05204.
2643 doi: 10.1029/2007JD008962
- 2644 Quaas, J., Boucher, O., & Lohmann, U. (2006). Constraining the total aerosol indi-
2645 rect effect in the LMDZ and ECHAM4 GCMs using MODIS satellite data. *At-*
2646 *mos. Chem. Phys.*, *6*, 947–955.
- 2647 Quaas, J., Ming, Y., Menon, S., Takemura, T., Wang, M., Penner, J., ... Schulz,
2648 M. (2009). Aerosol indirect effects - general circulation model intercomparison
2649 and evaluation with satellite data. *Atmos. Chem. Phys.*, *9*, 8697–8717. doi:
2650 10.5194/acp-9-8697-2009
- 2651 Quaas, J., Stevens, B., Stier, P., & Lohmann, U. (2010, 1). Interpreting the
2652 cloud cover - aerosol optical depth relationship found in satellite data using
2653 a general circulation model. *Atmos. Chem. Phys.*, *10*(13), 6129–6135. doi:
2654 10.5194/acp-10-6129-2010
- 2655 Ramanathan, V. (1975). Greenhouse effect due to chlorofluorocarbons: Climatic im-
2656 plications. *Science*, *190*(4209), 50–52. doi: 10.1126/science.190.4209.50
- 2657 Randles, C. A., Kinne, S., Myhre, G., Schulz, M., Stier, P., Fischer, J., ... Lu, P.
2658 (2013). Intercomparison of shortwave radiative transfer schemes in global
2659 aerosol modeling: results from the AeroCom Radiative Transfer Experiment.
2660 *Atmos. Chem. Phys.*, *13*(5), 2347–2379. doi: 10.5194/acp-13-2347-2013
- 2661 Rap, A., Scott, C. E., Spracklen, D. V., Bellouin, N., Forster, P. M., Carslaw,
2662 K. S., ... Mann, G. (2013). Natural aerosol direct and indirect radiative
2663 effects. *Geophysical Research Letters*, *40*(12), 3297–3301. Retrieved from
2664 <https://agupubs.onlinelibrary.wiley.com/doi/abs/10.1002/grl.50441>
2665 doi: 10.1002/grl.50441
- 2666 Regayre, L. A., Johnson, J. S., Yoshioka, M., Pringle, K. J., Sexton, D. M. H.,
2667 Booth, B. B. B., ... Carslaw, K. S. (2018). Aerosol and physical atmo-
2668 sphere model parameters are both important sources of uncertainty in aerosol
2669 ERF. *Atmos. Chem. Phys.*, *18*(13), 9975–10006. Retrieved from [https://](https://www.atmos-chem-phys.net/18/9975/2018/)
2670 www.atmos-chem-phys.net/18/9975/2018/ doi: 10.5194/acp-18-9975-2018
- 2671 Richardson, T. B., Forster, P. M., Andrews, T., & Parker, D. J. (2016). Under-
2672 standing the rapid precipitation response to co2 and aerosol forcing on a regional
2673 scale. *J. Climate*, *29*(2), 583–594. Retrieved from [https://doi.org/10.1175/](https://doi.org/10.1175/JCLI-D-15-0174.1)
2674 [JCLI-D-15-0174.1](https://doi.org/10.1175/JCLI-D-15-0174.1) doi: 10.1175/JCLI-D-15-0174.1
- 2675 Rosenfeld, D. (2006). Aerosol-cloud interactions control of earth radiation and latent
2676 heat release budgets. *Space Sci. Rev.*, *125*, 149. doi: 10.1007/s11214-006-9053
2677 -6
- 2678 Rosenfeld, D., Lohmann, U., Raga, G., O’Dowd, C., Kulmala, M., Fuzzi, S., ... An-
2679 dreae, M. (2008). Flood or drought: How do aerosols affect precipitation?
2680 *Science*, *321*, 1309. doi: 10.1126/science.1160606
- 2681 Rosenfeld, D., & Ulbrich, C. W. (2003). Cloud microphysical properties, processes,

- and rainfall estimation opportunities. *Meteorological Monographs*, *52*, 237-258. Retrieved from [https://doi.org/10.1175/0065-9401\(2003\)030<0237:CMPPAR>2.0.CO;2](https://doi.org/10.1175/0065-9401(2003)030<0237:CMPPAR>2.0.CO;2) doi: 10.1175/0065-9401(2003)030<0237:CMPPAR>2.0.CO;2
- Rotstayn, L. D., Collier, M. A., Shindell, D. T., & Boucher, O. (2015). Why does aerosol forcing control historical global-mean surface temperature change in CMIP5 models? *J. Climate*, *28*, 6608–6625. doi: 10.1175/JCLI-D-14-00712.1
- Samset, B. H., Myhre, G., Herber, A., Kondo, Y., Li, S.-M., Moteki, N., ... Zhang, K. (2014). Modelled black carbon radiative forcing and atmospheric lifetime in aerocom phase ii constrained by aircraft observations. *Atmos. Chem. Phys.*, *14*, 12465–12477. doi: 10.5194/acp-14-12465-2014
- Sandu, I., Brenguier, J.-L., Geoffroy, O., Thouron, O., & Masson, V. (2008). Aerosol impacts on the diurnal cycle of marine stratocumulus. *J. Atmos. Sci.*, *65*(8), 2705–2718. Retrieved from <https://doi.org/10.1175/2008JAS2451.1> doi: 10.1175/2008JAS2451.1
- Sato, Y., Goto, D., Michibata, T., Suzuki, K., Takemura, T., Tomita, H., & Nakajima, T. (2018, 1). Aerosol effects on cloud water amounts were successfully simulated by a global cloud-system resolving model. *Nature Comm.*, *9*(1). doi: 10.1038/s41467-018-03379-6
- Satoh, M., Noda, A. T., Seiki, T., Chen, Y.-W., Kodama, C., Yamada, Y., ... Sato, Y. (2018, Oct 29). Toward reduction of the uncertainties in climate sensitivity due to cloud processes using a global non-hydrostatic atmospheric model. *Progress in Earth and Planetary Science*, *5*(1), 67. Retrieved from <https://doi.org/10.1186/s40645-018-0226-1> doi: 10.1186/s40645-018-0226-1
- Schimel, D., Alves, D., Entling, I., Heimann, M., Joos, F., Raynaud, D., ... Wuebbles, D. (1996). Radiative forcing of climate change. In J. T. Houghton, L. G. Meiro Filho, B. A. Callander, N. Harris, A. Kattenburg, & K. Maskell (Eds.), *Climate change 1995: The science of climate change. contribution of working group i to the second assessment report of the intergovernmental panel on climate change* (pp. 69–131). Cambridge, United Kingdom and New York, NY, USA: Cambridge University Press.
- Schmidt, J., Ansmann, A., Bühl, J., & Wandinger, U. (2015). Strong aerosol–cloud interaction in altocumulus during updraft periods: lidar observations over central Europe. *Atmos. Chem. Phys.*, *15*, 10687–10700. doi: 10.5194/acp-15-10687-2015
- Schulz, M., Textor, C., Kinne, S., Balkanski, Y., Bauer, S., Bernsten, T., ... Takemura, T. (2006). Radiative forcing by aerosols as derived from the aerocom present-day and pre-industrial simulations. *Atmos. Chem. Phys.*, *6*, 5225–5246. doi: 10.5194/acp-6-5225-2006
- Schwartz, S. E. (2012, Jul 01). Determination of earth’s transient and equilibrium climate sensitivities from observations over the twentieth century: Strong dependence on assumed forcing. *Surv. Geophys.*, *33*(3), 745–777. Retrieved from <https://doi.org/10.1007/s10712-012-9180-4> doi: 10.1007/s10712-012-9180-4
- Schwartz, S. E. (2018). Unrealized global temperature increase: Implications of current uncertainties. *J. Geophys. Res.*, *123*, 3462–3482. doi: 10.1002/2017JD028121
- Schwartz, S. E., & Andreae, M. O. (1996). Uncertainty in climate change caused by aerosols. *Science*, *272*, 1121–1122.
- Seifert, A., Heus, T., Pincus, R., & Stevens, B. (2015). Large-eddy simulation of the transient and near-equilibrium behavior of precipitating shallow convection. *J. Adv. Model. Earth Syst.*, *7*(4), 1918–1937. Retrieved from <https://agupubs.onlinelibrary.wiley.com/doi/abs/10.1002/2015MS000489> doi: 10.1002/2015MS000489

- 2737 Seinfeld, J. H., Bretherton, C., Carslaw, K. S., Coe, H., DeMott, P. J., Dunlea,
2738 E. J., ... Wood, R. (2016). Improving our fundamental understanding of the
2739 role of aerosol-cloud interactions in the climate system. *Proc. Nat. Acad. Sci.*,
2740 *113*, 5781–5790. doi: 10.1073/pnas.1514043113
- 2741 Sekiguchi, M., Nakajima, T., Suzuki, K., Kawamoto, K., Higurashi, A., Rosenfeld,
2742 D., ... Mukai, S. (2003, 11). A study of the direct and indirect effects of
2743 aerosols using global satellite data sets of aerosol and cloud parameters. *J.*
2744 *Geophys. Res.*, *108*(D22), 4699. doi: 10.1029/2002JD003359
- 2745 Sena, E. T., McComiskey, A., & Feingold, G. (2016). A long-term study of aerosol-
2746 cloud interactions and their radiative effect at the southern great plains using
2747 ground-based measurements. *Atmos. Chem. Phys.*, *16*(17), 11301–11318.
2748 Retrieved from <https://www.atmos-chem-phys.net/16/11301/2016/> doi:
2749 10.5194/acp-16-11301-2016
- 2750 Sherwood, S. C., Bony, S., Boucher, O., Bretherton, C., Forster, P. M., Gregory,
2751 J. M., & Stevens, B. (2015). Adjustments in the forcing-feedback framework
2752 for understanding climate change. *Bull. Amer. Meteor. Soc.*, *96*, 217–228. doi:
2753 10.1175/BAMS-D-13-00167.1
- 2754 Shine, K. P., Cook, J., Highwood, E. J., & Joshi, M. M. (2003). An alternative
2755 to radiative forcing for estimating the relative importance of climate change
2756 mechanisms. *Geophysical Research Letters*, *30*(20). Retrieved from [https://](https://agupubs.onlinelibrary.wiley.com/doi/abs/10.1029/2003GL018141)
2757 agupubs.onlinelibrary.wiley.com/doi/abs/10.1029/2003GL018141 doi:
2758 10.1029/2003GL018141
- 2759 Skeie, R. B., Berntsen, T., Aldrin, M., Holden, M., & Myhre, G. (2018). Cli-
2760 mate sensitivity estimates – sensitivity to radiative forcing time series
2761 and observational data. *Earth System Dynamics*, *9*(2), 879–894. Re-
2762 trieved from <https://www.earth-syst-dynam.net/9/879/2018/> doi:
2763 10.5194/esd-9-879-2018
- 2764 Small, J. D., Chuang, P. Y., Feingold, G., & Jiang, H. (2009, 1). Can aerosol
2765 decrease cloud lifetime? *Geophys. Res. Lett.*, *36*(16). doi: 10.1029/
2766 2009GL038888
- 2767 Small, J. D., Jiang, J. H., Su, H., & Zhai, C. (2011, 12). Relationship between
2768 aerosol and cloud fraction over australia. *Geophys. Res. Lett.*, *38*, 23802. doi:
2769 10.1029/2011GL049404
- 2770 Smirnov, A., Holben, B., Eck, T., Dubovik, O., & Slutsker, I. (2000). Cloud-
2771 screening and quality control algorithms for the aernet database. *Remote*
2772 *Sensing of Environment*, *73*(3), 337 - 349. doi: [https://doi.org/10.1016/](https://doi.org/10.1016/S0034-4257(00)00109-7)
2773 [S0034-4257\(00\)00109-7](https://doi.org/10.1016/S0034-4257(00)00109-7)
- 2774 Smirnov, A., Holben, B., Slutsker, I., Giles, D., McClain, C. R., Eck, T., ... Jour-
2775 din, F. (2009). Maritime Aerosol Network as a component of Aerosol Robotic
2776 Network. *J. Geophys. Res.*, *114*, D06204. doi: 10.1029/2008JD011257
- 2777 Smith, C. J., Kramer, R. J., Myhre, G., Forster, P. M., Soden, B. J., Andrews,
2778 T., ... Watson-Parris, D. (2018). Understanding rapid adjustments to di-
2779 verse forcing agents. *Geophys. Res. Lett.*, *45*(21), 12,023-12,031. Retrieved
2780 from [https://agupubs.onlinelibrary.wiley.com/doi/abs/10.1029/](https://agupubs.onlinelibrary.wiley.com/doi/abs/10.1029/2018GL079826)
2781 [2018GL079826](https://agupubs.onlinelibrary.wiley.com/doi/abs/10.1029/2018GL079826) doi: 10.1029/2018GL079826
- 2782 Sorooshian, A., Feingold, G., Lebsock, M., Jiang, H., & Stephens, G. (2009). On the
2783 precipitation susceptibility of clouds to aerosol perturbations. *Geophys. Res.*
2784 *Lett.*, *36*, L13803. doi: 10.1029/2009GL038993
- 2785 Sourdeval, O., Gryspeerdt, E., Krämer, M., Goren, T., Delanoë, J., Afchine, A., ...
2786 Quaas, J. (2018, 1). Ice crystal number concentration estimates from lidar-
2787 radar satellite remote sensing – part 1: Method and evaluation. *Atmos. Chem.*
2788 *Phys.*, *18*(19), 14327–14350. doi: 10.5194/acp-18-14327-2018
- 2789 Stanelle, T., Bey, I., Raddatz, T., Reick, C., & Tegen, I. (2014). Anthropogenically
2790 induced changes in twentieth century mineral dust burden and the associated
2791 impact on radiative forcing. *J. Geophys. Res. Atmos.*, *119*(23), 13526–13546.

- doi: 10.1002/2014JD022062
- 2792
2793 Stephens, G. L., L'Ecuyer, T., Forbes, R., Gettleman, A., Golaz, J.-C., Bodas-
2794 Salcedo, A., . . . Haynes, J. (2010). Dreary state of precipitation in global
2795 models. *J. Geophys. Res.*, *115*, D24211. doi: 10.1029/2010JD014532
- 2796 Stephens, G. L., O'Brien, D., Webster, P. J., Pilewski, P., Kato, S., & Li, J.-
2797 l. (2015). The albedo of earth. *Rev. Geophys.*, *53*(1), 141-163. doi:
2798 10.1002/2014RG000449
- 2799 Stevens, B. (2015). Rethinking the lower bound on aerosol radiative forcing. *J. Cli-*
2800 *mate*, *28*, 4794-4819. doi: 10.1175/JCLI-D-14-00656.1
- 2801 Stevens, B., & Feingold, G. (2009). Untangling aerosol effects on clouds and precipi-
2802 tation in a buffered system. *Nature*, *461*, 607-613.
- 2803 Stevens, B., & Fiedler, S. (2017). Reply to "comment on 'rethinking the lower
2804 bound on aerosol radiative forcing'". *J. Climate*, *30*, 6585-6589. doi:
2805 10.1175/JCLI-D-17-0034.1
- 2806 Stier, P. (2016). Limitations of passive remote sensing to constrain global
2807 cloud condensation nuclei. *Atmos. Chem. Phys.*, *16*(10), 6595-6607. Re-
2808 trieved from <https://www.atmos-chem-phys.net/16/6595/2016/> doi:
2809 10.5194/acp-16-6595-2016
- 2810 Stier, P., Feichter, J., Kloster, S., Vignati, E., & Wilson, J. (2006). Emission-induced
2811 nonlinearities in the global aerosol system: Results from the ECHAM5-HAM
2812 aerosol-climate model. *J. Climate*, *19*, 3845-3862. doi: 10.1175/JCLI3772.1
- 2813 Stier, P., Schutgens, N. A. J., Bellouin, N., Bian, H., Boucher, O., Chin, M., . . .
2814 Zhou, C. (2013). Host model uncertainties in aerosol radiative forcing esti-
2815 mates: results from the AeroCom Prescribed intercomparison study. *Atmos.*
2816 *Chem. Phys.*, *13*(6), 3245-3270. doi: 10.5194/acp-13-3245-2013
- 2817 Stjern, C. W., Samset, B. H., Myhre, G., Forster, P. M., Hodnebrog, T., Ø. An-
2818 drews, Boucher, O., . . . Voulgarakis, A. (2017). Rapid adjustments cause weak
2819 surface temperature response to increased black carbon concentrations. *J.*
2820 *Geophys. Res. Atmos.*, *122*(11), 462-481. doi: 10.1002/2017JD027326
- 2821 Storelvmo, T. (2017). Aerosol effects on climate via mixed-phase and ice clouds.
2822 *Annual Review of Earth and Planetary Sciences*, *45*(1), 199-222. doi: 10.1146/
2823 annurev-earth-060115-012240
- 2824 Storelvmo, T., Heede, U., Leirvik, T., Phillips, P., Arndt, P., & Wild, M. (2018).
2825 Lethargic response to aerosol emissions in current climate models. *Geophys.*
2826 *Res. Lett.*, *45*. doi: 10.1029/2018GL078298
- 2827 Storelvmo, T., Kristjánsson, J. E., Lohmann, U., Iversen, T., Kirkevåg, A., & Se-
2828 land, Ø. (2008, 1). Modeling of the wenger-bergeron-findeisen process -
2829 implications for aerosol indirect effects. *Environ. Res. Lett.*, *3*(4), 045001. doi:
2830 10.1088/1748-9326/3/4/045001
- 2831 Ström, J., & Ohlsson, S. (1998). In situ measurements of enhanced crystal num-
2832 ber densities in cirrus clouds caused by aircraft exhaust. *J. Geophys. Res.*,
2833 *103*(D10), 1355-1361.
- 2834 Suzuki, K., Stephens, G. L., & Lebsack, M. D. (2013, 1). Aerosol effect on the warm
2835 rain formation process: Satellite observations and modeling. *J. Geophys. Res.*,
2836 *118*, 170-184. doi: 10.1002/jgrd.50043
- 2837 Takemura, T., Nozawa, T., Emori, S., Nakajima, T. Y., & Nakajima, T. (2005).
2838 Simulation of climate response to aerosol direct and indirect effects with
2839 aerosol transport-radiation model. *J. Geophys. Res. Atmos.*, *110*(D2). doi:
2840 10.1029/2004JD005029
- 2841 Tan, I., Storelvmo, T., & Choi, Y.-S. (2014, 1). Spaceborne lidar observa-
2842 tions of the ice-nucleating potential of dust, polluted dust, and smoke
2843 aerosols in mixed-phase clouds. *J. Geophys. Res.*, *119*(11), 6653-6665. doi:
2844 10.1002/2013JD021333
- 2845 Taylor, K. E., Stouffer, R. J., & Meehl, G. A. (2012). An overview of cmip5 and
2846 the experiment design. *Bull. Amer. Meteorol. Soc.*, *93*(4), 485-498. Retrieved

- 2847 from <https://doi.org/10.1175/BAMS-D-11-00094.1> doi: 10.1175/BAMS-D-
2848 -11-00094.1
- 2849 Tegen, I., Werner, M., Harrison, S. P., & Kohfeld, K. E. (2004). Relative impor-
2850 tance of climate and land use in determining present and future global soil
2851 dust emission. *Geophys. Res. Lett.*, *31*(5). doi: 10.1029/2003GL019216
- 2852 Textor, C., Schulz, M., Guibert, S., Kinne, S., Balkanski, Y., Bauer, S., . . . Tie,
2853 X. (2006). Analysis and quantification of the diversities of aerosol life
2854 cycles within aerocom. *Atmos. Chem. Phys.*, *6*(7), 1777–1813. Re-
2855 trieved from <https://www.atmos-chem-phys.net/6/1777/2006/> doi:
2856 10.5194/acp-6-1777-2006
- 2857 Thornton, J. A., Virts, K. S., Holzworth, R. H., & Mitchell, T. P. (2017, 1). Light-
2858 ning enhancement over major oceanic shipping lanes. *Geophys. Res. Lett.* doi:
2859 10.1002/2017GL074982
- 2860 Toll, V., Christensen, M., Gassó, S., & Bellouin, N. (2017, 1). Volcano and
2861 ship tracks indicate excessive aerosol-induced cloud water increases in a cli-
2862 mate model. *Geophys. Res. Lett.*, *44*(24), 12,492–12,500. doi: 10.1002/
2863 2017GL075280
- 2864 Toll, V., Christensen, M., Quaas, J., & Bellouin, N. (2019). Weak average liquid-
2865 cloud-water response to anthropogenic aerosols. *Nature*, *572*, 51–55. doi: 10
2866 .1038/s41586-019-1423-9
- 2867 Twohy, C. H., Petters, M. D., Snider, J. R., Stevens, B., Tahnk, W., Wetzell, M.,
2868 . . . Burnet, F. (2005). Evaluation of the aerosol indirect effect in marine
2869 stratocumulus clouds: Droplet number, size, liquid water path, and radiative
2870 impact. *Journal of Geophysical Research: Atmospheres*, *110*(D8). doi:
2871 10.1029/2004JD005116
- 2872 Twomey, S. (1959). The nuclei of natural cloud formation part ii: The supersatu-
2873 ration in natural clouds and the variation of cloud droplet concentration. *Ge-
2874 ofisica Pura e Applicata*, *43*, 243–249. doi: 10.1007/BF01993560
- 2875 Twomey, S. (1974). Pollution and the planetary albedo. *Atmos. Environ.*, *8*, 1251–
2876 1256. doi: 10.1016/0004-6981(74)90004-3
- 2877 Twomey, S. (1977). The influence of pollution on the shortwave albedo of clouds.
2878 *J. Atmos. Sci.*, *34*(7), 1149–1152. doi: 10.1175/1520-0469(1977)034<1149:
2879 TIOPOT>2.0.CO;2
- 2880 Twomey, S., & Warner, J. (1967). Comparison of measurements of cloud droplets
2881 and cloud nuclei. *Journal of the Atmospheric Sciences*, *24*(6), 702–703. doi: 10
2882 .1175/1520-0469(1967)024(0702:COMOCD)2.0.CO;2
- 2883 van Marle, M. J. E., Kloster, S., Magi, B. I., Marlon, J. R., Daniau, A.-L., Field,
2884 R. D., . . . van der Werf, G. R. (2017). Historic global biomass burning
2885 emissions for cmip6 (bb4cmip) based on merging satellite observations with
2886 proxies and fire models (1750–2015). *Geosci. Model Dev.*, *10*, 3329–3357. doi:
2887 10.5194/gmd-10-3329-2017
- 2888 Várnai, T., & Marshak, A. (2009, 3). MODIS observations of enhanced
2889 clear sky reflectance near clouds. *Geophys. Res. Lett.*, *36*(6), 6807. doi:
2890 10.1029/2008GL037089
- 2891 Vergara-Temprado, J., Holden, M. A., Orton, T. R., O’Sullivan, D., Umo, N. S.,
2892 Browne, J., . . . Murray, B. J. (2018). Is black carbon an unimportant
2893 ice-nucleating particle in mixed-phase clouds? *Journal of Geophysical
2894 Research: Atmospheres*, *123*(8), 4273–4283. Retrieved from [https://
2895 agupubs.onlinelibrary.wiley.com/doi/abs/10.1002/2017JD027831](https://agupubs.onlinelibrary.wiley.com/doi/abs/10.1002/2017JD027831) doi:
2896 10.1002/2017JD027831
- 2897 Vergara-Temprado, J., Miltenberger, A. K., Furtado, K., Grosvenor, D. P., Ship-
2898 way, B. J., Hill, A. A., . . . Carslaw, K. S. (2018). Strong control of southern
2899 ocean cloud reflectivity by ice-nucleating particles. *Proceedings of the Na-
2900 tional Academy of Sciences*, *115*(11), 2687–2692. Retrieved from [https://
2901 www.pnas.org/content/115/11/2687](https://www.pnas.org/content/115/11/2687) doi: 10.1073/pnas.1721627115

- 2902 Wang, M., Ghan, S., Liu, X., yer, T. S., Zhang, K., Morrison, H., ... Penner, J. E.
2903 (2012, 8). Constraining cloud lifetime effects of aerosols using a-train satellite
2904 observations. *Geophys. Res. Lett.*, *39*, 15709. doi: 10.1029/2012GL052204
- 2905 Wang, R., Andrews, E., Balkanski, Y., Boucher, O., Myhre, G., Samset, B. H., ...
2906 Tao, S. (2018). Spatial representativeness error in the ground-level observation
2907 networks for black carbon radiation absorption. *Geophysical Research Letters*,
2908 *45*(4), 2106-2114. Retrieved from [https://agupubs.onlinelibrary.wiley](https://agupubs.onlinelibrary.wiley.com/doi/abs/10.1002/2017GL076817)
2909 [.com/doi/abs/10.1002/2017GL076817](https://agupubs.onlinelibrary.wiley.com/doi/abs/10.1002/2017GL076817) doi: 10.1002/2017GL076817
- 2910 Wang, S., Wang, Q., & Feingold, G. (2003). Turbulence, condensation, and liq-
2911 uid water transport in numerically simulated nonprecipitating stratocumulus
2912 clouds. *J. Atmos. Sci.*, *60*(2), 262-278. doi: 10.1175/1520-0469(2003)060<0262:
2913 TCALWT>2.0.CO;2
- 2914 Wang, X., Heald, C. L., Ridley, D. A., Schwarz, J. P., Spackman, J. R., Perring,
2915 A. E., ... Clarke, A. D. (2014). Exploiting simultaneous observational con-
2916 straints on mass and absorption to estimate the global direct radiative forcing
2917 of black carbon and brown carbon. *Atmos. Chem. Phys.*, *14*(20), 10989–11010.
2918 Retrieved from <https://www.atmos-chem-phys.net/14/10989/2014/> doi:
2919 10.5194/acp-14-10989-2014
- 2920 Wang, X., Liu, J., Che, H., Ji, F., & Liu, J. (2018). Spatial and temporal evolution
2921 of natural and anthropogenic dust events over northern China. *Scientific Re-*
2922 *ports*, *8*(1), 2141. doi: 10.1038/s41598-018-20382-5
- 2923 Warren, S. G., & Wiscombe, W. J. (1980). A model for the spectral albedo of snow
2924 II: Snow containing atmospheric aerosols. *J. Atmos. Sci.*, *37*(1980). doi: 10
2925 [.1175/1520-0469\(1980\)037<2734:AMFTSA>2.0.CO;2](https://doi.org/10.1175/1520-0469(1980)037<2734:AMFTSA>2.0.CO;2)
- 2926 Watson-Parris, D., Bellouin, N., Deaconu, L., Schutgens, N., Yoshioka, M., Regayre,
2927 L. A., ... Stier, P. (submitted). Constraining uncertainty in aerosol direct
2928 forcing. *Geophys. Res. Lett.*
- 2929 Watson-Parris, D., Schutgens, N., Winker, D., Burton, S. P., Ferrare, R. A., & Stier,
2930 P. (2018). On the limits of CALIOP for constraining modeled free tropospheric
2931 aerosol. *Geophys. Res. Lett.*, *45*(17), 9260–9266. Retrieved from [https://](https://agupubs.onlinelibrary.wiley.com/doi/abs/10.1029/2018GL078195)
2932 agupubs.onlinelibrary.wiley.com/doi/abs/10.1029/2018GL078195 doi:
2933 10.1029/2018GL078195
- 2934 Webb, N. P., & Pierre, C. (2018). Quantifying Anthropogenic Dust Emissions.
2935 *Earth's Future*, *6*(2), 286–295. doi: 10.1002/2017EF000766
- 2936 Werner, F., Ditas, F., Siebert, H., Simmel, M., Wehner, B., Pilewskie, P., ...
2937 Wendisch, M. (2014). Twomey effect observed from collocated microphysi-
2938 cal and remote sensing measurements over shallow cumulus. *J. Geophys. Res.*
2939 *Atmos.*, *119*(3), 1534-1545. doi: 10.1002/2013JD020131
- 2940 White, B., Gryspeerd, E., Stier, P., Morrison, H., Thompson, G., & Kipling, Z.
2941 (2017). Uncertainty from the choice of microphysics scheme in convection-
2942 permitting models significantly exceeds aerosol effects. *Atmos. Chem. Phys.*,
2943 *17*, 12145-12175. doi: 10.5194/acp-17-12145-2017
- 2944 Wielicki, B. A., Barkstrom, B. R., Harrison, E. F., Lee, R. B., Louis Smith, G.,
2945 & Cooper, J. E. (1996, 1). Clouds and the earth's radiant energy system
2946 (CERES): An earth observing system experiment. *Bull. Amer. Meteorol. Soc.*,
2947 *77*(5), 853–868. doi: 10.1175/1520-0477(1996)077<0853:CATERE>2.0.CO;2
- 2948 Wilcox, E. M. (2012). Direct and semi-direct radiative forcing of smoke aerosols over
2949 clouds. *Atmos. Chem. Phys.*, *12*(1), 139–149. Retrieved from [https://www](https://www.atmos-chem-phys.net/12/139/2012/)
2950 [.atmos-chem-phys.net/12/139/2012/](https://www.atmos-chem-phys.net/12/139/2012/) doi: 10.5194/acp-12-139-2012
- 2951 Williams, E., Rosenfeld, D., Madden, N., Gerlach, J., Gears, N., Atkinson, L., ...
2952 Avelino, E. (2002, 10). Contrasting convective regimes over the amazon: Im-
2953 plications for cloud electrification. *J. Geophys. Res.*, *107*(D20), 8082. doi:
2954 10.1029/2001JD000380
- 2955 Winker, D. M., Tackett, J. L., Getzewich, B. J., Liu, Z., Vaughan, M. A., & Rogers,
2956 R. R. (2013). The global 3-D distribution of tropospheric aerosols as

- 2957 characterized by CALIOP. *Atmos. Chem. Phys.*, *13*(6), 3345–3361. Re-
 2958 trieved from <https://www.atmos-chem-phys.net/13/3345/2013/> doi:
 2959 10.5194/acp-13-3345-2013
- 2960 WMO. (2017). *World Meteorological Organization Cloud Atlas.* (cloudat-
 2961 las.wmo.int)
- 2962 Wood, R., Leon, D., Lebsock, M., Snider, J., & Clarke, A. D. (2012). Precipitation
 2963 driving of droplet concentration variability in marine low clouds. *Journal of*
 2964 *Geophysical Research: Atmospheres*, *117*(D19). doi: 10.1029/2012JD018305
- 2965 Wood, R., O, K.-T., Bretherton, C. S., Mohrmann, J., Albrecht, B. A., Zuidema,
 2966 P., ... Minnis, P. (2018). Ultraclean layers and optically thin clouds in the
 2967 stratocumulus-to-cumulus transition. part i: Observations. *J. Atmos. Sci.*,
 2968 *75*(5), 1631-1652. doi: 10.1175/JAS-D-17-0213.1
- 2969 Xue, H., & Feingold, G. (2006, 1). Large-eddy simulations of trade wind cumuli: In-
 2970 vestigation of aerosol indirect effects. *J. Atmos. Sci.*, *63*(6), 1605–1622. doi: 10
 2971 .1175/JAS3706.1
- 2972 Yamaguchi, T., Feingold, G., Kazil, J., & McComiskey, A. (2015). Stratocumu-
 2973 lus to cumulus transition in the presence of elevated smoke layers. *Geophys-
 2974 ical Research Letters*, *42*(23), 10,478-10,485. Retrieved from [https://agupubs
 2975 .onlinelibrary.wiley.com/doi/abs/10.1002/2015GL066544](https://agupubs.onlinelibrary.wiley.com/doi/abs/10.1002/2015GL066544) doi: 10.1002/
 2976 2015GL066544
- 2977 Yoshioka, M., Regayre, L., Pringle, K., Johnson, J., Mann, G., Partridge, D., ...
 2978 Carslaw, K. (2019). Ensembles of global climate model variants designed for
 2979 the quantification and constraint of uncertainty in aerosols and their radiative
 2980 forcing. *J. Adv. Model. Earth Syst.*
- 2981 Yuan, T., Remer, L. A., Pickering, K. E., & Yu, H. (2011, 2). Observational evi-
 2982 dence of aerosol enhancement of lightning activity and convective invigoration.
 2983 *Geophys. Res. Lett.*, *38*, 04701. doi: 10.1029/2010GL046052
- 2984 Yuan, T., Remer, L. A., & Yu, H. (2011, 7). Microphysical, macrophysical and
 2985 radiative signatures of volcanic aerosols in trade wind cumulus observed by the
 2986 A-Train. *Atmos. Chem. Phys.*, *11*, 7119–7132. doi: 10.5194/acp-11-7119-2011
- 2987 Zelinka, M. D., Andrews, T., Forster, P. M., & Taylor, K. E. (2014, 1). Quantifying
 2988 components of aerosol-cloud-radiation interactions in climate models. *J. Geo-
 2989 phys. Res.*, *119*(12), 7599-7615. doi: 10.1002/2014JD021710
- 2990 Zerefos, C. S., Tetsis, P., Kazantzidis, A., Amiridis, V., Zerefos, S. C., Luterbacher,
 2991 J., ... Papayannis, A. (2014). Further evidence of important environmen-
 2992 tal information content in red-to-green ratios as depicted in paintings by
 2993 great masters. *Atmospheric Chemistry and Physics*, *14*(6), 2987–3015. Re-
 2994 trieved from <https://www.atmos-chem-phys.net/14/2987/2014/> doi:
 2995 10.5194/acp-14-2987-2014
- 2996 Zhang, H., Zhao, S., Wang, Z., Zhang, X., & Song, L. (2016). The updated effective
 2997 radiative forcing of major anthropogenic aerosols and their effects on global
 2998 climate at present and in the future. *Int. J. Climatol.*, *36*(12), 4029-4044. doi:
 2999 10.1002/joc.4613
- 3000 Zhang, J., Reid, J., & Holben, B. (2005). An analysis of potential cloud artifacts in
 3001 MODIS over ocean aerosol optical thickness products. *Geophys. Res. Lett.*, *32*,
 3002 L15803. doi: 10.1029/2005GL023254
- 3003 Zhao, B., Liou, K.-N., Gu, Y., Jiang, J. H., Li, Q., Fu, R., ... He, C. (2018). Im-
 3004 pact of aerosols on ice crystal size. *Atmos. Chem. Phys.*, *18*(2), 1065–1078.
 3005 Retrieved from <https://www.atmos-chem-phys.net/18/1065/2018/> doi:
 3006 10.5194/acp-18-1065-2018
- 3007 Zhou, C., & Penner, J. E. (2014). Aircraft soot indirect effect on large-scale cir-
 3008 rus clouds: Is the indirect forcing by aircraft soot positive or negative? *Journal*
 3009 *of Geophysical Research: Atmospheres*, *119*(19), 11,303-11,320. doi: 10.1002/
 3010 2014JD021914
- 3011 Zhu, J., Penner, J. E., Yu, F., Sillman, S., Andreae, M. O., & Coe, H. (2019). De-

3012 crease in radiative forcing by organic aerosol nucleation, climate, and land use
3013 change. *Nature Communications*, *10*(423). doi: 10.1038/s41467-019-08407-7
3014 Zuidema, P., Redemann, J., Haywood, J., Wood, R., Piketh, S., Hipondoka, M., &
3015 Formenti, P. (2016). Smoke and clouds above the southeast atlantic: Upcom-
3016 ing field campaigns probe absorbing aerosol's impact on climate. *Bull. Amer.*
3017 *Meteorol. Soc.*, *97*(7), 1131-1135. doi: 10.1175/BAMS-D-15-00082.1

Table 1. Best estimates and uncertainty ranges of radiative forcing of aerosol-radiation and aerosol-cloud interactions, and total aerosol radiative forcing, in W m^{-2} , as given by successive Assessment Reports of the IPCC. Uncertainty ranges are given at the 90% confidence level. The First Assessment Report did not have the scientific understanding needed to quantify aerosol radiative forcing, although they noted that it was potentially substantial. All values are for radiative forcing, except for the Fifth Assessment Report, which are for effective radiative forcing. Adapted from Table 8.6 of Myhre, Shindell, et al. (2013).

Assessment report	Forcing period	Aerosol-radiation interactions	Aerosol-cloud interactions	Total
2 (Schimel et al., 1996)	1750–1993	-0.50 (-1.00 to -0.25)	N/A (-1.5 to 0.0)	N/A
3 (J. Penner et al., 2001)	1750–1998	N/A	N/A (-2 to 0.0)	N/A
4 (Forster et al., 2007)	1750–2005	-0.50 (-0.90 to -0.10)	-0.70 (-1.80 to -0.30)	-1.3 (-2.2 to -0.5)
5 (Boucher et al., 2013)	1750–2011	-0.45 (-0.95 to +0.05)	-0.45 (-1.2 to 0.0)	-0.9 (-1.9 to -0.1)

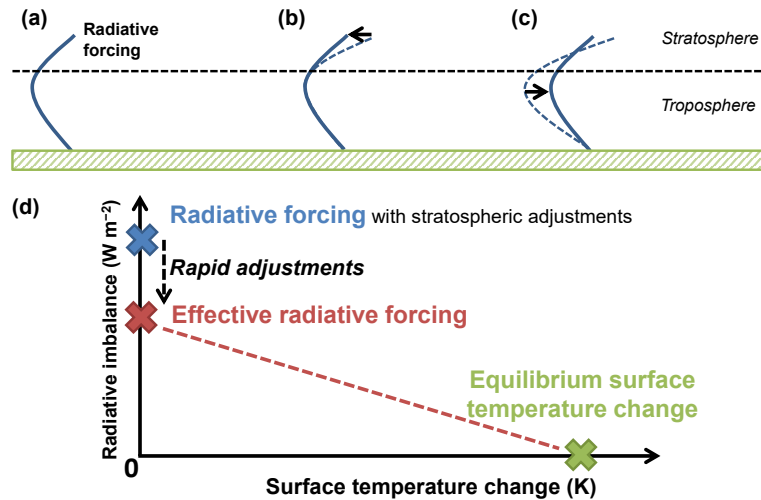


Figure 1. (a) Instantaneous radiative forcing: A perturbation is applied, but the vertical profiles of temperature (solid line) and moisture remain unperturbed. (b) Stratosphere-adjusted radiative forcing: Stratospheric temperatures respond (transition from dashed to solid line). (c) Effective radiative forcing: the perturbation also triggers rapid adjustments in the troposphere, but surface temperatures have not yet responded. (d) The system returns to radiative balance by a change in surface temperature.

Table 2. Mathematical definitions and descriptions of the variables of Equations 8, 15, and 24. The first column gives the number of the section where the uncertainty range for each variable is assessed. τ_a and τ_c are the aerosol and cloud optical depths, respectively. N_d is the cloud droplet number concentration. \mathcal{L} is the liquid cloud water path. \mathcal{C} is the cloud fraction, and \mathcal{C}_{liq} and \mathcal{C}_{ice} are the liquid and ice cloud fractions, respectively. R is the sum of shortwave and longwave radiation at the top of the atmosphere, R_{atm} is the radiation absorbed in the atmosphere, and R_{SW}^\downarrow is the downwelling shortwave radiation at cloud top. α_c and α_{clear} are the cloud and cloud-free albedos, respectively. Angle brackets denote global-area weighted temporal averaging

Section	Mathematical definition	Description
4	τ_a^{PD}	Present-day (2005–2015) τ_a
4	$\Delta\tau_a = \tau_a^{\text{PD}} - \tau_a^{\text{PI}}$	Change in τ_a between present-day (2005–2015) and preindustrial (1850)
4	$\Delta \ln \tau_a = \Delta\tau_a/\tau_a^{\text{PD}}$	Relative change in τ_a over the industrial era
6	$\Delta \ln N_d = \Delta N_d/N_d$	Relative change in N_d over the industrial era
Aerosol-radiation interactions		
5	$S_\tau^{\text{clear}} = \partial R_{\text{clear}}/\partial\tau_a$	Sensitivity of R to changes in τ_a in clear (cloud-free) sky
5	$S_\tau^{\text{cloudy}} = \partial R_{\text{cloudy}}/\partial\tau_a$	Sensitivity of R to changes in τ_a in cloudy-sky
5	$c_\tau = \frac{\langle \tau_c \Delta\tau_a \mathcal{C} \rangle}{\langle \tau_c \Delta\tau_a \rangle}$	Effective cloud fraction for RFari
7	dR/dR_{atm}	Sensitivity of R to changes in atmospheric absorption
7	$dR_{\text{atm}}/d\tau_a$	Sensitivity of atmospheric absorption to changes in τ_a
Aerosol-cloud interactions		
6	$\beta_{\ln N - \ln \tau} = \frac{\partial \ln N_d}{\partial \ln \tau_a}$	Sensitivity of N_d to changes in τ_a
6	$S_N = \left. \frac{\partial R}{\partial \ln N_d} \right _{\mathcal{L}, \mathcal{C}}$	Sensitivity of R to changes in N_d at constant \mathcal{L} and \mathcal{C}
6	$c_N = \frac{\langle \mathcal{C}_{\text{liq}} \alpha_c (1 - \alpha_c) \beta_{\ln N - \ln \tau_a} \frac{\Delta\tau_a}{\tau_a} R_{\text{SW}}^\downarrow \rangle}{\langle \alpha_c (1 - \alpha_c) \rangle \langle \beta_{\ln N - \ln \tau_a} \rangle \langle \frac{\Delta\tau_a}{\tau_a} \rangle \langle R_{\text{SW}}^\downarrow \rangle}$	Effective cloud fraction for RFaci
8	$\beta_{\ln \mathcal{L} - \ln N} = \frac{\partial \ln \mathcal{L}}{\partial \ln N_d}$	Sensitivity of \mathcal{L} to changes in N_d
8	$S_{\mathcal{L}, N} = \frac{\partial R}{\partial \mathcal{L}} \frac{d\mathcal{L}}{d \ln N_d}$	Sensitivity of R to changes in \mathcal{L} mediated by changes in N_d
8	$c_{\mathcal{L}} = \frac{\langle \mathcal{C}_{\text{liq}} \alpha_c (1 - \alpha_c) \beta_{\ln \mathcal{L} - \ln N_d} \beta_{\ln N_d - \ln \tau_a} \frac{\Delta\tau_a}{\tau_a} R_{\text{SW}}^\downarrow \rangle}{\langle \alpha_c (1 - \alpha_c) \rangle \langle \beta_{\ln \mathcal{L} - \ln N_d} \rangle \langle \beta_{\ln N_d - \ln \tau_a} \rangle \langle \frac{\Delta\tau_a}{\tau_a} \rangle \langle R_{\text{SW}}^\downarrow \rangle}$	Effective cloud fraction for rapid adjustments in \mathcal{L}
8	$\beta_{\mathcal{C} - \ln N} = \frac{\partial \mathcal{C}}{\partial \ln N_d}$	Sensitivity of \mathcal{C} to changes in N_d
8	$S_{\mathcal{C}, N} = \frac{\partial R}{\partial \mathcal{C}} \frac{d\mathcal{C}}{d \ln N_d}$	Sensitivity of R to changes in \mathcal{C} mediated by changed in N_d
8	$c_{\mathcal{C}} = \frac{\langle (1 - \mathcal{C}_{\text{ice}}) (\alpha_c - \alpha_{\text{clear}}) \beta_{\mathcal{C} - \ln N} \beta_{\ln N - \ln \tau_a} \frac{\Delta\tau_a}{\tau_a} R_{\text{SW}}^\downarrow \rangle}{\langle (\alpha_c - \alpha_{\text{clear}}) \rangle \langle \beta_{\mathcal{C} - \ln N} \rangle \langle \beta_{\ln N - \ln \tau_a} \rangle \langle \frac{\Delta\tau_a}{\tau_a} \rangle \langle R_{\text{SW}}^\downarrow \rangle}$	Effective cloud fraction for rapid adjustments in cloud fraction

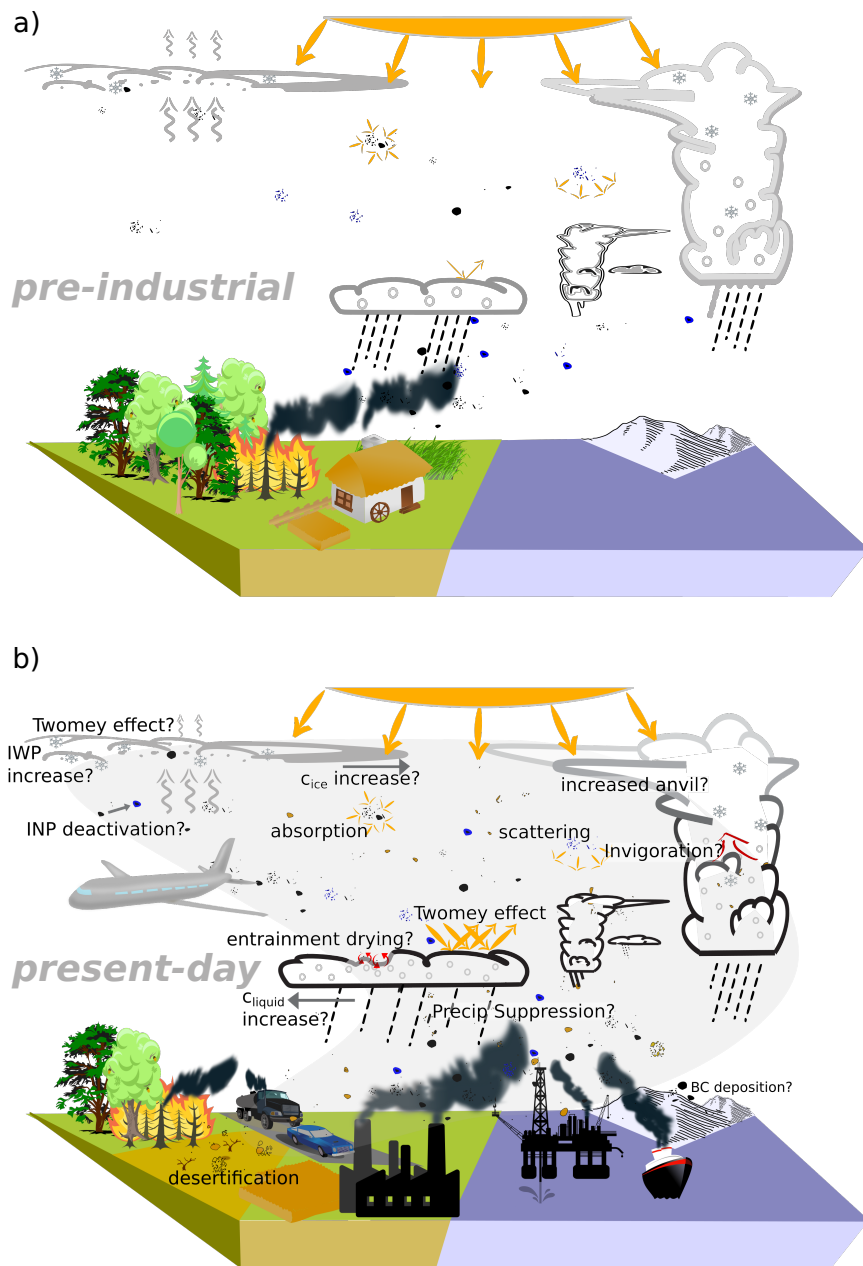


Figure 2. Simplified representation of the impact of anthropogenic aerosol emissions on the Earth system in (a) the preindustrial and (b) the present-day atmosphere. A schematic representation of known processes relevant for the effective radiative forcing of anthropogenic aerosol is summarised for present-day conditions in panel (b), but the same processes were active, with different strengths, in preindustrial conditions. Processes where the impact on the effective radiative forcing remains qualitatively uncertain are followed by a question mark. C_{liquid} and C_{ice} denote liquid and ice cloud fractions, respectively. LWP and IWP stand for liquid and ice water path, respectively. INP stands for ice nucleating particle.

Table 3. Estimates of effective cloud fraction for aerosol-radiation interactions, c_{τ} , in the 9 global aerosol-climate models that participated in H. Zhang et al. (2016). Models that share the same host model use different aerosol and/or cloud schemes.

Model name	Reference	c_{τ}
CAM5.3-CLUBB	Bogenschutz et al. (2013)	0.693
ECHAM6-HAM2	Neubauer et al. (2014)	0.552
GEOS-5	Barahona et al. (2014)	0.596
HadGEM3-A-GLOMAP	Bellouin, Mann, et al. (2013)	0.728
ModelE2-TOMAS	Y. H. Lee et al. (2015)	0.667
NCAR_CAM5.3-CLUBB_MG2		0.680
NCAR_CAM5.3_MG2	Gettelman and Morrison (2015)	0.637
NCAR_CAM5.3	Liu et al. (2012)	0.673
SPRINTARS	Takemura et al. (2005)	0.704
SPRINTARS-KK	Takemura et al. (2005)	0.697
	<i>Mean</i>	<i>0.663</i>
	<i>Median</i>	<i>0.677</i>
	<i>Standard deviation</i>	<i>0.054</i>

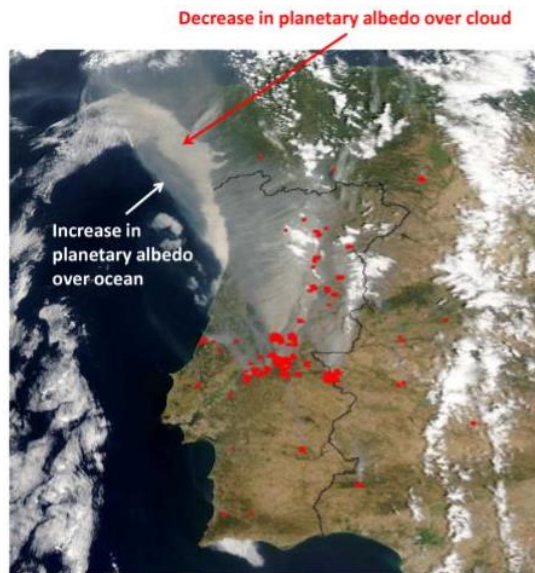


Figure 3. True-colour satellite image taken by the Moderate Resolution Imaging Spectrometer (MODIS) showing a plume of smoke from forest fires in Portugal on 3 August 2003. Fires are shown by the red spots, the smoke plume appears in grey. From J. Haywood (2015).

Table 4. Ranges obtained by this review in the 16–84% confidence interval for the variables of Equations 8, 15, and 24. The ranges of radiative forcing (RF) and rapid adjustments (RA) components estimated from the variables are shown in italics. The bounds for total aerosol effective radiative forcing (ERF) are shown in bold. ari stands for aerosol-radiation interactions and aci for aerosol-cloud interactions. Optical depths τ_a are given at $0.55 \mu\text{m}$. Sensitivities (S terms) are given in W m^{-2} over the shortwave and longwave spectrum, and in parentheses also in terms of relative changes in planetary albedo for sensitivities that are predominantly acting in the shortwave spectrum. LES stands for Large Eddy Simulation.

Section	Variable	Lower bound	Upper bound	Line of evidence
4	τ_a^{PD}	0.12	0.16	Satellite retrievals
4	$\Delta\tau_a$	0.02	0.04	Global modeling
4	$\Delta \ln \tau_a = \Delta\tau_a/\tau_a^{\text{PD}}$	0.14	0.29	Modeling/satellite
6	$\Delta \ln N_d = \Delta N_d/N_d$	0.06	0.18	Modeling/satellite
Aerosol-radiation interactions				
5	$S_\tau^{\text{clear}} [\text{W m}^{-2} \tau_a^{-1}]$	−27 (0.08)	−20 (0.06)	Global modeling
5	c_τ	0.59	0.71	Global modeling
5	$S_\tau^{\text{cloudy}} c_\tau [\text{W m}^{-2}]$	−0.1	+0.1	Global modeling
5	<i>RF of ari</i> [W m^{-2}]	−0.37	−0.12	
7	dR/dR_{atm}	−0.3	−0.1	Global modeling
7	$dR_{\text{atm}}/d\tau_a [\text{W m}^{-2} \tau_a^{-1}]$	17	35	Global modeling
7	<i>RA of ari</i> [W m^{-2}]	−0.25	−0.05	
7	<i>ERF of ari</i> [W m^{-2}]	−0.58	−0.23	
Aerosol-cloud interactions				
6	$\beta_{\ln N - \ln \tau}$	0.3	0.8	Modeling/satellite
6	$S_N [\text{W m}^{-2}]$	−27 (0.079)	−26 (0.076)	Satellite retrievals
6	c_N	0.19	0.29	Modeling/satellite
6	<i>RF of aci</i> [W m^{-2}]	−1.20	−0.35	
8	$\beta_{\ln \mathcal{L} - \ln N}$	−0.3	−0.011	Satellite analyses
8	$S_{\mathcal{L}, N} [\text{W m}^{-2}]$	−54	−56	Mixed
8	$c_{\mathcal{L}}$	0.21	0.29	Mixed
8	<i>RA of aci (liquid-water path)</i> [W m^{-2}]	0.00	+0.50	
8	$\beta_{c - \ln N}$	0	0.1	Global modeling, LES
8	$S_{c, N} [\text{W m}^{-2}]$	−91	−153	Satellite analysis
8	c_c	0.76	1.07	Mixed
8	<i>RA of aci (cloud fraction)</i> [W m^{-2}]	−1.35	0.0	
8	<i>ERF of aci</i> [W m^{-2}]	−2.00	−0.30	
11	Total aerosol ERF [W m^{-2}]	−2.50	−0.65	
11	(constrained by observational inferences)	−1.60	−0.65	

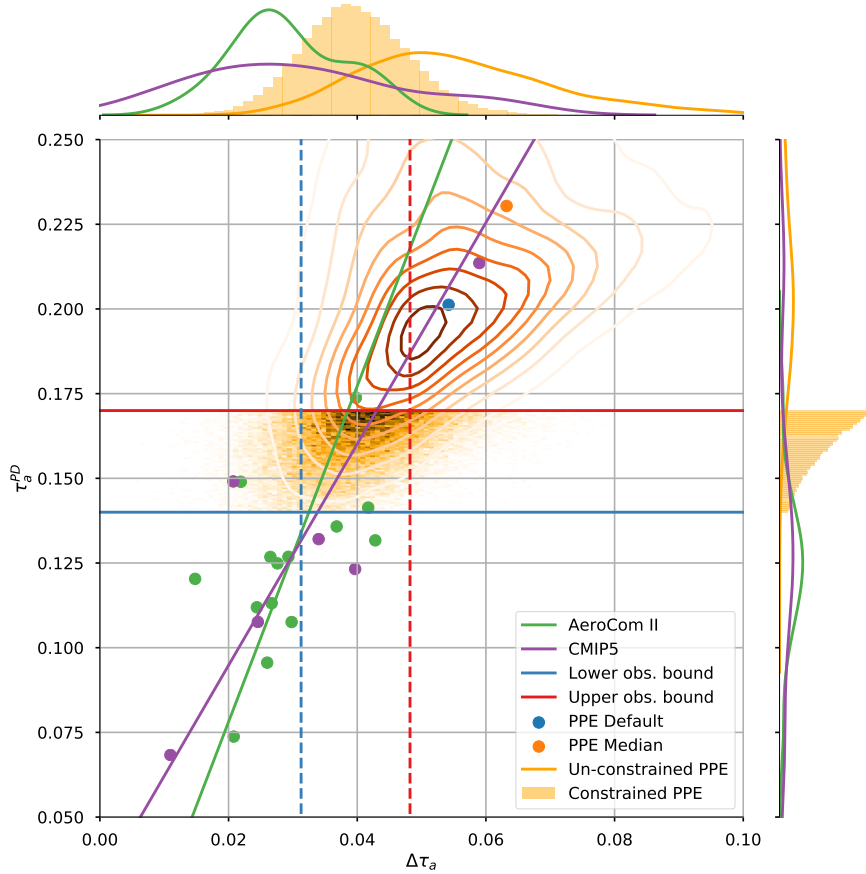


Figure 4. Distributions, standard deviation and best-fit lines of the present-day aerosol optical depth, τ_a^{PD} against the industrial-era change in aerosol optical depth at $0.55\mu\text{m}$, $\Delta\tau_a$, between 1850 and present-day, simulated for cloud-free conditions by AeroCom Phase II and CMIP5 sstClimAerosol models. The full joint-probability distribution sampled from the emulated HadGEM-UKCA 26 aerosol parameter Perturbed Parameter Ensemble (PPE) is shown as contour lines, and the constrained distribution as a hex-density. The default and median model runs of the PPE are also shown for completeness. The horizontal lines show the 1σ observational uncertainty range in globally-averaged τ_a^{PD} , while the vertical lines show the resulting 1σ range in $\Delta\tau_a$ of the constrained PPE. Figure adapted from Watson-Parris et al. (submitted).

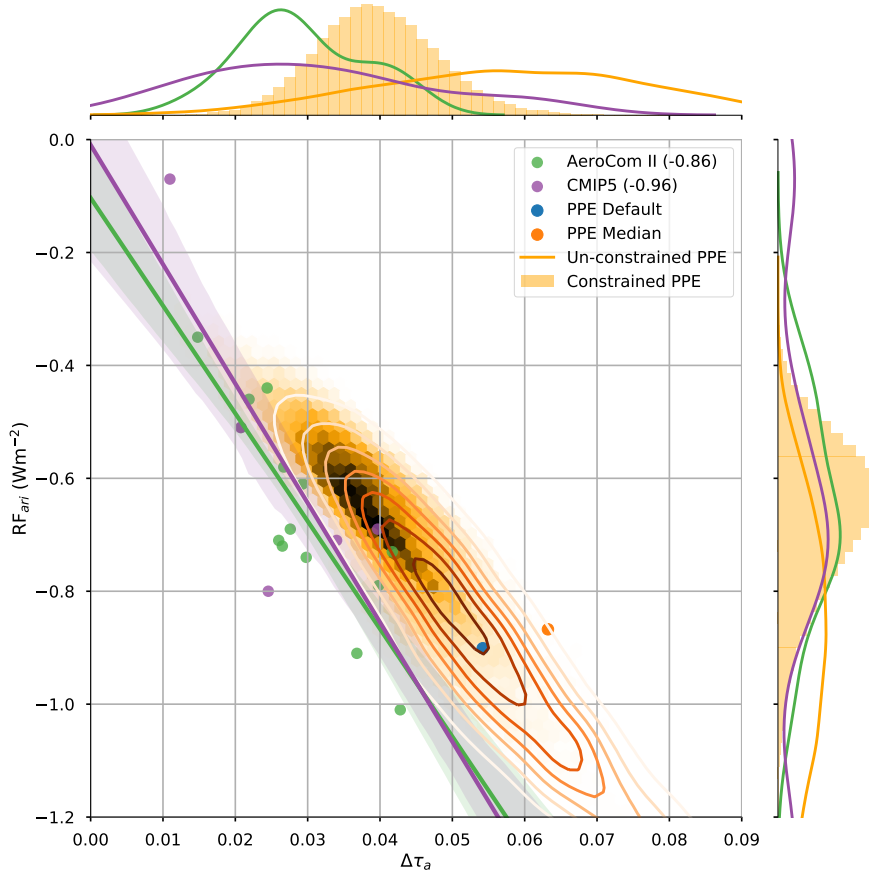


Figure 5. Clear-sky radiative forcing of aerosol-radiation interactions, RF_{ari} in $W m^{-2}$, as a function of the industrial-era change in aerosol optical depth at $0.55 \mu m$, $\Delta\tau_a$ in AeroCom models (green), CMIP5 models (purple). The slopes of the lines of best fit for each dataset are -19.1 and $-21 W m^{-2} \tau_a^{-1}$, respectively. The joint-distribution of the full emulated HadGEM-UKCA 26 aerosol parameter Perturbed Physics Ensemble (PPE) is shown with contours, while the samples consistent with τ_a^{PD} is shown as a hex-density. The slope for the PPE is $-14 W m^{-2} \tau_a^{-1}$. The default and median model runs are also shown for completeness. The 1σ uncertainty in the fits are shaded and the correlation coefficients are indicated in the parentheses in the legend. Figure adapted from Watson-Parris et al. (submitted).

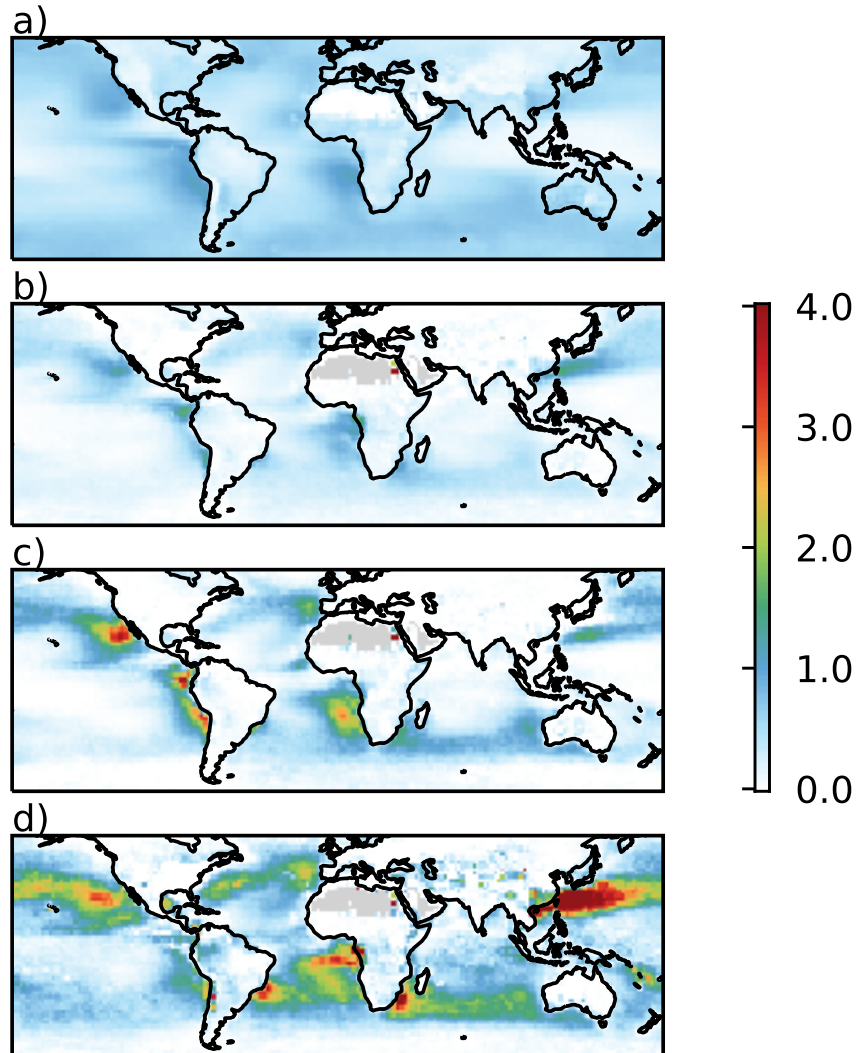


Figure 6. (a) Liquid cloud fraction C_{liq} , multiplied by 2 to be legible on the shared color scale. (b–d) The effective cloud fractions for b) the radiative forcing of aerosol-cloud interactions (c_N), c) rapid adjustments in liquid water path (c_L) and d) rapid adjustments in liquid cloud fraction (c_C). Distributions have been calculated using cloud retrievals by MODIS (Platnick et al., 2017), CERES cloud albedo (Wielicki et al., 1996) and the anthropogenic aerosol fraction from Bellouin, Quaas, et al. (2013).

Table 5. Ranges obtained by this review for the radiative forcing (RF), rapid adjustments (RA), and effective radiative forcing (ERF) of aerosol-radiation interactions (ari), aerosol-cloud interactions (aci), and total aerosol ERF. All values are in W m^{-2} . Compared to Table 4, ranges are given as 5-95% confidence intervals.

Variable	Lower bound	Upper bound
RFari	-0.45	-0.05
RAari	-0.35	-0.05
ERFari	-0.70	-0.15
RFaci	-1.60	-0.20
RAaci (liquid-water path)	-0.05	+0.80
RAaci (cloud fraction)	-2.20	+0.20
ERFaci	-3.10	-0.10
Total aerosol ERF (constrained by observational inferences)	-3.60 -2.0	-0.40 -0.40

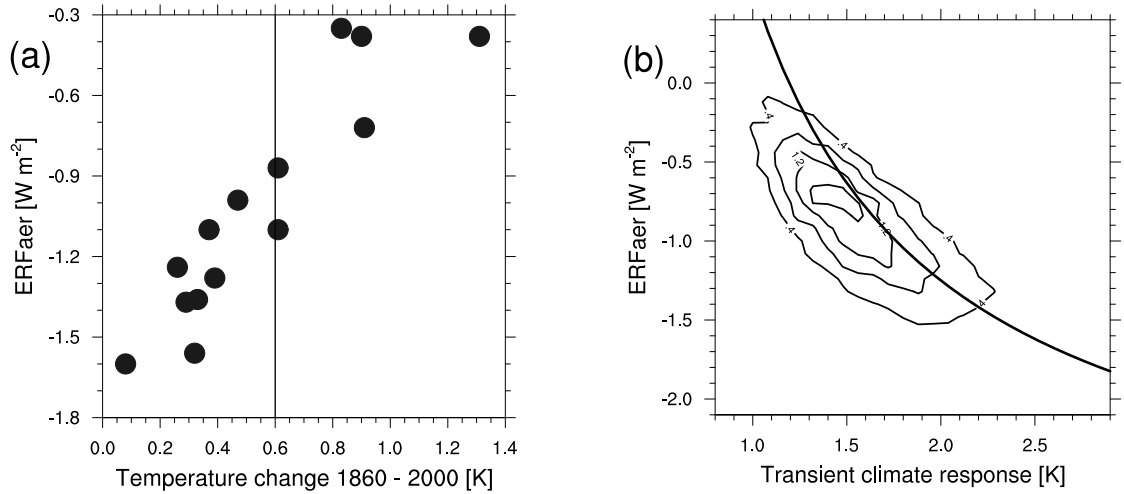


Figure 7. (a) Scatterplot of the change in global annual mean surface temperature between 1860 and 2000 and aerosol ERF, ERF_{aer} , from 14 models of the CMIP5 ensemble. The vertical line at 0.6 K corresponds to the approximately observed change. After Rotstayn et al. (2015). (b) Joint histogram of the probability density function, normalised to 1, between aerosol ERF (2010 vs. 1765) and transient climate response (the global-mean surface temperature increase at time of CO_2 doubling) from a large ensemble obtained with the simple emissions-based climate model of Smith et al. (2018). Superimposed is the relation determined from an energy balance model assuming an immediate temperature response to the total forcing. The total forcing here consists of the greenhouse-gas forcing in 2011 (3.1 Wm^{-2} , Myhre, Shindell, et al., 2013) plus aerosol ERF; the temperature increase in 2011 (relative to preindustrial) is taken as 1 K; and the transient sensitivity is translated to transient climate response for the ERF of doubled CO_2 taken as 3.7 Wm^{-2} .

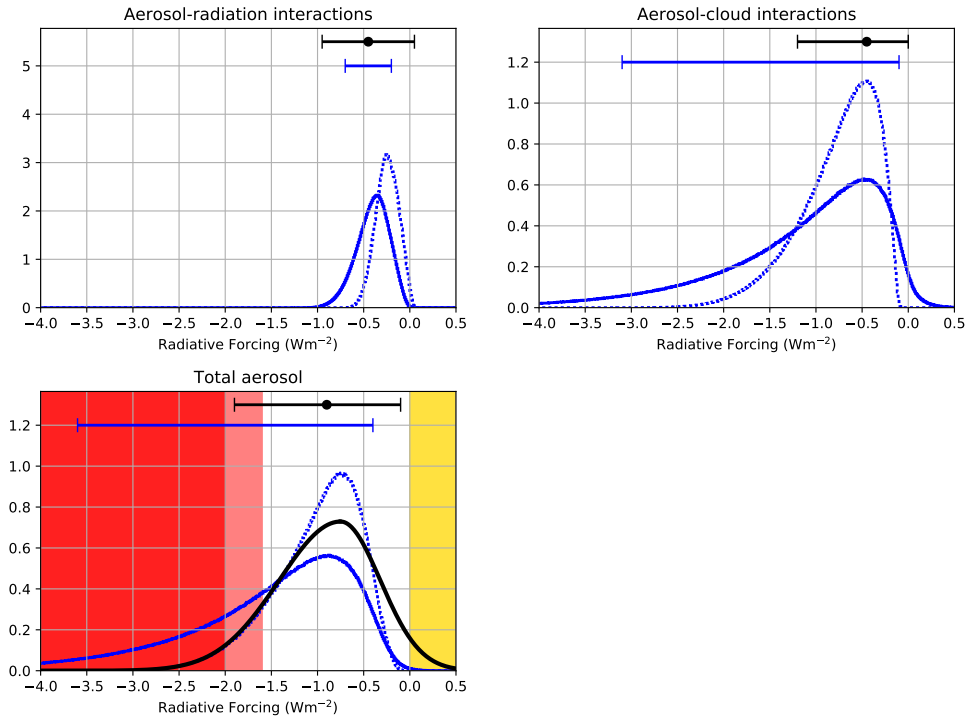


Figure 8. Probability distribution functions of aerosol radiative forcing (dashed lines) and effective radiative forcing (solid lines), in W m^{-2} , as derived by this review (blue) and by the Fifth Assessment Report of the IPCC (Myhre, Shindell, et al., 2013) (black). Those distributions functions are obtained based on understanding of the aerosol, cloud, and radiation physics. The top row shows distributions for (left) aerosol-radiation interactions and (right) aerosol-cloud interactions. The bottom row shows distributions for their sum. Corresponding 5-95% confidence intervals (90% likelihood of being in that range) for the effective radiative forcing are shown at the top of each panel, again in blue for this review and in black for the IPCC assessment. The IPCC intervals also show the best estimate as a dot. For total aerosol, colored regions indicate aerosols ERFs that are inconsistent with inferences based on observed changes in temperature (red shading for the 5-95% confidence interval, pink shading for the 17-84% confidence interval) and inconsistent with observed changes in surface radiation (yellow shading).